CRANFIELD UNIVERSITY

Ahmed Aseeri

Modelling and Simulation of Fuel Cell/Photovoltaic Hybrid Power System

School of Engineering

MSc
Academic Year: 2010 - 2012

Supervisor: Dr A. Savvaris
November 2012

CRANFIELD UNIVERSITY

School of Engineering

MSc

Academic Year 2010 - 2012

Ahmed Aseeri

Modelling and Simulation of Fuel Cell/Photovoltaic Hybrid Power System

Supervisor: Dr A. Savvaris
November 2012

This thesis is submitted in partial fulfilment of the requirements for the degree of MSC

ABSTRACT

Due to an ever increasing demand for power consumption and a rising public awareness of the impact on the environment, renewable energy based on Hybrid Power Systems (HPS) (e.g. fuel cell, wind or solar) to supply electricity has attracted a growing research interest. Photovoltaic (PV) power generation systems are among the most promising renewable energy technology solutions. Fuel Cell (FC), on the other hand, is emission-free and quieter than hydrocarbon fuel-powered engines. It saves fuel and is cleaner for the environment. Such systems can generate electricity from clean sources to power loads located in inaccessible or remote areas.

The aim of this thesis is to investigate the potential for utilising an FC/PV hybrid power system to provide power for a water pump, which supply an elevated water tank (6,500 litres/day consumption) to a small community located in a remote area. The HPS consists of a photovoltaic solar panel, a 1.2 KW Nexa Proton Exchange Membrane Fuel Cell (PEMFC), a Lead acid battery bank, a bidirectional DC/DC converter, one directional DC/DC converter and a water pump. The thesis will commence with a literature review, giving an overview of energy demand and future trend, describing the different HPS configurations and giving some examples of similar projects carried out by other researchers and organisations. A system component description is also covered. The thesis will then move on to describing the HPS simulation model development using Matlab/Simulink simulation environment, concluding with the test cases used to validate the model based on the 1.2 KW Nexa PEMFC and PV panels.

In the case study, the system utilizes photovoltaic (PV) as the primary power generator, PEMFC as the secondary back-up power generator and a battery bank (to store any excess power) as power storage device. The advantage of the proposed system is that, in addition to being environmentally friendly, it also has lower maintenance costs, noise and carbon footprint. Two main scenarios were explored to validate the hybrid system performance, at two different geographical and environmental conditions.

The first case is based in Saudi Arabia, where it is hot and sunny for most of the year. This scenario permits higher utilization of the power generated from the PV

cells and reduces the dependence on power produced by the fuel cell. The second case scenario is based in the UK, where it is cold and cloudy for most of the year. The Sunlight here is at minimum, leading to higher dependence on the fuel cells for the system operation

ACKNOWLEDGEMENTS

I thank to God (Allah) by the strength and faith that he has given me, which has allowed me to accomplish this and all other achievements in my life. Then I would like to thank all those people who gave me direct or indirect support which was like a bright star in very dark night that kept me heading to my goal.

First I would like to express my sincere gratitude to my supervisor, Dr. A. Savvaris for his enthusiasm, encouragement, support and guidance on fundamentally and theoretical important matters throughout the whole research work.

I am very grateful to my friends and colleagues at Cranfield University and especially Abdulhakim Oheda for his help and support.

I would like extend my thanks to my brother Mohammed who never stops supporting me in all my life. And especial thanks to my wife Aisha and my daughters Sulaf and Elaf for their ultimate support and patience, who suffered a lot for my absence days and nights.

TABLE OF CONTENTS

LIST OF FIGURES

LIST OF TABLES

SUBSTANCES

a-Si	Amorphous Silicon
CdTe	Cadmium Telluride
CO_2	Carbon dioxide
GaAs	Gallium Arsenide
H_2	Hydrogen
H_2O	Water
KOH	Potassium hydroxide
Li_2CO_3	Molten carbonate melts
mc-Si	Multi crystalline
O_2	Oxygen
sc-Si	Mono crystalline
Si	Silicon
µm-Si	Micromorph silicon

ABBREVIATIONS

AC	Alternating Current
AFC	Alkaline Fuel Cell
AM	Air Mass
APL	Alternative Power Library
BP	International Company for Solar Cell
BPWM	Bipolar Pulse Width Modulation
CHP	Combined Heat and Power Generation
DC	Direct Current
EL	Electrolyser Component
EPIA	European Photovoltaic Industry Association
FC	Fuel Cell
ISET	Institute of Solar Energy Supply Technology
I-U	Current-Voltage
MCFC	Molten Carbonate Fuel Cell
MPPT	Maximum Power Point Tracking
MW	Megawatt
NOCT	Normal Operating Cell Temperature

PAFC	Phosphoric Acid Fuel Cell
FC	Fuel Cell
MCFC	Molten Carbonate Fuel Cell
PEM	Proton Exchange Membrane
PEMFC	Proton Exchange Membrane Fuel Cell
PV	Photovoltaic
SOFC	Solid Oxide Fuel Cell
APU	Auxiliary Power
DC	Direct Current
TRL	Technology Reading Level
UC	Ultra-Capacitor
HPS	Hybrid Power System

LIST OF SYMBOLS

k_{H2}	Hydrogen valve molar constant [kmol s^{-1} atm]
k_{H2O}	Water valve molar constant [kmol s−1 atm]
k_{O2}	Oxygen valve molar constant[kmol s^{-1} atm]
k_{an}	Anode valve constant [kmol s^{-1} atm]
q_{H2}	Molar flow of hydrogen [kmol s^{-1}]
q_{H2O}	Molar flow of water [kmol s^{-1}]
q_{O2}	Molar flow of oxygen [kmol s^{-1}]
q_{H2}^{in}	Hydrogen input flow [kmol s^{-1}]
q_{H2}^{out}	Hydrogen output flow [kmol s^{-1}]
q_{H2}^{r}	Hydrogen flow that reacts [kmol s^{-1}]
P_{H2}	Hydrogen partial pressure [atm]
P_{H2O}	Water partial pressure [atm]
P_{O2}	Oxygen partial pressure [atm]
τ_{H2}	Hydrogen time constant [s]
τ_{H2O}	Water time constant [s]
τ_{O2}	Oxygen time constant [s]
M_{H2}	Molar mass of hydrogen [kg kmol s^{-1}]
M_{H2O}	Molar mass of water [kg kmol s^{-1}]
M_{O2}	Molar mass of oxygen [kg kmol s^{-1}]
V_{an}	Volume of the anode channel [m^3]

V_{ca}	Volume of the cathode channel [m^3]
R	Universal gas constant [J $kmol^{-1}$ K]
r_{h-o}	Oxygen flow ratio
C_{O2}	Oxygen concentration [%]
T	Stack Temperature [K]
N_o	Number of FCs in the stack
I	Stack current [Amp]
F	Faraday's constant [C $kmol^{-1}$]
k_r	Modelling constant [kmol s^{-1}A]
V_{Cell}	DC output voltage of FC system
E	Nernst voltage [V]
E_o	Open cell voltage [V]
η_{ohmic}	Over voltage due to ohmic loss
η_{act}	Activation over voltage
B	Activation voltage constant [A^{-1}]
C	Activation voltage constant [V]
$q_{methanol}$	Methanol flow rate [kmol s^{-1}]
CV	Conversion factor
τ_1, τ_2	Time constants
U	Utilization rate
k_3	PI gain
τ_3	Time constant of the PI controller
s	s domain
R_{int}	Stack internal resistance [Ω]
X	Line reactance [Ω]
I_L	Light current [A]
I_s	Saturation current [A]
I_d	Diode current (A
I	Load current [A]
I_{sc}	Short circuit current [I]
V	Output voltage [V]
V_{oc}	Open circuit voltage [V]
R_s	Series resistance [Ω]
R_{sh}	Shunt resistances [Ω]

n	Diode ideality factor
k	Boltzman's constant, 1.13×10^{-23} [j/k]
q	Electron charge, 1.6×10^{-19} [C]
G_0	Reference solar radiation, 1000 [W/m²]
Ns	Number of cells in series, 60/Panel
Eg	Gap energy voltage, [eV]
T_0	Reference junction temperature, [K]
NOCT	Normal operating cell temperature [°C]

1 INTRODUCTION

1.1 Background and Motivation

Due to the ever-increasing demand for power consumption and rising public awareness of the impact on the environment, renewable energy hybrid power generation systems (e.g. fuel cell, wind or solar) have attracted a growing research interest. Photovoltaic (PV) power generation systems are among the promising renewable energy technology solutions. Fuel Cell (FC), on the other hand, is emission-free and quieter than hydrocarbon fuel-powered engines. It saves fuel and is cleaner for the environment. This is the main drive behind this research project, with the aim of investigating the potential of utilising a hybrid FC/PV system to power venues of use such as environmental and technical monitoring equipment, along with some novel application on relatively high power equipment (pumps - lifting equipment for weirs and sluices).

1.2 Project Aims and Objectives

Aims:

The aim of this project is to model and design an FC/PV Hybrid Power System (HPS), to investigate the potential for utilising an FC/PV hybrid power system to provide power for a water pump to pump water to an elevated water tank, which then supplies water (6,500 litres/day consumption) to a small community located in a remote area.

Objectives:

The main objectives of the project are summarised as follows:

- Designing and developing the experimental FC/PV power hybrid system
- Developing a simulation model of the FC/PV HPS which describes the system operation and the load profile
- Comparing between experimental and simulation results
- Energy management and control of the hybrid system.

1.3 Thesis Layout

Chapter two of this report gives an overview of the energy demand and future trend. Chapter three describes the different Hybrid Power System configuration and gives

some examples of similar projects carried out by other researchers and organisations. In chapter four, a description of the system component is given.

The simulation model used in this project is explained in chapter five. Chapter six describes the experimental setup including the photovoltaic solar panel, Nexa 1.2 PEM fuel cell module set-up, DC/DC one directional converter, DC/DC bidirectional converter, water pump and control strategy.

Chapter seven presents a study case, results and discussions and finally the conclusion, future work and recommendations are given in chapter 8.

1.4 Research Gap and Contribution to Knowledge

In the last few decades Hybrid Power System (HPS) attracted many researchers, due to the increase of fuel prices and high cost associated with running power transmission lines to remote areas. Many different configurations of HPS have been proposed in the literature as will be shown in more details in chapter 3 of this thesis. Many of these studies investigated different configurations of HPS as part of micro power generation connected to a power network, or as standalone HPS to power remote loads. However, for the specific application considered in this thesis little research has been carried-out. In addition, comparison of the system performance at two different geographical locations based on the literature search has not been attempted before. The developed FC model was adjusted using experimental data from the test-rig to improve the model performance and to more accurately represent the real system behaviour. Finally, a controller was implemented to manage the power between the different power sources and meet the demand for different times of the day.

2 ENERGY OVERVIEW

2.1 Introduction

Since the beginning of the last century, fossil fuel has been and still is the main energy source to meet the world's increased energy demand. The improved quality of life is pushing the world's energy consumption year after year. As a result of extensive fossil fuel consumption, millions of tonnes of pollutant gases have been released into the atmosphere, which is believed to be the main cause of global warming [1]. There is growing high pressure on governments around the world to meet future energy demand and to reduce CO_2 emissions at the same time. During the years 2007 and 2008, oil prices hit their highest ever since the Second World War. The world realised that oil is no longer a cheap energy source. Besides the sudden increase in oil prices, more scientific evidence has pointed out that burning fossil fuel is the main reason behind global warming and climate changes. The reasons above and the expected growth of the world's energy demands have put world leaders under heavy pressure to invest and investigate new sustainable sources of energy, to reduce CO_2 emissions and to close the gap of the predicated increases in future energy demand. This chapter will highlight the expected world energy growth and different energy sources available or under development.

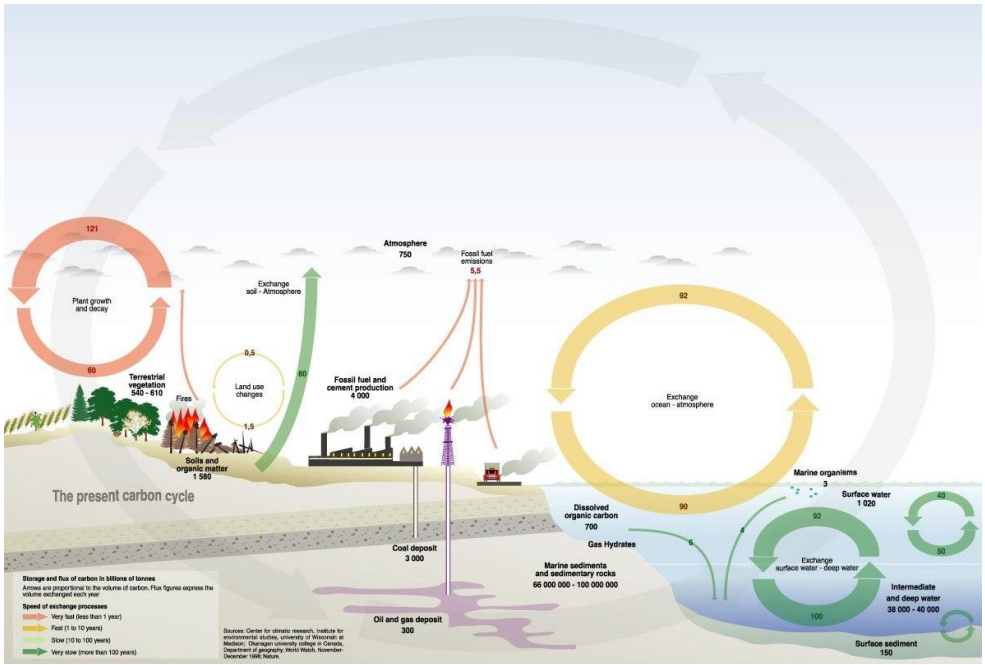

Figure 2.1 Carbon cycle [2]

2.2 Expected World Energy Demand

Despite the recession the world economy went through during 2008, it is estimated that the world's energy consumption will grow up by about 49% from 2007 until the year 2035, with an average increase of 1.4 % per year as shown in figure 2 [3]. However, energy demand in fast growing economy countries like China and India is expected to grow dramatically in the next two decades as shown in figure 2.3. Both countries were consuming about 10% of the world's energy consumption in 1990, but their consumption had jumped to 20% by the year 2007. By 2035 it is predicted that about 30% of the overall world energy consumption will be shared between China and India [3]. For example, car ownership increased in 2007 in China and India by 37% and 17% respectively [4]. On the other hand, the US share in world energy consumption will drop from 21% in 2007 to 16% by the year 2035. This is due to high improvement in building and equipment efficiency [3].

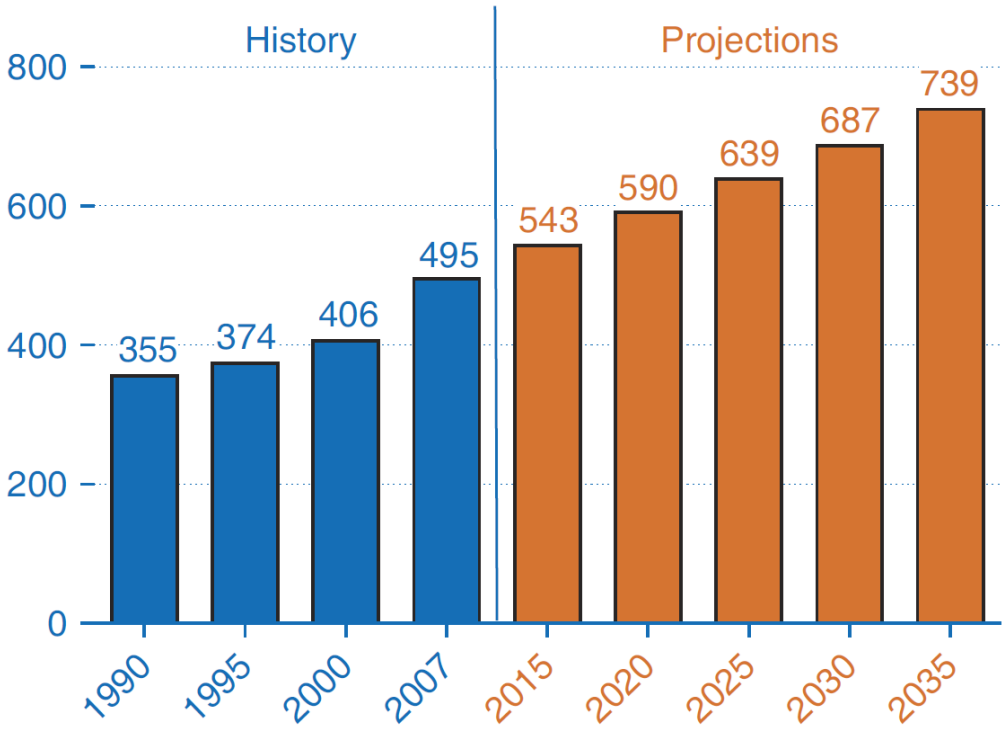

Figure 2.2 World's energy consumption (quadrillion Btu) [3]

Fossil fuel will continue to play a big role as the main source of current and future expected energy growth. The non-even distribution of oil around the world will risk energy supply stability, especially during natural disasters or political conflicts.

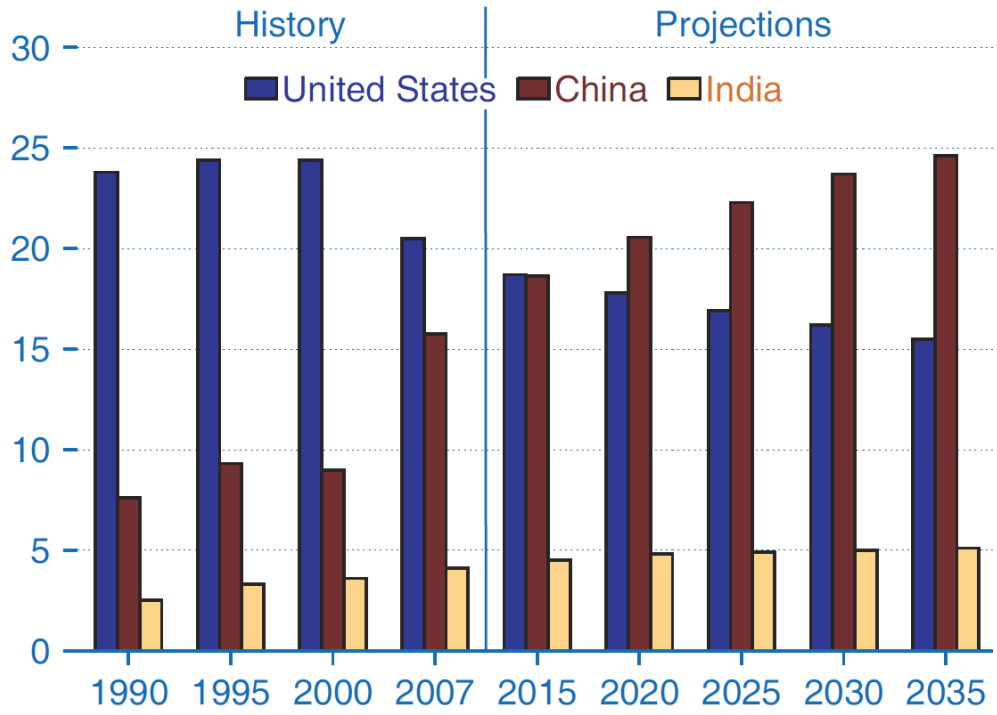

Figure 2.3 Shares of world's energy consumption in the USA, China, and India (percentage of world total) [3]

The other problem with oil supply is the increasing gap between oil predicted future demand and expected new discovery. Figure 2.4 shows the actual oil discoveries in grey bars and oil consumption in dotted black lines for the period from 1930 to 2008. As a result of the first oil crisis, consumption hit a peak in 1979. For the following five years the world's consumption decreased owing to the world economy slow down and the introduction of more efficient transport vehicles. As per the grey bars shown in Figure 2.4, most of the major oil fields were discovered early last century. This includes the world's largest oil field, Ghawar, discovered in Saudi Arabia in 1948 and Burgan Kuwait's big oil field discovered the late 1930s. It is important to note that oil discovery was far greater than oil consumption until 1984; since then, oil consumption has been exceeding discoveries. In the future the already existing large gap between new oil discoveries and predicted production demand will continue to increase. The future projected growth demand is shown in red. The yellow bars are the estimated future oil discoveries [4].

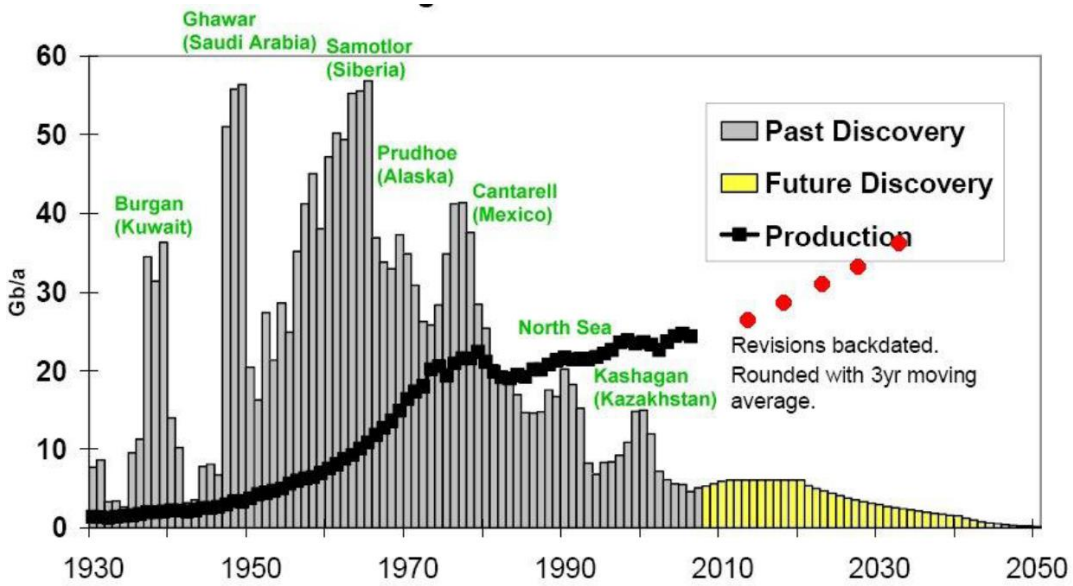

Figure 2.4 The growing gap between the oil past and future discoveries [4]

2.3 Energy Alternatives

The world is working hard to find reliable alternatives to the oil that has dominated energy supply since early last century. The problem is not because we are going to run out of oil, but due to the following main reasons [6]:

- Expected oil consumption to rise far above the production rate.
- To reduce CO_2 emission and improve cities' air quality, and reduce the effect of global warming.
- Ensure sustainable security of energy supply.
- Reduce the dependence on imported oil.

Energy supply can be divided into two main categories.

1. Conventional Energy Sources
    - Oil
    - Coal
    - Natural Gas
    - Nuclear Energy
2. Sustainable energy
    - Hydroelectric Power
    - Wind Energy
    - Photovoltaic (PV)
    - Concentrated Solar Power
    - Fuel Cell
    - Geothermal power

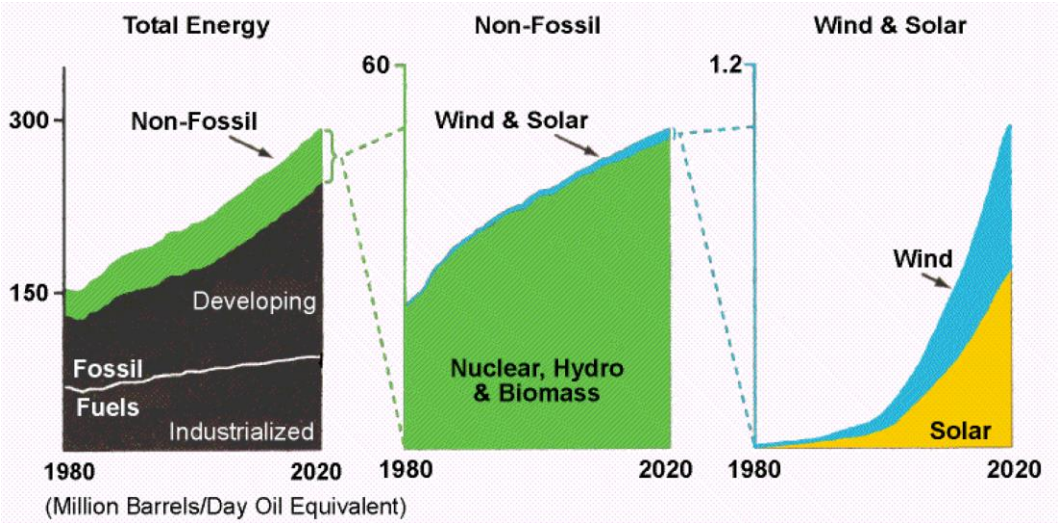

Figure 2.5 Expected growth of demand growth of different energy sources. [5]

2.4 Chapter Summary

This chapter presents an overview of the challenges the world is facing to secure energy, to meet the dramatically growing future demand due to the improved quality of life and high growth in new markets like China and India. On the other side there is growing public pressure on the government to invest in renewable energy to reduce the dependence on–imported oil and gas with the aim of reducing CO_2 emissions**,** which are believed to be the main cause of global climate change.

3 HYBRID POWER SYSTEMS

Chapter 2 presented how, in the last few years, energy consumption and prices have hit their highest record since the last energy crisis in the late 1970s. Besides energy prices, strong environmental campaigns to reduce global warming have enhanced the interest in renewable green energy power generation. Solar, wind power and hydrogen as a power carrier are the most attractive green sources of renewable energy. The European Photovoltaic Industry Association (EPIA) estimated that electricity produced by PV will cover about 12% of electricity demand generated in Europe by 2020[6]. Due to the fact that solar and wind generated power is affected by weather changes, using hydrogen as power storage and then generating electrical power via fuel cells also showed great potential as a green power source for the future. FCs have many advantages, such as low or even zero CO_2 emission, high efficiency and low maintenance cost. Also, in the last few years, fuel cell technology has dramatically improved and, as a result of that, the cost has dropped rapidly. However, none of these technologies have reached the optimum level as yet.

In this chapter, a concise technical explanation of numerous widely used Hybrid Power System (HPS) configurations shall be given. Several examples of Hybrid Power System (HPS) configurations shall be presented.

3.1 Introduction

In general, HPS can be defined as the combination of multi-power generators and storage devices which are connected to each other and controlled to meet a certain power demand.

As mentioned earlier, solar and wind power are sensitive to weather changes, while currently FCs are still very expensive and need a pure or high concentration of hydrogen gas. As a result, a combination of many power generators and storage components is required to form a multi-source HPS to improve reliability and availability, to meet energy demand. HPS can be utilised to power any load, whether as a stand-alone or connected to existing grid power generation, in remote areas, such as wireless communication antenna, villages, well water pumps etc., or in any remote, rural areas.

Combining more than one source of energy generators with a good control system has improved system quality and reliability. Hybrid systems have attracted researcher attention worldwide [9, 11, 12, 13, and 14].

The many combinations of Hybrid Power Systems (HPS) have been indicated in many literatures, as shown below:

1. PV/Wind/FC/electrolyser system [9, 13, 14].
2. Diesel/FC system
3. Wind/diesel system
4. PV/wind/battery system [20]
5. PV/diesel system[19]
6. PV/battery system
7. Wind/PV/hydrogen storage system
8. PV/ Wind system [10, 17].
9. PV/FC system [10]
10. PV/Wind/Batteries system [11]
11. PV/Wind/Solar concentration/ Electrolyser/H2 storage/FC system[12,16]
12. PV/Wind/FC system [14]
13. PV/Wind/Hydro/FC/electrolyser/batteries [18]

This is evidence to support the argument that photovoltaic (PV) and wind power are among the most promising sustainable energy sources. However, due to the fact that wind and PV power are dependent on weather conditions, it is not practical to meet the required energy demand just by stand-alone photovoltaic and/or wind sustainable energy systems. An additional power back-up is required. This could be a power generator(s) and/or a power storage device(s) integrated with each other to make up a Hybrid Power System (HPS). The energy storage device could be a battery bank, a super-capacitor bank, a hydrogen electrolyser integrated with a fuel cell system or a mixture of two or more of these devices

An important point to consider before designing an HPS to serve a specific geographic location is to investigate the availability and visibility of energy sources at that site which can be utilised to meet the power requirement. Prior to building an HPS for a specific location, it is very important to understand the power demand needed and the available resources in the area. As such, the energy designer’s role includes analysing the solar, wind and other possible energy sources in the location. This will allow the designing engineer to select HPS components to achieve an optimum design.

3.2 Typical HPS Configurations

3.2.1 PV/Battery/Diesel HPS

It requires significant financial investment to design a stand-alone PV system that is sizeable enough to survive in the toughest weather conditions. As such, an integrated PV hybrid system can offer a more cost-effective option. In order to optimize the system design and improve its availability, a diesel generator and battery bank could be connected to the system. During the time when the PV generator cannot meet the necessary power or during challenging weather conditions, the diesel generator can contribute the important difference to ensure a proper power supply and recharge the batteries at the same time. During low load demand, the PV system will recharge low batteries [19]. The advantages are:

1. Diesel generators are easy to operate and maintain even by unqualified operators
2. Availability of spare parts and consumables
3. Simple maintenance which does not need special qualification
4. Batteries technology has improved and achieved a crucial level of maturity
5. H Batteries with advanced technological capabilities becoming widely available to consumers.

The disadvantages are:

1. Batteries shall be well charged to achieve a good electricity release yield
2. Dangerous gases are released from batteries such as H2 and O2, especially in poorly ventilated locations
3. Diesel generators offer a poor yield proportionate to power required at approx. 40%
4. Batteries life is considered short compared with other system components.

3.2.2 PV/Battery/FC HPS

In this configuration fuel cells replaced the diesel generator and other components and configurations are unchanged. FC in this system will be used to recharge the batteries and compensate the power shortage whenever PV cannot meet power demand. PV/FC is a promising system and is expected to replace PV/Diesel HPS in the near future. FC has many advantages over diesel or petrol generator such as [1, 10]:

1. FC is environmentally friendly, with very low or even zero carbon emissions and very low noise level
2. High energy conversion efficiency of up to 50% compared with low diesel generator efficiency of about 8 to 15 % [1].
3. Lower operation and maintenance cost, due to minimal rotating parts
4. FC can operate at partial load whilst maintaining good efficiency, while diesel generator can only work on the rated load.

The high capital cost of FC is considered to be its main disadvantage. However, FC cost is expected to reduce in the future as FC is produced in mass production.

3.2.3 Wind/PV/Electrolyser/FC/H2 Storage System

Depending on the application and the available resources at any specific location, HPS can be either a simple or a very complicated system composed of multi power generators and storage devices. Connecting more components can improve HPS system availability and reliability to meet power demand. As an improvement to PV-Battery-FC HPS explained in section 2.2.2, a wind generator can be connected. Normally For critical application, the system will normally be designed for the worst weather case, which means that during good weather conditions generated power will be far greater than demand. Therefore, another form of energy storage other than batteries is needed. In this system a water electrolyser is used to store access energy into H2, which will be compressed and stored in a tank. The stored H2 can be used to power FC to back up PV and wind generators as needed.

H2 production and storage efficiency can reach up to 50% which, if considered carefully during HPS design, can help to optimize and reduce the size of the PV generator [9]. The main benefit of this configuration is that the system is environmentally friendly and the water can be recirculated in a closed loop without the need for refuelling or water top-up for a long time. Figure 3.1 shows a typical arrangement of PV-Wind-FC-Electrolyser-FC-H2 storage HPS.

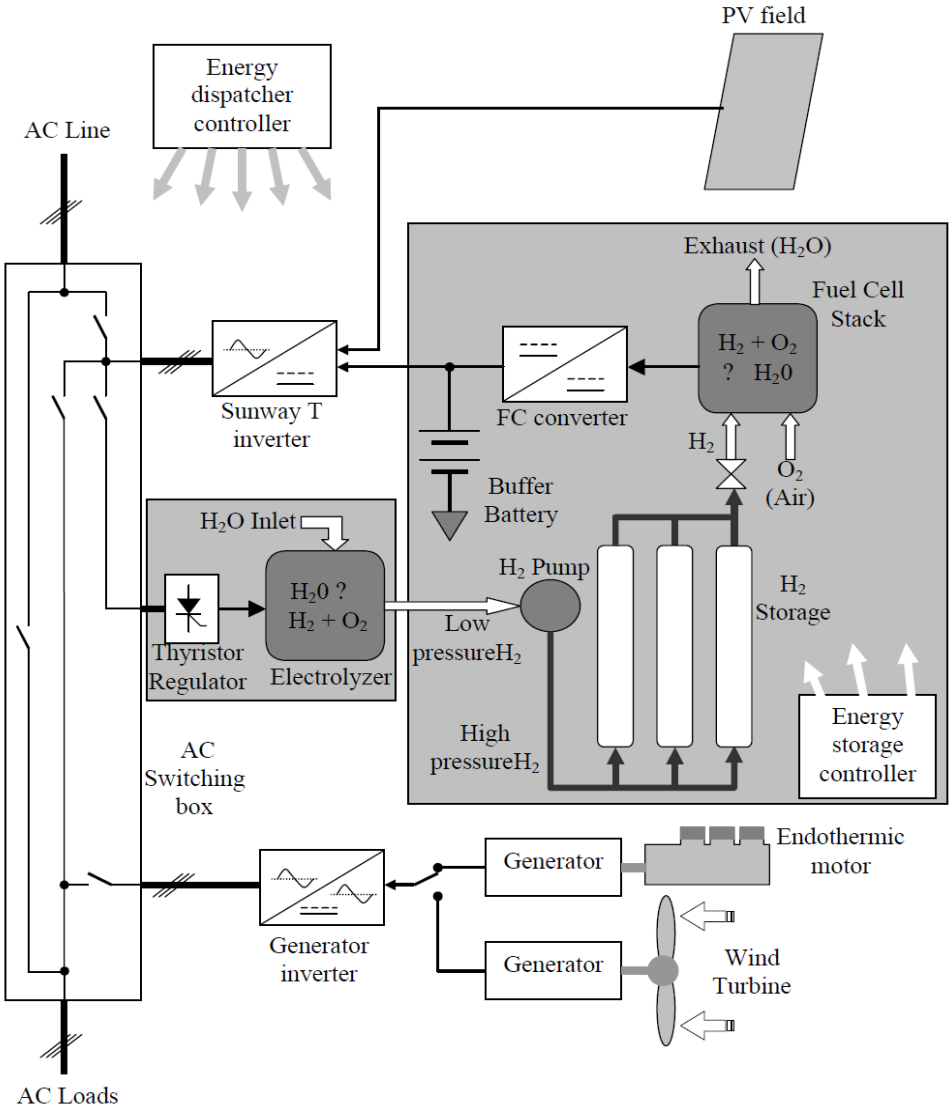

Figure 3.1 Hybrid Wind-Solar-Fuel-cell generator block schematic [9]

3.3 Hybrid Power System Connections

The most important step after defining the HPS components is how to connect them to achieve the best configurations. HPS components can be connected to each other in two typical configurations: DC coupled or AC coupled [27].

3.3.1 DC Coupled HPS

A DC coupled HPS is a system whose components (energy storage and energy generator devices) are all connected to a DC bus. All device output shall be converted into DC then connected to the main DC bus as per figure 3.2. The DC bus depending on the application will be then connected to a DC or an AC load via a DC/AC inverter. Each power generator is connected via a one-directional DC/DC converter to the DC bus while storage devices are connected via bi-directional

DC/DC converters to allow for battery charging and discharging or powering the electrolyser.

DC Coupled Advantages:

1 Simple and easy to implement [28]

2 Stable energy supply even during battery charging process.

DC coupled disadvantages [28]:

1. Low overall efficiency

2. Limited overall DC/AC inverter capacity is a bottleneck for future system expansion.

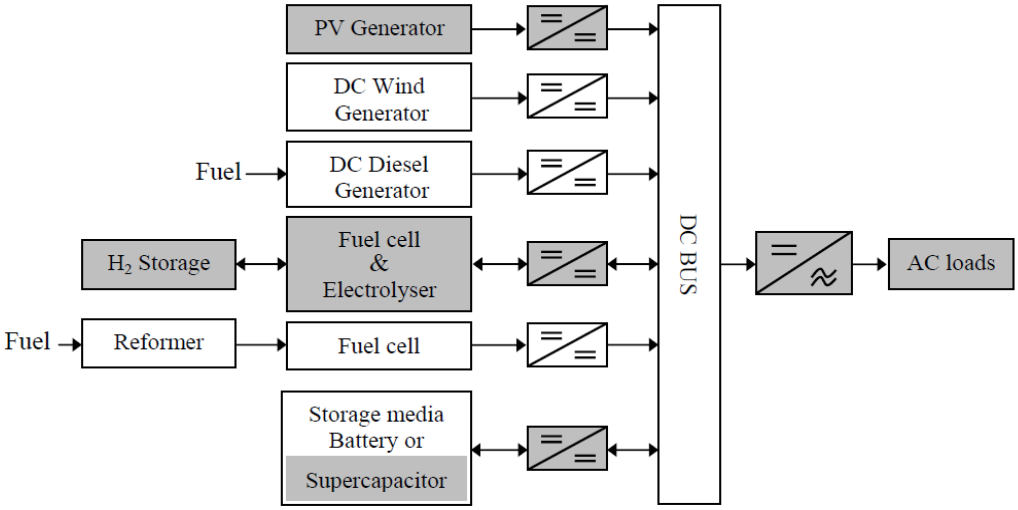

Figure 3.2 DC coupled HPS block diagram [27]

3.3.2 AC Coupled HPS

An AC coupled HPS is a system whose components (energy storage and energy generator devices) are all connected to an AC bus. Each device output is directly inverted to AC voltage via the DC/AC inverter and then connected to the AC bus as shown in figure 3.3. Because each inverter is designed and sized specifically to its generator, AC coupled HPS performance and efficiency is better than DC coupled HPS [27, 28]. In this configuration each generator can supply the load independently from the other generator. This will give the system more flexibility in meeting changeable load demand. For example when the required load is very low, only one generator will supply the power and other generator's power storage will remain in standby mode.

AC coupled HPS have the following advantages over the DC coupled configuration [19, 27, and 28]:

1 Higher overall system efficiency
2 Smaller power management unit (PMU)
3 Better overall system availability
4 If a diesel generator is used, its operation can be optimized. This will reduce the required operating time and therefore the maintenance cost
5 Easier to modify and expand to meet power demand growth.

The main disadvantage of the AC coupled is its complicated control system, which is required to maintain optimum synchronization between system components.

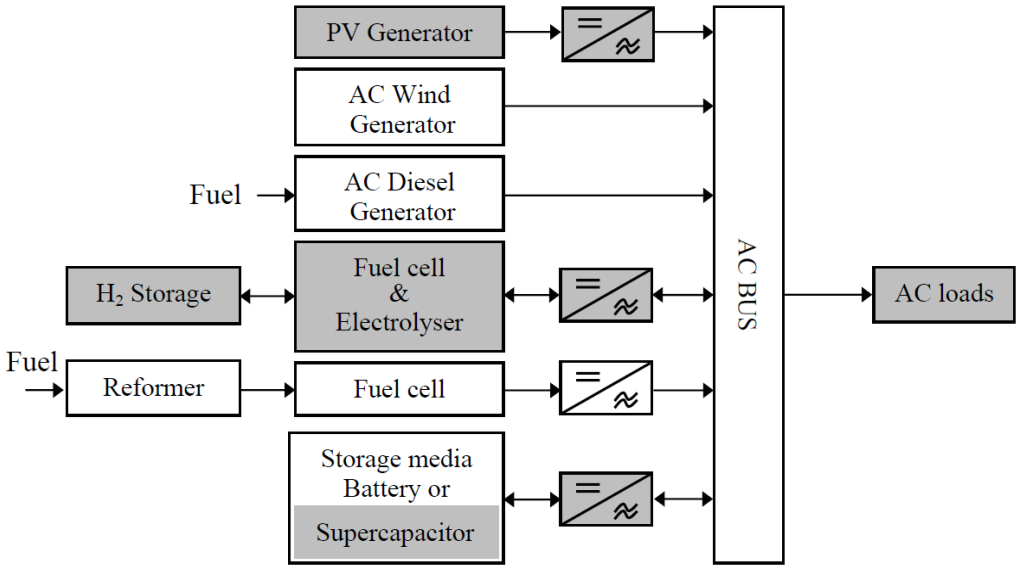

Figure 3.3 AC coupled HPS block diagram [27]

3.4 General Overview of Similar Projects

3.4.1 PV/ FC Integrated Power System for Remote Telecommunication Repeater

This project was developed by the Schatz Energy Research Centre to supply a back-up power system to a remote PV-power radio-telephone repeater. The power system has to meet the meet the National Park (in north-western California) requirement, which insists on having a system that can generate power and create no noise or air pollution. Therefore a PEMFC power system has been integrated into the hybrid power system. The fuel cell starts automatically to compensate the power shortage when the solar panel cannot keep the battery at the minimum charge level [29].

3.4.2 PV/FC/Electrolyser Water Pumping System

This project is based on about 150 watt water pump power by PV/FC HPS. The system is also equipped with an Electrolyser to utilize any access of solar power in generating hydrogen. In order to maximize the efficiency of the system design, the Maximum Power Point Tracking (MPPT) control technique was implemented [31].

In this project it was shown that, by using MPPT control strategy, the hybrid component units can always utilize the available local power to the best extent. This supports the main aim to maximize use of the available local sources of renewable energy, which is the main point of successful HPS design.

3.4.3 PV/Diesel Generator/Batteries HPS Project Tanzania

This project was design and implemented by CONERGY/ Schott Solar 2006, to power a village including households and community services in Tanzania. The HPS consisted of:

- 30kw solar generator
- 25kVA diesel generator
- 240kWh battery bank

The cost analysis of this system shows that renewable based HPS is more cost competitive than conventional energy generators. Figure 3.4 shows how for the long run the PV/Diesel generator/batteries HPS is more economical compared to a Diesel generator [31].

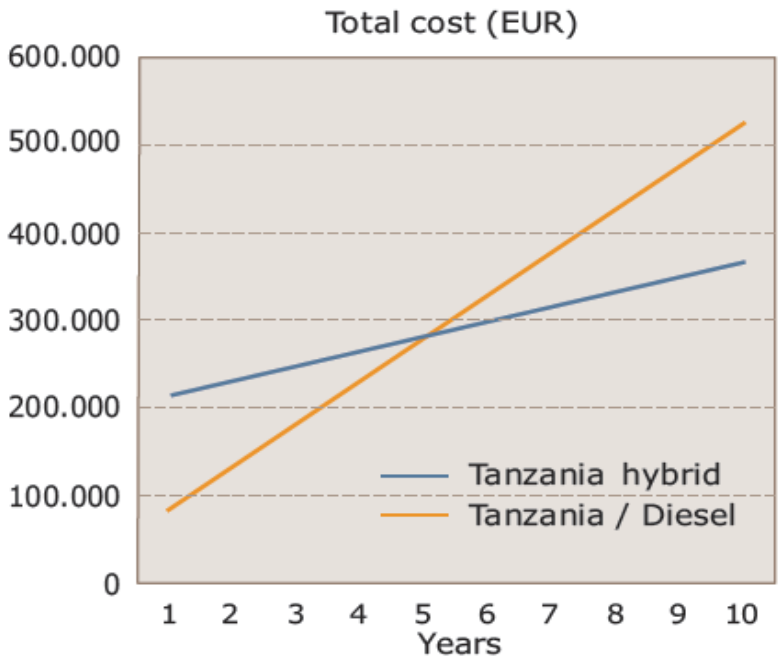

Figure 3.4 Economical comparison: diesel vs. hybrid systems (life cycle costs) [30]

3.5 The Propose HPS

The proposed HPS architectural is shown in figure 3.5. The solar panels are the prime power source, which are connected in parallel to the battery bank in order compensate for any power shortage from the solar panels. At night time or during bad weather conditions where Solar panel/batteries bank cannot meet the power demand, the Fuel Cell will be used to power the load and charge the batteries.

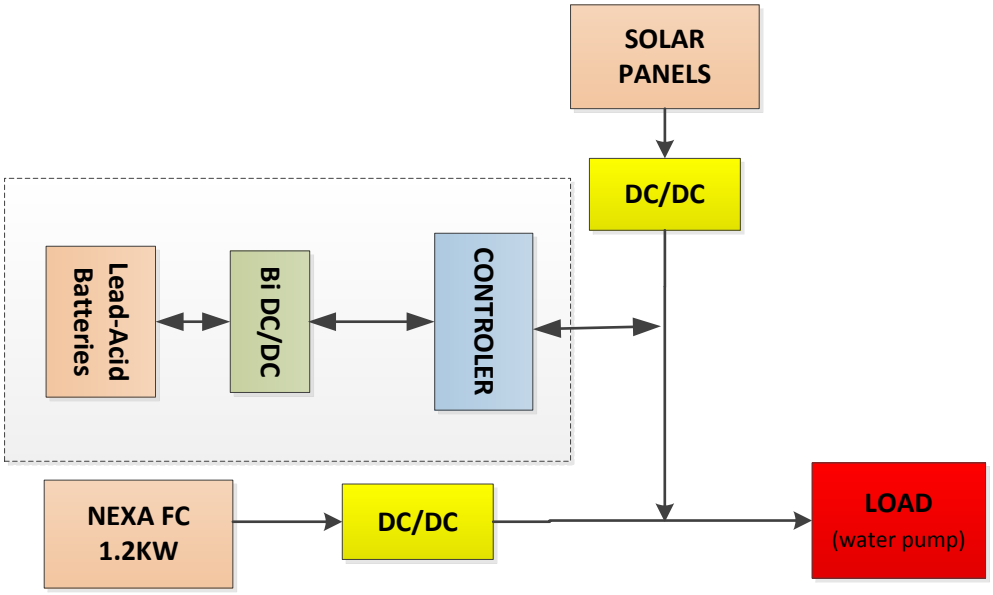

Figure 3.5 the hybrid system set-up schematic diagram

3.6 Chapter Summary

Due to fluctuations and interruptions in power generated from renewable sources such as wind, solar and hydro energy, the Hybrid Power System configuration was introduced by integrating more than one energy generation source in one system to work together to meet specific energy demand. This chapter presented the architecture of commonly used HPS such as PV/battery/Diesel HPS and the way they could be connected (i.e. DC or AC coupled). Following that two examples from experimental systems that were deployed to assess the technology and its readiness level were covered. Finally the PV/Battery/FC HPS architecture that will be used in this investigation was presented.

4 HPS COMPONENTS DESCRIPTION

Due to fluctuation and interruption in power generated from renewable sources like wind, solar and hydro energy, considering a form of energy storage to backup power fluctuation is very important. Therefore, short-term and/or long-term energy storage, such as batteries or super-capacitors and/or hydrogen storage tanks, must be used to achieve a reliable and safe operation and to maintain the required power supply during power fluctuation, failure or high power peak conditions. To achieve this, system components should be selected carefully and the control system must ensure that HPS components are well managed and monitored properly. This chapter will cover a brief description of the important hybrid system components used in this project and developed in the laboratory: (1) Hydrogen System, (2) Photovoltaic generator, (3) Batteries (or super-capacitor), (4) power management system.

4.1 Hydrogen System and Component

4.1.1 An Introduction to Hydrogen

Hydrogen (H_2) is one of the most commonly available gases on earth. Because H_2 is an unstable element, it cannot be found in its base form as pure hydrogen atoms. Alternatively, water (H_2O) is a very reliable source of hydrogen which covers about two-thirds of the earth's surface. To extract hydrogen from water energy, it is required to separate hydrogen from oxygen (O_2).

Hydrogen can be produced by breaking water components via electrolysis into Hydrogen and Oxygen as per the following chemical reaction:

$$H_2O \Rightarrow H_2 + \tfrac{1}{2} O_2 \qquad (4.1)$$

Because pure hydrogen is difficult to store and transport and water electrolysis is still costly compared with the other forms of hydrogen production process, producing Hydrogen by fuel reforming is a viable alternative option to overcoming Hydrogen storage and distribution challenges, especially for fuel cell powered vehicles [23].

There are many reforming techniques, such as partial oxidation (POX), auto thermal reforming (ATR), and steam reforming (SR), which can be used for Hydrogen production from widely used fuels such as diesel, Petrol and LPG, [23]. In the recent years, there has been a high global trend to produce hydrogen electrolytically from renewable electric sources of energy such as wind and solar energy. If considering the advanced technology of photobiological, and photoelectrochemical process, solar

energy alone can become the main driver of hydrogen production from water [24]. Table 4.1 summarises the hydrogen production technologies available.

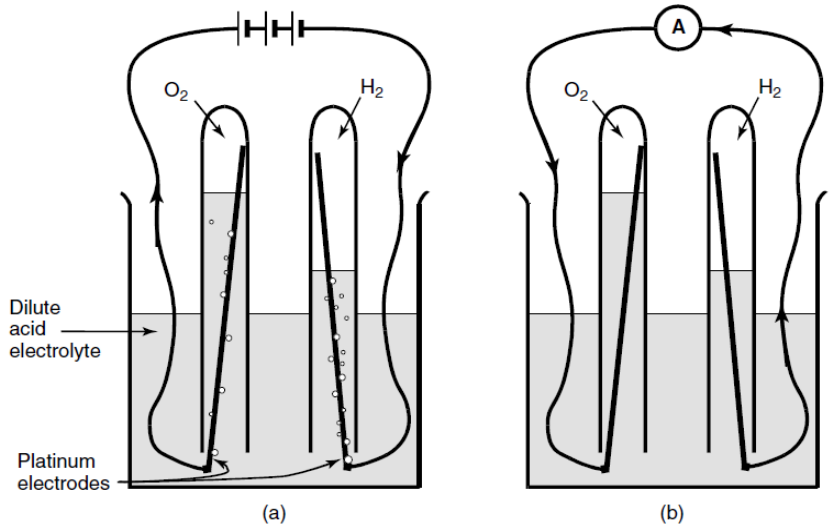

Figure 4.1 (a) water electrolysis. (b) current flows. The O_2 and H_2 are reacting to form water (The arrows show electron flow from – to +) [21]

Table 4.1 Hydrogen production technologies [26]

Hydrogen production technology	Benefits	Barriers
Electrolysis: splitting water using electricity	Commercially available with proven technology; Well-understood industrial process; modular; high purity hydrogen, convenient for producing H_2 from renewable electricity.	Competition with direct use of renewable electricity
Reforming (stationary and vehicle applications): splitting hydrocarbon fuel with heat and steam	Well-understood at large scale; widespread; low cost hydrogen from natural gas; opportunity to combine with large scale CO_2 sequestration (‘carbon storage’)	Small-scale units not commercial; hydrogen contains some impurities - gas cleaning may be required for some applications; CO_2 emissions; ; primary fuel may be used directly
Gasification: splitting heavy hydrocarbons and biomass into hydrogen and gases for reforming	Well-understood for heavy hydro-carbons at large scale; can be used for solid and liquid fuels; possible synergies with synthetic fuels from biomass- biomass gasification being demonstrated	Small units very rare; hydrogen usually requires extensive cleaning before use; biomass gasification still under research; biomass has land-use implications; competition with synthetic fuels from biomass
Thermochemical cycles using cheap high temperature heat from nuclear or concentrated solar energy	Potentially large scale production at low cost and without greenhouse gas emission for heavy industry or transportation; International collaboration on research,	Complex, not yet commercial, research and development needed over 10 years on the process: materials, chemistry technology; high temperature nuclear reactor, or solar

	development and deployment	thermal concentrators
Biological production: bacteria produce hydrogen directly in some conditions	Potentially large resource	Slow hydrogen production rates; large area needed; most appropriate organisms not yet found; still under research

4.1.2 What is a Fuel Cell

A fuel cell can be defined as a device which converts the chemical energy stored in hydrogen, or hydrogen-containing fuels, directly into electricity, plus potentially useful heat.

Typically, fuel cell main components are: a fuel electrode (positive anode), an oxidant electrode (negative cathode). An electrolyte (ion-conducting membrane) is sandwiched by the anode and cathode. In general, a fuel cell operates by feeding hydrogen to the anode side and oxygen to the cathode side. At the anode side a catalyst enhances Hydrogen atoms to separate into electrons and protons. Electrons travel through the external circuit to generate electricity while Protons move through the membrane (electrolyte). At the cathode side, both electron and proton meet with Oxygen to form water (H_2O) and release heat as shown in Figure 4.2.

As an example, the PEMFC has the following reactions:

$$\text{Anode:} \quad H_2\,(g) \rightarrow 2H^+ + 2e- \qquad (4.2)$$

$$\text{Cathode:} \quad 1/2O_2\,(g) + 2H^+ + 2e^- \rightarrow H_2O\,(l) \qquad (4.3)$$

$$\text{Overall:} \quad H_2\,(g) + 1/2O_2\,(g) \rightarrow H_2O\,(l) + \text{electric energy} + \text{heat} \qquad (4.4)$$

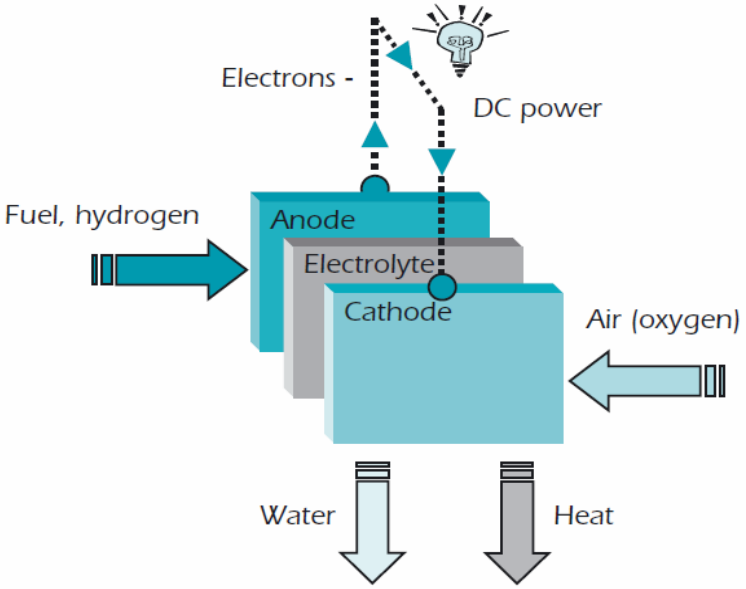

Figure 4.2 Fuel cell basic components [25]

Fuel cells and batteries share the same operating concept, as they both convert chemical energy into electricity through electrochemical reaction. The main

advantage of the fuel cell over the battery is that the fuel cell will continue to produce electricity as long as the fuel is being supplied. Compared with an internal combustion engine, the fuel cell has much higher efficiency due to the fact that the fuel cell has no rotating parts and converts fuel directly into electricity.

4.1.3 Fuel Cell History

The fuel cell was invented by an English scientist called William Grove in 1839 [22]. Since then, there had been no noticeable investigation or study until the 1960s, when extensive fuel cell research began at NASA. NASA did an extensive study and investigation to develop AFC) and (PEMFC) for a space programme (Gemini, Apollo, space lap) [22]. Table 4.2 shows a brief history of fuel cell development.

Table 4.2 Fuel cell history [22]

1800	W. Nicholson and Carlisle described the process of using electricity to break water.
1835	William Grove fuel cell demonstration.
1889	Separate teams: Mond and C. Langer/C Wright and C. Thompson/ L. Cailleteton and L. Colardeau performed various fuel cell experiments.
1896	W. Jacques constructed a carbon batter.
Early 1900's	E. Baur and students conducted experiments on high temperature devices.
1960s	T. Grubb and L. Niedrach invented PEMFC at GE
1990s – Present	Worldwide extensive fuel cell research on all fuel cell types.

4.2 Types of Fuel Cells

Fuel cells are normally classified based on their electrolyte material. It determines many factors such as the kind of chemical reaction, the type of catalysts required, operating temperature and fuel used to generate electricity. So each type of fuel cell is suitable for different applications. The following sections will describe briefly the main available fuel cell-types as listed below:

4.2.1 Proton Exchange Membrane Fuel Cell (PEMFC)

The PEMFC – which is also called Polymer Electrolyte Membrane Fuel Cells (PEMFC) – are working at low temperatures of about 60 to 80 ^{0}C. Due to PEMFC low operating temperature, rated power can be reached fast with a quick warming time. The PEMFC's high efficiency (of about 40 to 50%) and high power density are important advantages which make PEMFC a promising future competitor in

transportation and stationary application. In addition to the above, the PEMFC's light weight and small volume is another feature which is beneficial in automotive applications where weight is playing an important role. The PEMFC is made of two electrodes (positive- cathode and negative-anode), an electrolyte and a catalyst as per Figure 4.3. The anode conducts free electrons that are released from hydrogen molecules so they can be used in an external circuit, and has channels etched into it which disperse the hydrogen gas over the catalyst's surface. The cathode conducts the electrons to the catalyst and also has Oxygen distribution channels to distribute the oxygen to the catalyst's surface. The catalyst is normally made of cloth or carbon paper coated with a very thin platinum layer. It increases the reaction rate between oxygen and hydrogen without actually taking part in the reaction. Finally, the electrolyte is the proton exchange membrane; it is the ionic conducting medium between the cathode and anode [21, 24].

In the PEMFC process, hydrogen enters into the anode side and then makes contact with the platinum on the catalyst as per the reaction shown in equation (4.4). In this reaction Hydrogen is to dissociate into protons and electrons. The electrons are forced to travel through an external circuit (provide electric current) to do useful work before completing the reaction**,** while the protons are conducted through the membrane to the cathode side. Oxygen is forced through the catalyst on the cathode side and when the electrons reach there, they re-combine with the protons and oxygen to form water and heat as the reaction in equation (4.6) and shown in Figure 4.3.

$$H_2 \rightarrow 2H^+ + 2e^- \tag{4.5}$$

$$4H^+ + 4e^- + O_2 \rightarrow 2H_2O \tag{4.6}$$

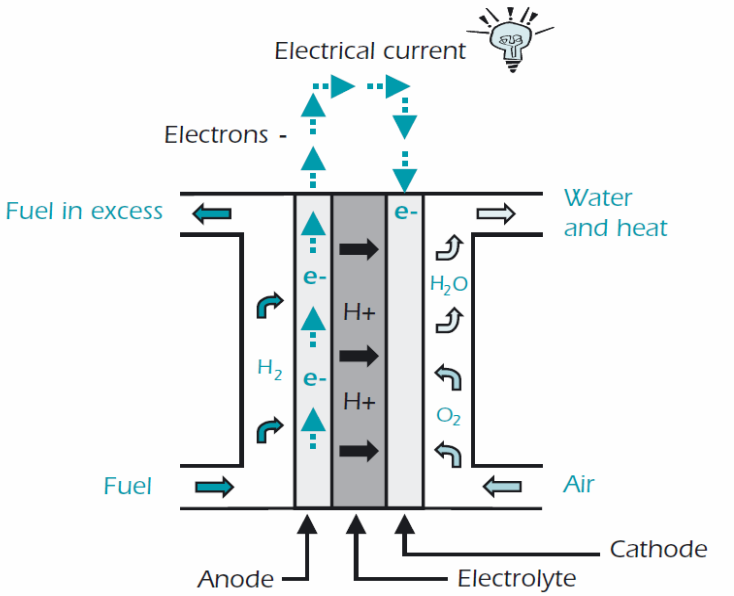

Figure 4.3 Proton exchange membrane fuel cell [25]

4.2.2 Solid-Oxide Fuel Cell (SOFC)

The electrolyte of SOFC is a solid electrolyte called non-porous ceramic compound [25]. SOFC can be fuelled by either Carbone Monoxide (CO) or hydrogen. Figure 4.4 shows reaction on both sides of the cathode and anode. SOFCs operate at a very high temperature of about 800-1000 ^{0}C with overall expected efficiencies of about 50 to 60. A Precious-metal catalyst can be removed when operating SOFC at about 1,000 ^{0}C which will reduce fuel cell cost. As another advantage of SOFC, it can operate with higher sulphur content fuel unlike other types of fuel cell. Due to the suitability of using SOFCs to generate electricity in medium and large scale, SOFCs can be used to power buildings and/or factories. Disadvantages of high temperature operation are the slow start-up, and durability and reliability problems. Frequent start up and shut down can lead to operation start-up problems [12].

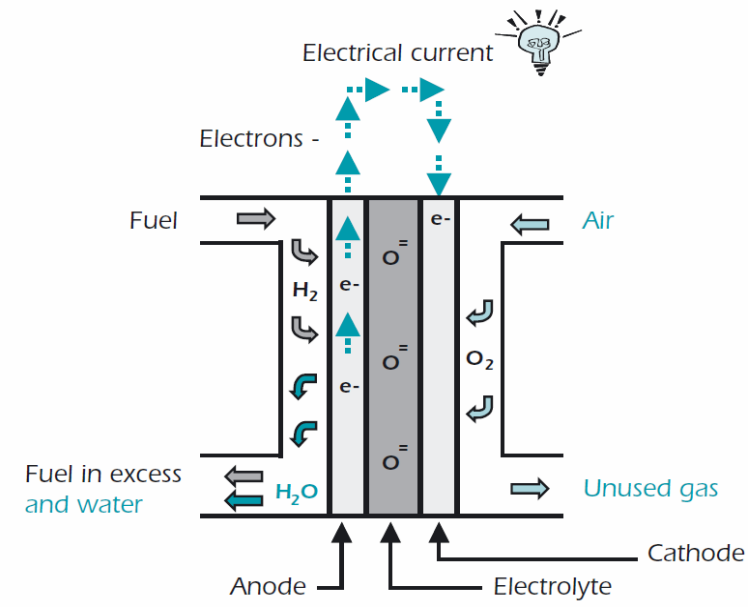

Figure 4.4 Solid Oxide Fuel Cell [25]

4.2.3 Alkaline Fuel Cell (AFC)

The AFC is an old technology, which first used by the NASA space programme to produce electricity and water on board spacecraft missions. In AFC types of fuel cells, the potassium hydroxide solution is always used as the electrolyte. They do not require a precious metal catalyst at the cathode and anode [21, 25]. The reaction at the anode is given by equation (4.7).

$$2H_2 + 4OH^- \rightarrow 4H_2O + 4e^- \tag{4.7}$$

In this reaction, released electrons pass through an external circuit to the cathode and react with oxygen and water to form new OH^- as in equation (7).

$$O_2 + 4e^- + 2H_2O \rightarrow 4OH^- \tag{4.8}$$

The most significant issue of the alkaline fuel cell is that it is very susceptible to contamination by carbon dioxide (CO_2). Therefore, it requires purification of both hydrogen and oxygen. This purification process makes alkaline fuel cells a very expensive technology and, therefore, an unlikely candidate to be commercialised on a large scale [10].

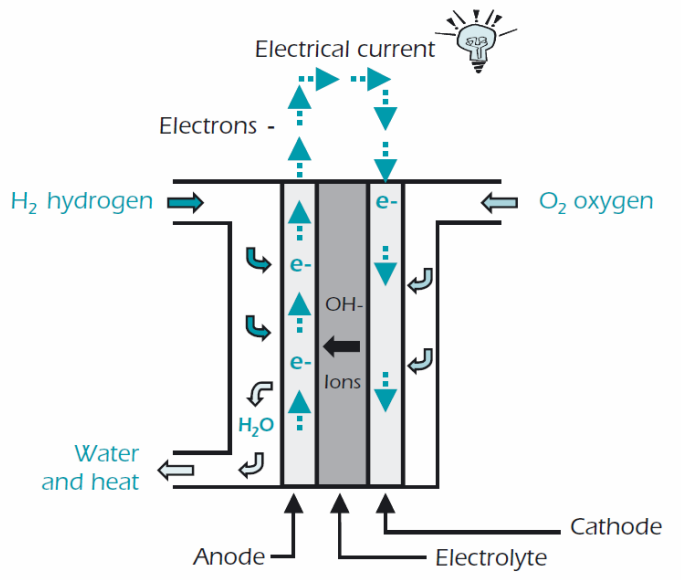

Figure 4.5 Alkaline Fuel Cell fuel cell [25]

4.2.4 Molten Carbonate Fuel Cell (MCFC)

The electrolyte of MCFC is a mixture of a molten carbonate salt mixture suspended in a porous, chemically inert ceramic lithium aluminium oxide ($LiAlO_2$) matrix [19]. The molten carbonate salt mixture is normally a mixture of either lithium and sodium carbonates or lithium and potassium. The operating temperature of MCFC is around (600-700◦c). The advantage of this high temperature operation is that no precious metal catalyst is required at electrodes, and high conductive ionic alkali carbonates are used to transfer electrons. Figure 4.6 shows the chemical reaction of both MCFCs cathode and anode, when fuelled by either hydrogen (H_2) or carbon monoxide (CO_2).

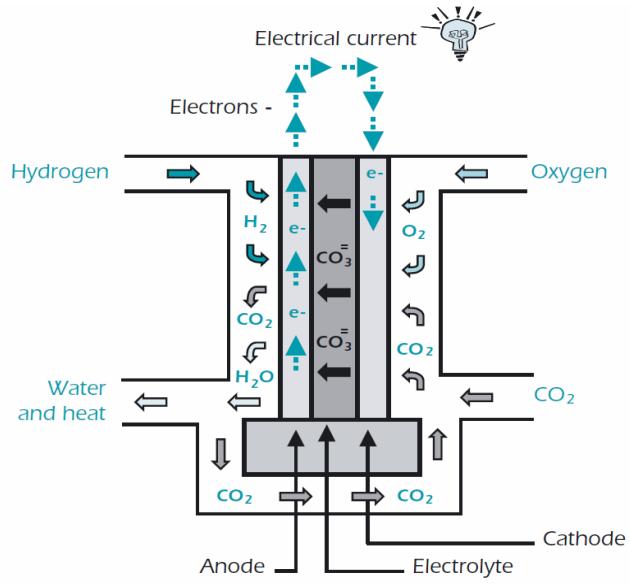

Figure 4.6 Molten Carbonate Fuel Cell [25]

As shown in Figure 4.6, it can be seen that MCFCs require oxygen and carbon dioxide to be delivered to the cathode. This, in turn, gets converted to carbonate ions, which provide the means of an ion transfer between the cathode and the anode. Subsequently, the carbonate ions are converted back at the anode. Disadvantages of MCFCs are mainly associated with durability. Component breakdown and corrosion are again an issue because of the high operating temperature and the corrosive electrolyte.

4.2.5 Phosphoric Acid Fuel Cell (PAFC)

The PAFC use an inorganic acid as electrolyte, which concentrates 100 % phosphoric acid (H_3PO_4). The acid works like a membrane in the PEM cells conducting protons. At low temperatures, the ionic conductivity of phosphoric acid is low; therefore PAFCs are operated at the upper end of the range 150-220^{0}C. They work in a similar way to the PEM fuel cell, as with the PEM FCs, platinum (Pt) or Pt alloys are used as the catalyst at both electrodes and the protons migrate through phosphoric acid electrolyte [19].

The PAFCs operate at an efficiency of around 37 to 42% of electricity generation, and operating efficiency can reach up to 85% in case of co-generation application. The waste heat can be used to heat water or generate. The other advantage of PAFCs is that CO_2 does not affect the electrolyte or cell performance and can be easy operated with reformed fossil fuels. Because of that PAFCs are more tolerant of impurities in reformate than PEM cells. Disadvantages of PAFCs are typically large and heavy, they are expensive because they require an expensive platinum catalyst like the PEM fuel cells. A summary of fuel cell types is shown in table 4.3.

Table 4.3 Fuel cell type summary [25, 32]

Fuel cell type	Electrolyte	Operating Temperature (°C)	Catalyst	Prime cell component	Electrical efficiency (%)
PEMFC	Ion Exchange Membranes	~ 80	Platinum	Carbon-based	40-50
AFC	Potassium hydroxide	65 -220	Platinum	Carbon-based	60
PAFC	Concentrated Phosphoric Acid	~205	Platinum	Graphite-based	37-42
MCFC	molten-carbonate-salt	~650	Nickel	Stainless-based	50-60
SOFC	ceramic	800 - 1000	Pervskites	Ceramic	60-70

4.3 Fuel Cell Applications

The unique feature of fuel cells is that the technology could potentially be used in applications with a broad range of power needs: stationary, transportation and portable power could all use fuel cell technology to provide power to their facilities…etc. In stationary applications, many fuel cell systems have been installed all over the world in hospitals, nursing homes, hotels, office buildings and schools. In transportation, all the major automotive manufactures have a fuel cell vehicle either in development or in testing at the present time and several have begun leasing and testing in larger quantities. Therefore, fuel cell electric vehicles can be a viable alternative to battery powered vehicles. As a portable power source, fuel cells can provide power as long as fuel is supplied, plus they are quiet and have zero emission [36]. Figure 4.7 provides a summary of fuel cell types, used fuel and range of applications.

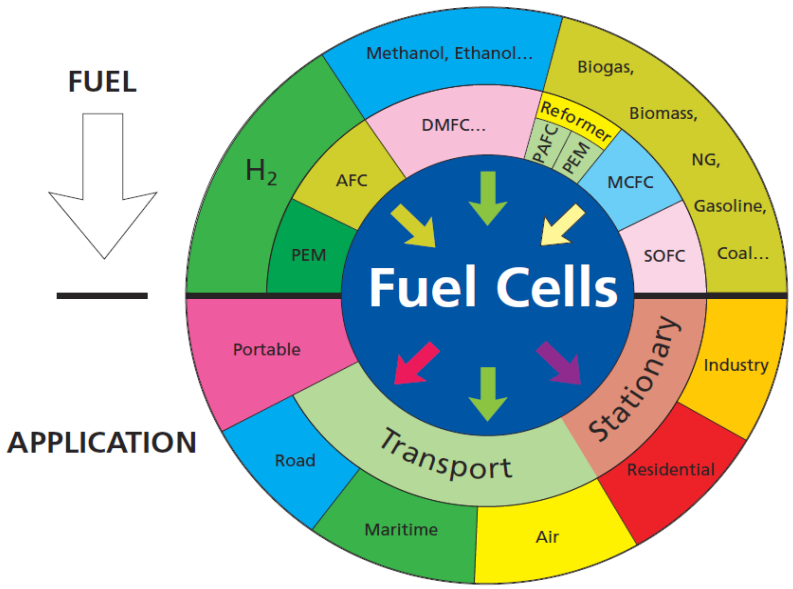

Figure 4.7 Fuel cell technologies, possible fuels and applications [26]

PEMFC was selected to be part of the HPS of this project, because PEMFC has many advantages over the other types such as low operating temperature and relatively good efficiency. Also it is compact and easy to operate and require minimum maintenance compared to other types of fuel cells.

4.4 Photovoltaic Cell (Solar Panel)

The term "photovoltaic" comes from the Greek word (phos) meaning "light", and "voltaic", meaning electrical, from the name of the Italian physicist Volta, after whom a unit of electrical potential, the volt, is named. The term "photovoltaic" has been in use since 1849 [45].

The photovoltaic (or photovoltaic cells) is a device that converts solar radiation directly into DC electrical energy. The only fuel photovoltaic needed to produce electricity is sunlight.

4.4.1 History

The French physicist Alexander Edmond Becquerel recognised the photovoltaic effect in 1839. However, the first solar cell was built in 1883 by Charles Fritts, who coated the semiconductor selenium with an extremely thin layer of gold to form the junctions. Charles' new device only achieves efficiency of about 1% [45].

Although extensive research started in 1950, commercial production did not begin until the 1970s after the oil crises [45]. Table 4.4 highlights photovoltaic historical development.

Table 4.4 Photovoltaic History [39, 40, 41, 46]

Year	Development
1839 - 1899	**Discovery of basic phenomena and properties of PV materials**
1839	Edmund Becquerel (19 years old French experimental physicist) discovered the photovoltaic effect while experimenting with an electrolytic cell made up of two metal electrodes.
1873	Willoughby Smith discovered the photoconductivity of selenium.
1883	Charles Fritts, an American inventor, describes the first solar cells made from selenium wafers
1888	"solar cell" first US patent for Edward Weston
1900 - 1949	**Theoretical explanation of the photovoltaic effect and first solar cells**
1905	Albert Einstein publishes paper on theory behind “photoelectric effect” along with paper on relativity theory
1916	Einstein’s theory on photoelectric effect was proofed by Robert Millikan
1922	Einstein wins Nobel prize for 1904 paper on photoelectric effect
1950 - 1969	**Intensive space research**
1951	A grown p-n junction enabled the production of a single-crystal cell of germanium.
1954	Bell Labs exhibits first high-power silicon PV cell. The New York Times forcasts that solar cells will eventually lead to a source of "limitless energy of the sun".
1955	Western Electric sells commercial licenses for silicon PV technologies
1963	Sharp Corporation produces a viable photovoltaic module of silicon solar cells. Japan installs a 242-watt PV array on a lighthouse, the world's largest array at that time.
1966	NASA launches Orbiting Astronomical Observatory with a 1-kilowatt PV array
1968	The OVI-13 satellite was launched with two CdS panels.
1970 - 1979	**Establishment of large photovoltaic companies**
1972	• Solar Power Corporation was established • The French install a Cadmium Sulphide (CdS) PV system in a village school in Niger to run an educational TV
1974	Japan formulated Project Sunshine. Tyco Labs grew the first EFG, 1-inch-wide ribbon by an endless-belt process.
1975	• Solec International and Solar Technology International were established. • The American government encouraged JPL Laboratories research in the field of photovoltaic systems for application on Earth
1976	Kyocera Corp begins production of Silicon ribbon crystal solar modules
1977	US Dept. of Energy establishes US Solar Energy Research Institute in Golden, CO
1980 - 1989	**Large standalone systems installations** Continued improvements in efficiency and cost enables PV to become a popular power source for consumer electronic devices, such as calculators, watches, radios, lanterns and other small battery charging applications
1981	A 90.4-kW PV system was dedicated at Lovington Square Shopping Center (New Mexico)

1982	• Worldwide PV production exceeded 9.3 MW • ARCO Solar's Hisperia, California, 1-MW PV plant went on line with modules on 108 dual-axis trackers.
1984	• 1 MW photovoltaic power plant began to operate in Sacramento, California • BP Solar Systems with EGS donations built a 30 kW photovoltaic system connected to public electric grid nearby Southampton
1989	BP Solar got a thin film technology patent for a solar cells production in 1989
1990 – 1999	**Large photovoltaic companies co-operation**
1990	Germany launches $500MM “100,000 Solar Roofs” program.
1991	The Solar Energy Research Institute was redesignated as the U.S. Department of Energy's National Renewable Energy Laboratory by President George Bush.
1993	The National Renewable Energy Laboratory's Solar Energy Research Facility (SERF), opened in Golden, Colorado.
1994	Japan begins "70,000 Solar Roofs" PV subsidy program
1998	California initiates $112MM “Emerging Renewable Program” to fund rebates for <30 kW residential and commercial PV systems
2000	**Renewable energy and the Stock exchange**
2002	NASA successfully conducts two tests of a solar-powered, remote controlled aircraft called Pathfinder Plus
2003	The world's largest photovoltaic plant was connected to the public grid in Hemau near Regensburg (Bavaria), Germany
2004	Five manufacturers — Sharp, Kyocera, Shell Solar, BP Solar and RWE SCHOTT Solar — account for 60 percent of the PV market.
2009	The level of announced capacities worldwide in 2009 was around 24 GW.
2011	Honda Soltec Co., Ltd. will this year release a new thin-film solar cell with improve compact design which is more flexible for roof installation. Honda is expecting the module conversion efficiency to exceed 13.0%, which can be ranked among the most efficient CIGS-based thin-film solar cells [46].

4.4.2 General Description of Photovoltaic

When sunlight hits a PV cell, the photons of the absorbed sunlight dislodge the electrons from the atoms of the cell. The free electrons are forced to move through the cell, creating and filling in holes in the cell. It is this movement of electrons and holes that generates electricity. The conversion process of sunlight into electricity is known as the photovoltaic effect. The electrons are accelerated to n-region (N-type material), and the holes are dragged into (p-type material) as shown in figure 4.8. The electrons from n-region flow through the external circuit and provide the electric power to the load [47].

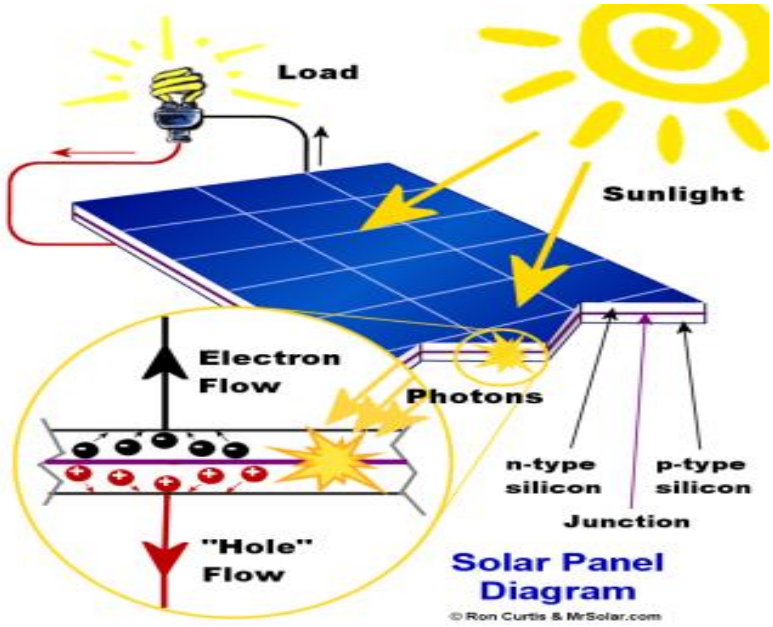

Figure 4.8 Solar Panel Diagram [47]

Figure 4.8 shows the basic component of a PV energy system. Because each cell is normally producing less than 2 W at about 0.5 V DC, it is important to connect PV cells in series-parallel configuration to produce the required power. Figure 4.9 shows how PV cells are connected together to form modules and how modules are connected to form arrays. There are no rules on the size of a module or an array. A module can be sized from a few watts to hundreds of watts. Power rating an array can vary from hundreds of watts megawatts [47, 48]. Figure 4.9 illustrates the configuration of PV cell, module and array.

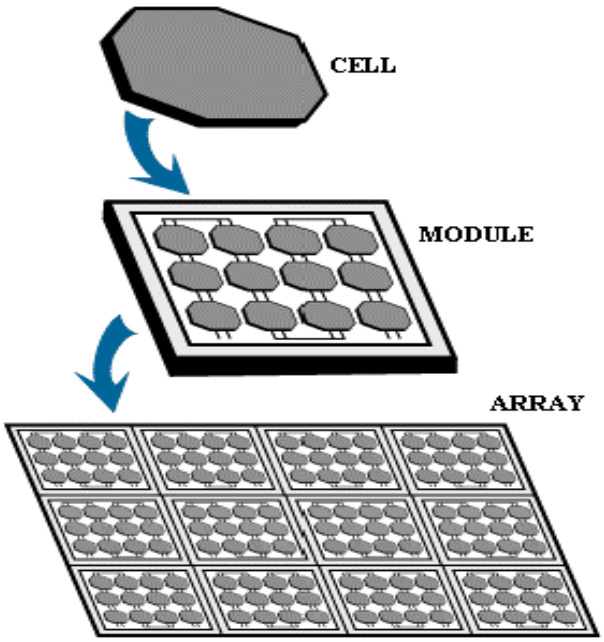

Figure 4.9 PV cell module and array [47]

4.4.3 Photovoltaic Types

PV can be calcified into two main categories based on technology used for manufacturing PV cells. Mainly, crystalline silicon which is the most commonly used technology for PV cells production; and thin film, which is new growing and demanding technology. Figures 4.10 and 4.11 summarize available PV cells technologies in the market.

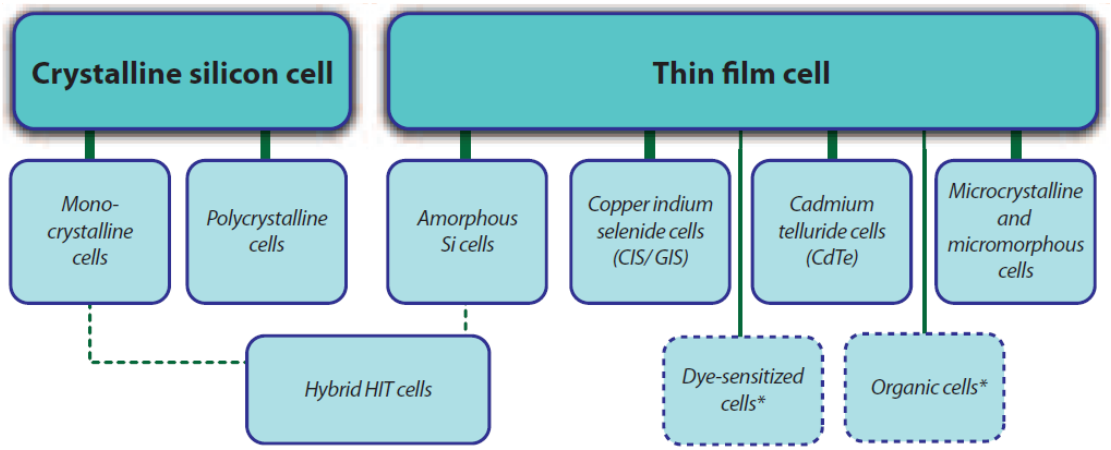

(* Research, experiment, ** Aerospace, concentrators)

Figure 4.10 PV cell types [45]

Crystalline Silicon

Ultra-pure silicon is used to produce crystalline cells, similar to the silicon used in semiconductor chips production. 150 to 200 microns silicon wafers are commonly used in manufacturing crystalline PV cells [45]. The wide availability of silicon on earth is the most important advantage of silicon cells.

Thin Film

Thin film is a flexible thin sheet of PV cells which is manufactured by deposing about 0.3 to 2 micrometres of semiconductor materials onto stainless steel or glass sheets. Because the semiconductor layers are very thin, the cost of material is much cheaper than the process and manufacturing equipment cost [45]. As shown in Table 4.2, the energy conversion efficiency is the most important difference between PV cells technologies.

Table 4.5 Comparison of solar cell efficiencies

Type	Standard Product %	Maximum Lab Efficiency %
Mono crystalline (sc-Si)	15 - 20	23.4
Multi crystalline (mc-Si) (Poly-crystalline)	13 - 16	17.3
20 shows the Amorphous silicon (a-Si)	6 - 8	8.3
Cadmiumtelluride (CdTe)	8 -10	10.9
Copper indium(gallium) 10-12% 12.2% 19.0% diselenide (CIS/CIGS)	10 - 10	12.2
Micromorph silicon (µm-Si)	9 - 11	12
Dye sensitized solar cell	4 - 8	8
Organic solar cell	2- 5	5

Figure 4.11 shows the commonly used types of PV cells available in the market. In recent years the share of thin film PVs have started to increase, due to the flexibility it gives for installation and easy handling [43].

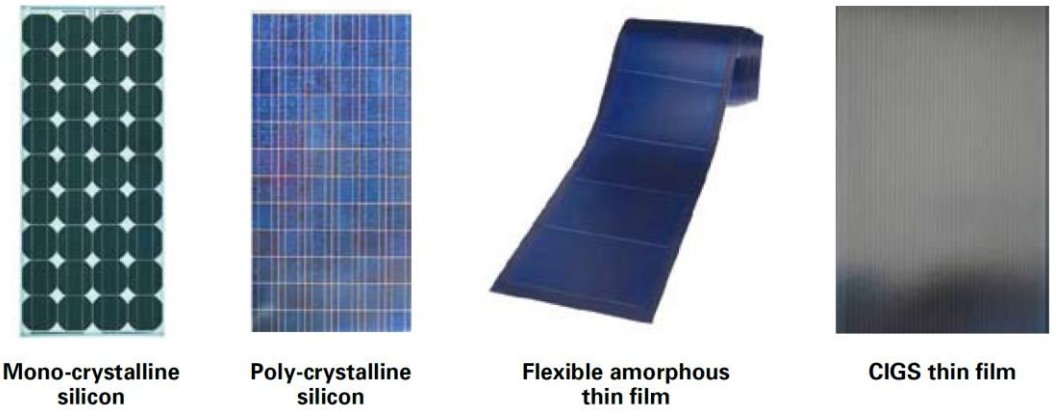

Figure 4.11 PV cell types [43]

Multi crystalline (mc-Si) Photovoltaic Solar panels are most widely used, since it has the optimum value for money, compared to other types available in the market. Multi crystalline is at affordable price while in the same time the standard product efficiency is varying between 13 to 16 %, therefore Multi crystalline solar panels were selected to be used in this project.

4.5 Chapter Summary

This chapter described Hybrid Power System components in detail. The chapter started by highlighting the importance of hydrogen, its production and storage. It then introduced Fuel Cells, with definition, how they work, followed by a general description of each type and their different common applications.

The chapter also introduced the Photovoltaic Cell (PV), by presenting PV development process history, how PV works and the different types of PV available in the market and relevant efficiency of each type.

5 EXPERIMENTAL SETUP

Throughout this chapter, the experimental configuration and the lab components set-up of the hybrid system will be presented. Figure 5.1 shows the main system components, which include two main sources of power (Nexa system and PV panels) connected in parallel.

This configuration was chosen because:

- Such system is designed for remote area, it is important to increase system reliability and to reduce the frequency of fuel transportation.
- Solar panel and batteries bank are connected in parallel to form the primary source of energy.

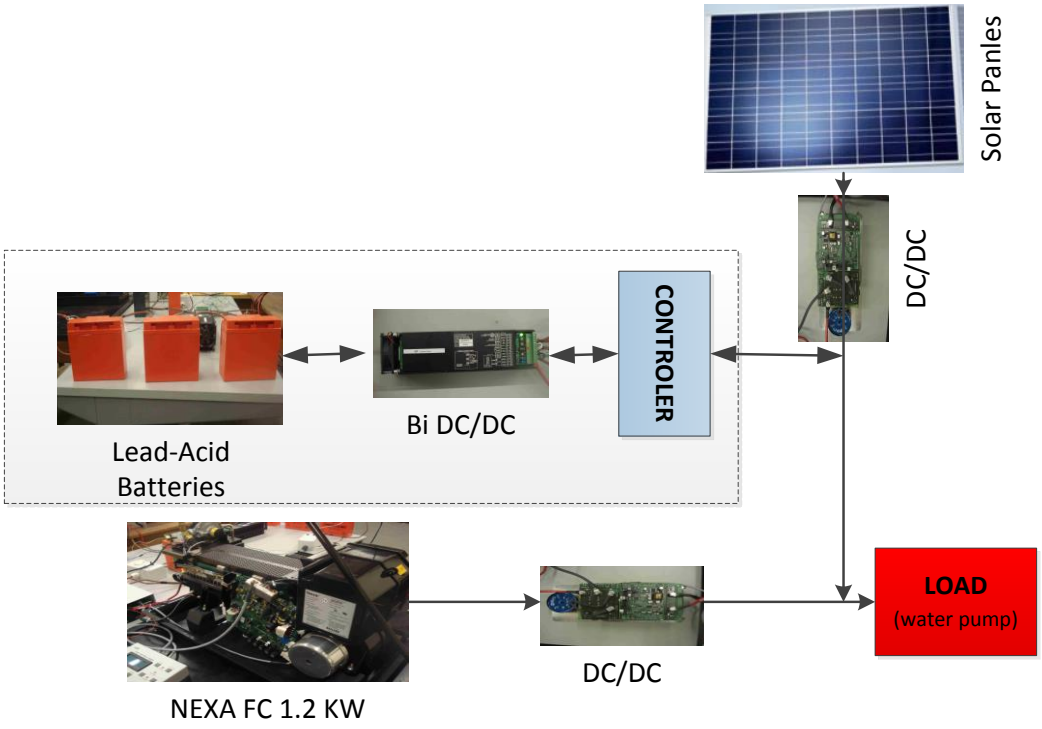

Figure 5.1 The HPS Experimental setup set-up schematic diagram

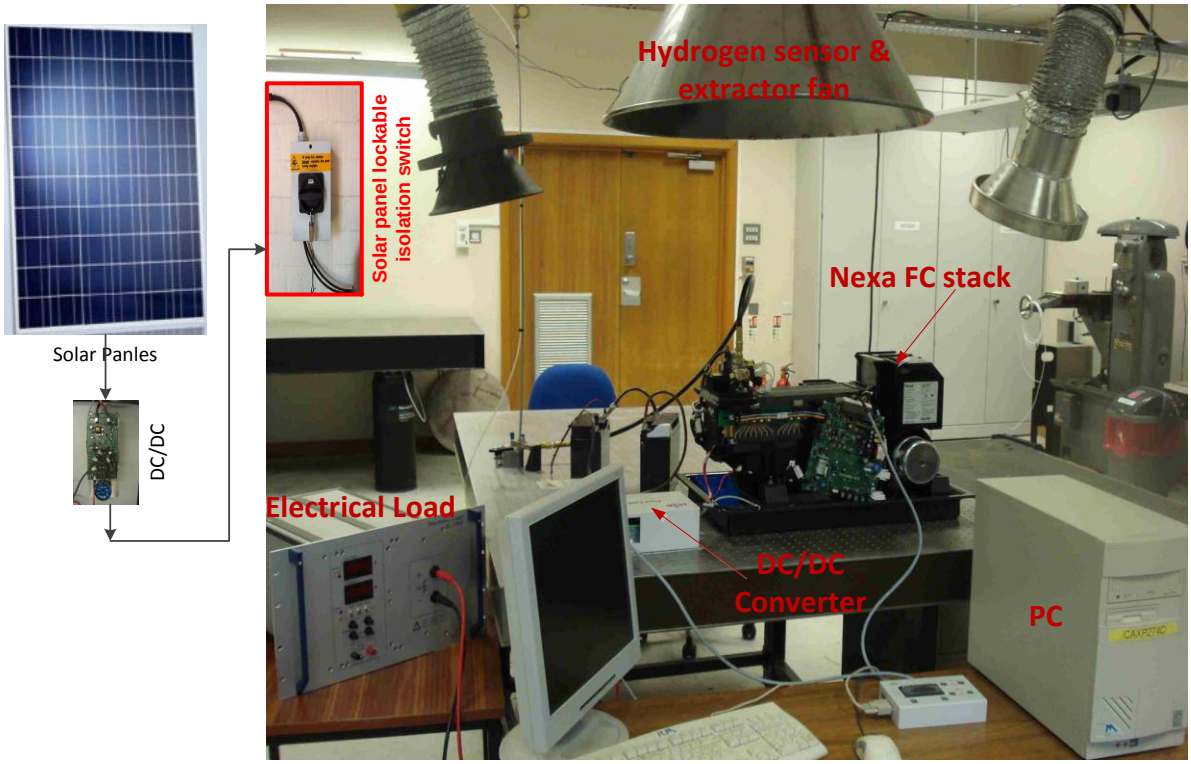

Figure 5.2 The HPS Experimental setup Cranfield

In this configuration, the batteries are connected in parallel via a bidirectional DC/DC converter, to allow stable operation and faster response to compensate the unstable PV unstable electric generation. This arrangement allows for a high degree of operation flexibility, which means the load can be powered by a single source of energy or combination of all three sources (Fuel cell, PV or/and batteries). The following sections will cover general safety instructions, the configuration of hybrid components including the Nexa 1.2 PEMFC system, Solar Panel and associated axillary components.

5.1 Safety Requirement

It is very crucial before starting the laboratory to ensure that our work is safe to personnel, equipment and building, especially when dealing with Hydrogen. The following precautions have been taken:

- Test facility located away from any occupied building
- Hydrogen cylinder has been installed outside the laboratory and equipped with isolation valve
- Test facility has been equipped with extraction fan and gas leak sensor connected to alarm system.

- All electric sources are equipped with isolation switches and because solar panels will produce electric any time where there is sun, its isolation switch was equipped with lockable isolation switch.
- Any person using the laboratory shall use Personal Protective Equipment (PPE)

5.1.1 Why Should Hydrogen be Handled with Special Care?

Although hydrogen is not a toxic gas, special care should be taken when handling it because [54]:

- Hydrogen is colourless, odourless and tasteless and its leakage is hard to detect
- Hydrogen is flammable over a wide range of concentrations
- The ignition energy for hydrogen is very low
- Hydrogen burns with a nearly invisible bluish flame, unless it is contaminated with impurities, in which case a pale-yellow flame is easily visible in the dark
- The temperature of burning hydrogen in air is a high 2,044 C, as compared with 1,246 F for gasoline), and warm hydrogen gas rises rapidly because of its buoyancy
- It is the lightest of all gases, with a specific gravity of 0.0695
- A single volume of liquid hydrogen expands to about 850 volumes of gas at standard temperature and pressure when vaporized. At 2 133.6 metres elevation, this expansion rate is increased to approximately 1,000 volumes of gas at standard temperature.

5.2 **Photovoltaic (PV) Panels**

Two Schott poly 230 Photovoltaic solar panels were installed on the roof of the laboratory building facing south with a 30 degree incline to maximize utilizing sun light. Each panel can deliver a maximum of 230 watts. The panels are connected to each other in a series to deliver maximum overall nominal power of about 460 watts. Because solar panels will generate electricity as long as the sun is shining on the PV cells, it is very important to avoid any electrical risk by ensuring that the electrics are isolated. To achieve, the PV solar panels are equipped with a lockable switch which is kept locked off whenever the solar is in use, as shown in figure 5.5. The PV panels

are connected to the hybrid system via a DC/DC convertor, as illustrated in the architecture diagram shown in figure 5.1.

Figure 5.3 Solar panel lockable isolation switch

5.3 **Nexa 1.2 PEMFC module Set-up**

The BALLARD 1.2 kW Nexa fuel cell power module has been installed in the laboratory, in order to obtain experimental data. This data has been used to validate the developed mathematical model shown in Chapter 6. The system contains a pre-assembled fuel cell stack integrated with the auxiliary equipment required to operate the system safely. Figure 5.3 shows the assembled Nexa fuel cells in the laboratory together with all auxiliary and control systems [33].

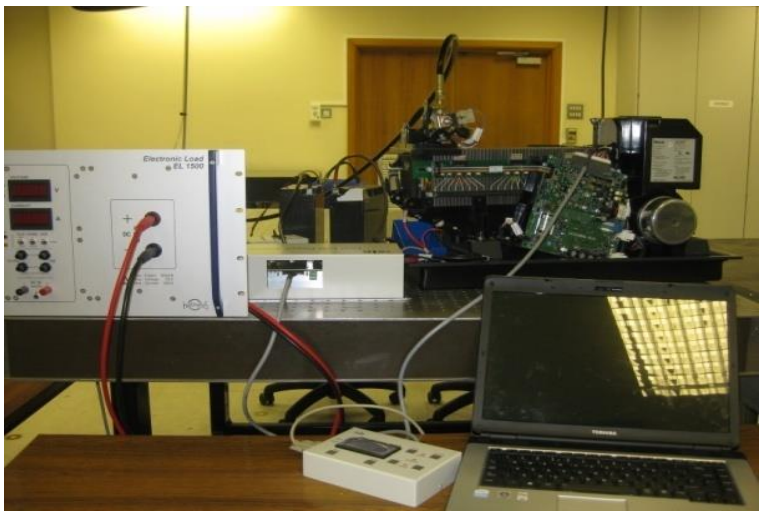

Figure 5.4 Fuel cell assemblies in the laboratory.

The system is supplied as an integrated package which includes all auxiliary components such as the control system, hydrogen delivery, cooling air fan and oxidant air fan. The system is also equipped with accurate sensors to be used for system operation control and to provide performance data, which can be stored automatically for later analysis. [33].

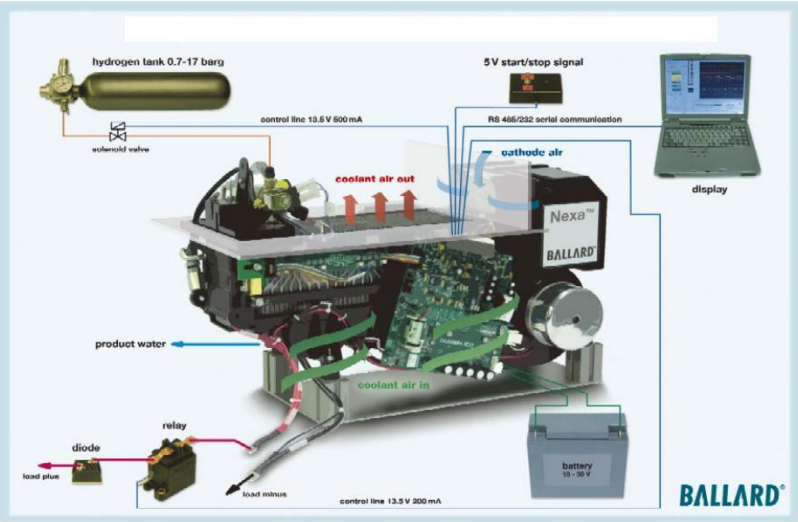

Figure 5.5 Installation of Nexa FC system

An illustration for the Nexa system configuration at the laboratory is show in figure 6.4. This figure also shows the hydrogen storage cylinder and the auxiliary start-up battery, which needs to be connected during start up and shutdown. The package is equipped with a serial communication port to allow computer interface data recording.

The Nexa 1.2 technical specifications are listed in Table 5.1.

5.3.1 Nexa Safety Features

The Nexa system is automatically controlled and protected and equipped with alarm and interlock systems to protect equipment from damage and to ensure operator safety. The Nexa system is equipped with the following protection and monitoring mechanisms at all times:

- Oxygen monitoring sensor to measure ambient oxygen concentration and shut down Nexa system automatically when oxygen concentration falls below the low level
- Nexa system is equipped with hydrogen leak detection installed at fuel inlet assembly to shut down the system when a hydrogen leak is detected
- Each individual cell output voltage is continuously monitored and, whenever cell failure is detected, the Nexa system will shut down
- Fuel cell main operating parameters (like stack current, operating temperature, output voltage and fuel inlet pressure) are continuously monitored to ensure they are within the allowable operating limits, warning alarm and system shut down whenever any of the operating parameters have been exceeded.

Table 5.1 Nexa1.2 power module specification [33]

Output	Requirement	Quantity
Power	Rated power	1200 W
	Voltage	26V (at rated power)
		22V to 50V (operating voltage range)
	Start-up time	2 minutes
Emissions	Noise	72 dBA
	Water	870 ml/hr
Physical	Dimensions (L*W*H)	56*25*33cm
	Mass	13 Kg
Lifetime	Operating life	1500 hours
	Cyclic life	500
	Shelf life	2 years
Input	**Requirement**	**Quantity**
Fuel	Purity	99.99% H_2 (vol)
	Pressure	70-1720 kPa(g)
	Acceptable impurities	0.01% (vol) (total inert fluids)
		2 ppm (vol) (CO and CO_2 combined)
		1 ppm (vol) (total hydrocarbon)
		500 ppm (vol) (oxygen)
	Consumption	<18.5 SLPM (fuel consumption at rated power)
Power conditioning	Current ripple (Maximum acceptable current ripple at 120 Hz, with respect to average DC net output current)	24.7% RMS 35% peak-peak
DC power supply	Voltage	18V to 30V (allowable range of input voltage)
	Power	60 W (drawing power during start-up)
Operating environment	Location	Indoors & outdoors (acceptable locations for use)
	Temperature range	3 ^{0}C – 40 ^{0}C (Range of acceptable ambient, cooling air and oxidant air temperatures)
	Relative Humidity	0% - 95% (non-condensing)

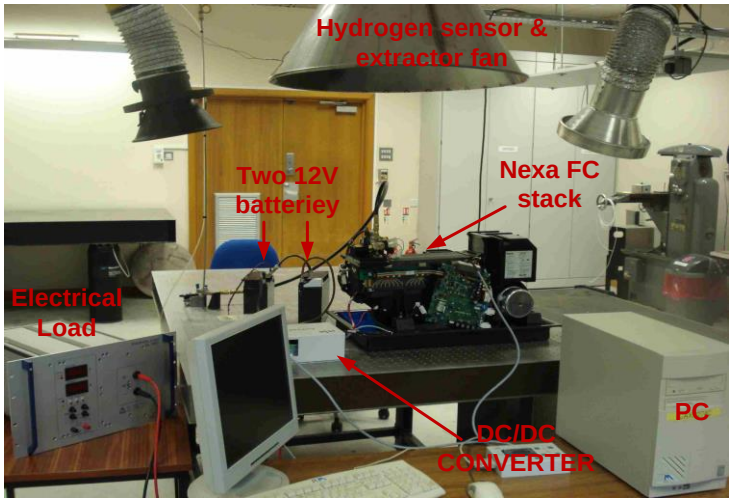

Figure 5.6 Experimental setup at Cranfield University

5.4 **DC/DC One Directional Converter**

The BSZ PG 1200 one directional DC/DC converter is customized to work with NEXA PEMFC by Isle ® as shown in figure 5.5. The BSZ PG 1200 converted comes equipped with a communication port to communicate with the Nexa PEMFC control system, which improves control system responses and converter efficiency.

An important feature of this converter is that its output voltage is filtered and is equipped with a current back flow protection to protect the fuel cell. The converter operation is a controlled built-in micro controller. Table 5.2 lists the converter specification summary.

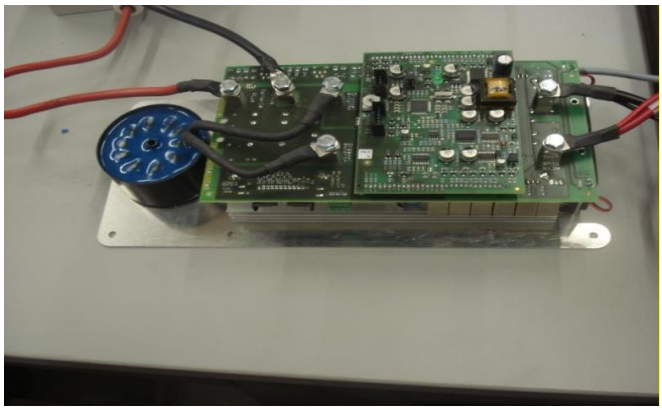

Figure 5.7 One directional DC/DC BSZ PG 1200 converter

Table 5.2 One directional DC/DC BSZ PG 1200 converter

Description	**Unit**	**Value**
Output voltage range	Voltage (V)	11-15 / 22-30
Accuracy of output voltage	%	2%
Nominal output current	Amber (A)	100/50
Maximum output current	Amber (A)	110/55
Maximum output power	Watt (W)	1200
Maximum output current ripple	%	2
Operating input voltage range	Voltage VDC	26-48
Maximum input voltage	Voltage (VDC)	50
Minimum voltage drop input to output	Voltage (VDC)	2
Power consumption standby	Watt (W)	2
Ambient temperature	Degree (°C)	0°C…40°C
Efficiency	%	96% (24V)
Short-circuit proof		Yes
Thermal protection	Degree (°C)	Internal 80°C
Mechanical dimensions (HxBxT)	mm	(320 x 14 x 80) mm

5.5 **DC/DC bidirectional converter**

Zahn Electronics bidirectional high performance step down converter (model no. DC6350F-S) was used to connect the battery to the HPS, which allowed battery charging and discharging as shown in figure 5.6. This converter consists of two quadrants (sourcing and sinking current), crystal controlled, dual Half H Bridge, configured in a buck topology programmed for Voltage Loop (VLP). With a high switching frequency of about 31,250 Hz, a fast response can be achieved.

Another feature, Zahn convert, is a compact design, integrated package, with an input power fitter, power supply and regeneration circuit. The unit Power supply is from a DC power source in this project either from battery, solar panel or fuel cell.

In order to protect the converter, the unit temperature is controlled. To keep the transistor temperature within the safe range, the current to the load is automatically reduced to protect the unit. [48].

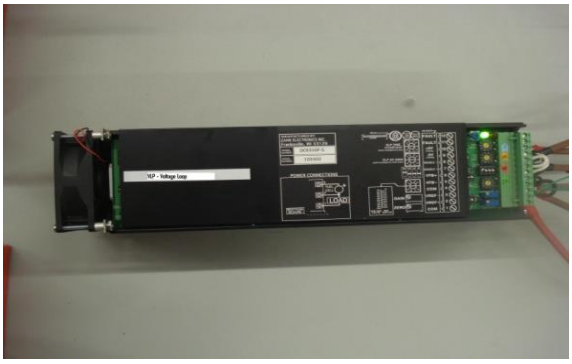

Figure 5.8 Bidirectional DC6350F-S converter

5.6 **Electrical load (water pump)**

For this study a 373 watt fixed speed DC motor water pump was selected as shown in table 5.3. Because all the parameters of the system (the water depth in the well, the tank height and piping length) are constant, the pump power and flow are also constant and will be presented by constant electrical load.

Table 5.3 Water pump specification

Water pump	Unit	Value
Type		Shallow well jet Pump.
Quantity		1
Power Max.	Watt (W)	373
Flow rate Max.	litre/hour (l/hr)	2,274
Suction left Max	Meter (m)	7.6
Discharge pressure Max.	Psig	58
Suction pipe size	Inch	1
Discharge pipe size	Inch	1

5.7 **Control Logic**

This section presents HPS control logic, bases and assumption in order to maximize the operational efficiency of the system.

The control logic will define all the power management of the HPS and will describe the interaction between the HPS components. Solar power is defined as the primary power source and backed-up by the batteries, which are the secondary power system. The FC is defined as the secondary power system.

The main power supply will be normally by solar power and any access power to the power demand will be stored in the battery bank. If solar power fails to meet the load demand, the power will be supplied from the battery bank. For that purpose a battery

charge controller is used to manage energy flow from/into the battery bank and the HPS. There are three main operating conditions:

1. Normal operation condition, if $P_{PV} > P_{Load}$ then $P_{BC} = P_{PV} - P_{Load}$. It means that the power from the PV generator is high enough to power the load, and the excess power is used to charge the battery bank.
2. The second scenario is the $P_{PV} < P_{Load}$ then $P_{BD} = P_{Load} - P_{PV}$. It means that the power produced by PV is not enough to power the load, therefore this power needs to be backed-up by the battery.
3. The third scenario, the $P_{PV} = 0$ and $P_{BD} > P_{Load}$. It means that no power is produced by the PV and then the battery is the main power supply, if the battery charge is equal or greater than 70%.
4. The fourth scenario, the $P_{PV} = 0$ and $P_{BD} = 0$ then, $P_{FC} = P_{Load} + P_{BC}$. It means no power is produced by PV or the battery. Then the main power supply is by fuel cell and power will be supplied by PLoad.

It is important to ensure the battery is protected against excessive charge, therefore the PV panel or FC are disconnected by the battery charge controller once the battery reaches its maximum charge. In case the FC is in operation, a signal will be sent to reduce FC power ($P_{FC)}$ to match the required load or switch it to the standby condition.

Table 5.4 Principal control parameters of PV-FC

Parameters	Unit	Description
P_{PV}	Watt (W)	PV generator output power
P_{BC}	Watt (W)	Battery charging power
P_{BD}	Watt (W)	Battery discharging (output) power
P_{Load}	Watt (W)	Load power demand
P_{FC}	Watt (W)	Fuel Cell output power

5.8 PI Controller

The proposed HPS system is normally installed in remote areas, therefore it is very important to keep it simple and easy to handle. There is no need to have a very sophisticated control system with a very fast response. As explained in section 5.7, the system is based on start and stop. Once the water level in the tank reaches the minimum level the pump will start pumping water. The primary power will be provided by the Solar panel which will be backed up by the batteries which are connected in parallel. In this case there is no controller required, since the power will be supplied by the solar panel and any power shortage, due to any fluctuation in solar energy, will

be compensated by the batteries. When the solar power and battery cannot provide the power the system will stop and then, after at least 3 seconds, the FC will start to power either/or both the water pump and the the batteries. In order to control this process a simple PI controller was developed as shown in figure 5.7.

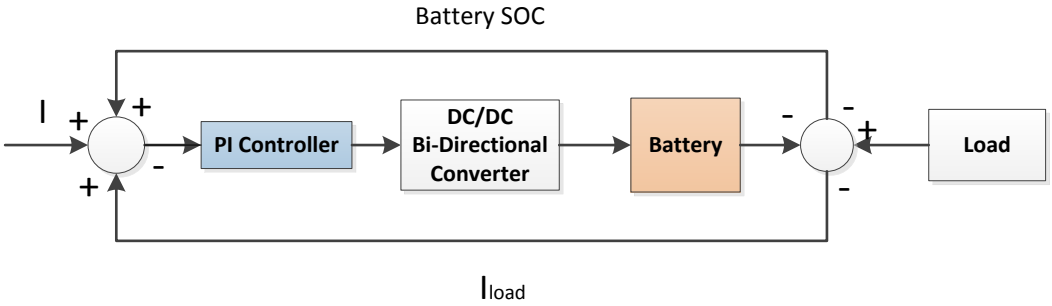

Figure 5.9 PI controller schematic diagram

5.9 **Chapter summary**

This chapter began by introducing the hybrid power system set-up schematic diagram. It then explained the safety considerations and requirements for working in the laboratory, with especial precautions needed when handling hydrogen. A description of the system components used in the experimental set-up was then given, with a summary of each component specifications and functions including Schott ply 230 photovoltaic solar panels, BALLARD Nexa PEMFC, One directional and bidirectional DC/DC converter. Finally, the control strategy was explained.

6 HPS SIMULATION MODELS

The model is a computer simulation based on a mathematical model which describes the characteristics and behaviour of the actual system. There are many computer programmes that can be used to perform a simulation model. One of the most widely used programs in simulation is Matlab/Simulink.

Regardless of the tools or computer programs which are used to perform the simulation, it is important to define the following for any system before developing the mathematical model:

- Define the system boundary
- Simplify the system by dividing it into smaller sub-components. For each sub-component the following need to be defined:
  - Model inputs data
  - Model output data

It is very important to link all system components via a process flow diagram, which describes the relation between each individual component and how they are connected to each other. The mathematical relation between model input and output data is then derived for all the system components. Once the model is established, the next step is to validate it by comparing simulation model results with experimental results.

This chapter will describe in detail the mathematical models of each system component as shown in the schematic diagram figure 6.1.

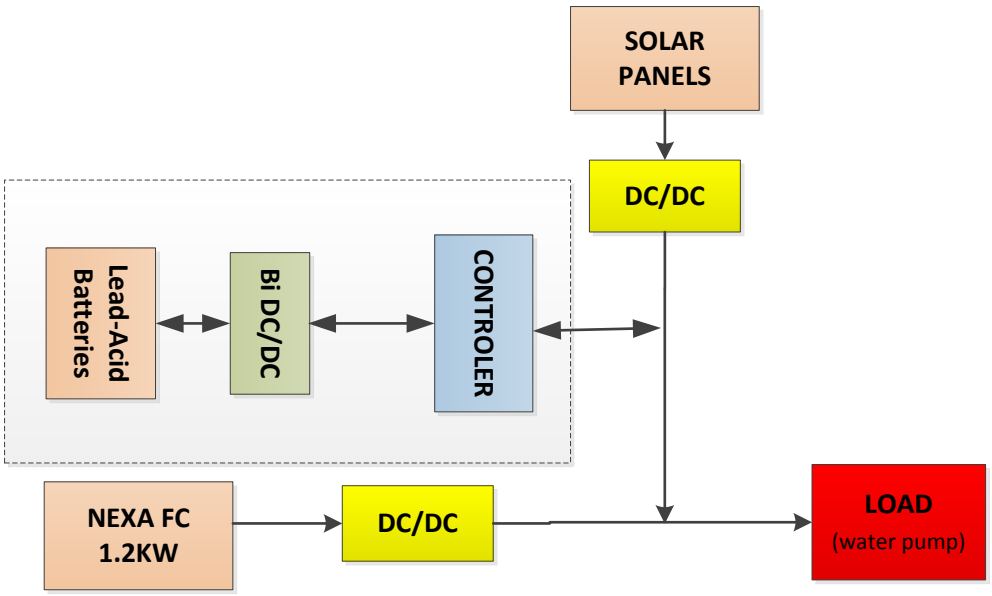

Figure 6.1 Hybrid System Schematic Diagram

6.1 Fuel Cell Modelling

In order to understand the system behaviour and optimize performance of the system, a simulation model of the complete system was developed in Matlab/Simulink. The first step was to build an “accurate” mathematical model of FC. This would be then followed by modelling the PV, batteries and load. The assumptions used in the FC model are listed below [22]:

- One-dimensional treatment
- Assume all gases are ideal and uniformly distributed.
- Laminar flow
- Constant pressure in the fuel cell gas flow channels
- Incompressible flow
- Isotropic and homogeneous electrolyte, electrode and bipolar material structures.
- A negligible ohmic potential drop in components
- Mass and energy transport is modelled from a macroperspective using volume average conservation equation.

6.1.1 Fuel Cell Stack Modelling

Several models were investigated; some based on thermodynamic modelling, others on electrochemical modelling or on semi-empirical modeling. El-Sharkh, et al. [35] introduced a dynamic model for a stand-alone PEMFC power plant for residential applications. With some modifications this model can be used to simulate PEMFC of a 1.2kW as follows:

PEMFC model

The relationship of gas flow and its partial pressure through a valve can be written as: [23]

$$k_{H2} = \frac{qH_2}{PH_2} \tag{6.1}$$

and

$$k_{H2O} = \frac{qH_{2O}}{PH_{2O}} \tag{6.2}$$

and

$$k_{O2} = \frac{qO_2}{PO_2} \tag{6.3}$$

Where

k_{H2}	Hydrogen valve molar constant [kmol s−1 atm]
k_{H2O}	Water valve molar constant [kmol s−1 atm]
k_{O2}	Oxygen valve molar constant [kmol s−1 atm]
q_{H2}	Molar flow of hydrogen [kmol s−1]
q_{H2O}	Molar flow of water [kmol s−1]
q_{O2}	Molar flow of oxygen [kmol s−1]
P_{H2}	Hydrogen partial pressure [atm]
P_{H2O}	Water partial pressure [atm]
P_{O2}	Oxygen partial pressure [atm]

For hydrogen, the derivative of the partial pressure can be calculated using the ideal gas law as follows: [23]

$$\frac{d}{dt}PH_2 = \frac{RT}{V_{an}}\left({}^{in}_{qH_2} - {}^{out}_{qH_2} - {}^{r}_{qH_2}\right) \quad (6.4)$$

The relationship between the hydrogen flow and the stack current can be written as:

$${}^{r}_{qH_2} = \frac{N_o}{2F} = 2krI \quad (6.5)$$

Where

R	Universal gas constant [J kmol−1 K]
T	Stack Temperature [K]
N_o	Number of FCs in the stack
q^{in}_{H2}	Hydrogen input flow [kmol s−1]
q^{out}_{H2}	Hydrogen output flow [kmol s−1]
q^{r}_{H2}	Hydrogen flow that reacts [kmol s−1]
Van	Volume of the anode channel [m3]
F	Faraday's constant [C kmol−1]
kr	Modelling constant
I	Stack current [Amp]

Using equation (5.4), Equation (5.5) can be rewritten in the s domain as:

$$PH_2 = \frac{\frac{1}{k_{H2}}}{1+\tau_{H2}\,s}\left({}^{in}_{qH_2} - {}^{out}_{qH_2} - {}^{r}_{qH_2}\right) \quad (6.6)$$

Where:

$$\tau_{H2} = \frac{V_{an}}{k_{H2}RT}\,s \quad (6.7)$$

The partial pressure of oxygen PO_2 and water PH_2O can be derived using equation (6.6). Equations (6.8) and (6.9), describe the polarization curves for the PEMFC where the FC voltage is the sum of three terms, the Nernst instantaneous voltage E in terms of gas molarities, activation over voltage ηact, and ohmic over voltage ηohmic. Polarization curve be mathematically expressed as per equation 6.8.

$$V_{cell} = E + \eta_{act} + \eta_{ohmic} \tag{6.8}$$

Where η_{act} is a function of the oxygen concentration CO_2 and stack current I (A) and η_{ohmic} is a function of the stack current and the stack internal resistance R^{int} (Ω). Assuming constant temperature and oxygen concentration, equation (6.7) can be rewritten as: [12]

$$V_{Cell} = E - B \ln (CI) - R^{int} I \tag{6.9}$$

Where constants, B = 0.04777V and C = 0.0136A−1. [37]

The Nernst voltage in terms of gas molarities can be written as: [38]

$$E = N_o \left[E_o + \frac{RT}{2F} \log \left[\frac{PH_{2qO_2}^{0.5}}{PH_2O} \right] \right] \tag{6.10}$$

Where

τ_{H2}	Hydrogen time constant
k_{H2}	Hydrogen valve molar constant [kmol s−1 atm]
s	s domain
V_{cell}	DC output voltage of FC system [V]
E	Nernst voltage [V]
Eo	Open cell voltage [V]

6.2 PEMFC Model Validation

The PEMFC model is based on thermodynamic modelling as described in detail in section 6.1. Experimental data was obtained from a Nexa FC, which had been used as inputs to the simulation model. Figure 6.2 shows a comparison between experimental and simulation cell voltage step down for Nexa 1.2kw. As it can be seen from figure 6.2 there is a good match between the experimental simulation results. However, during the start up the model did not show accurate match with the experimental result. This is because the system during start up is going through

unstable condition which affected the accuracy. Most models are neglecting the start-up conditions from the model due the system instability during start up.

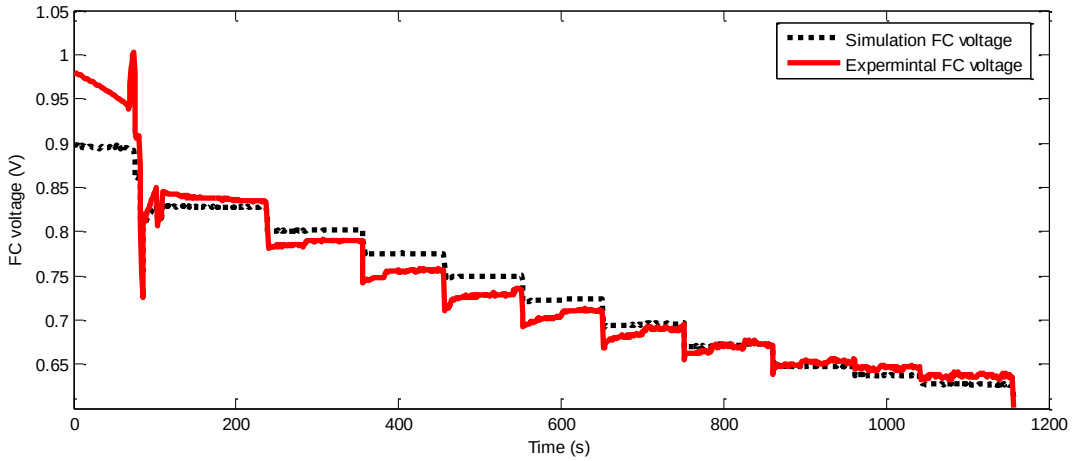

Figure 6.2 Experimental and simulation FC cell voltage comparison

6.3 Polarisation Characteristics

As shown in Figure 6.3, the BALLARD Nexa polarisation characteristics provided by the manufacturer, the system power ranges from the maximum 1.200 kW to zero at system idle. While open circuit is about 43 V and drop to approximately 26 V at the rated power [33]. The illustrated measurements in Figure 6.3 are based on defined conditions which are at room temperature and sea level.

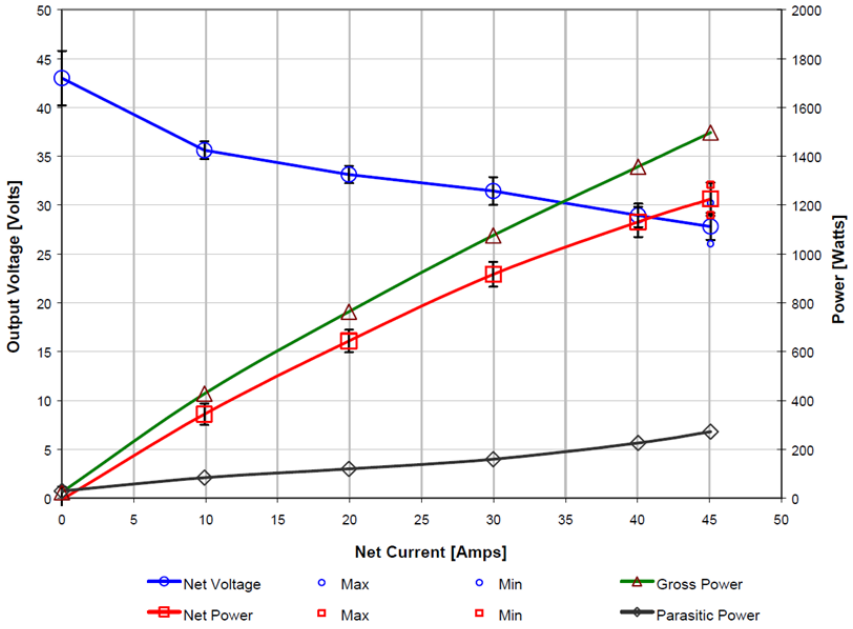

Figure 6.3 Nexa polarisation and power curves [33].

In this study the dynamic electrochemical approach was adopted. Figures 6.4 and 6.5 show the developed simulation model in Matlab Simulink. A new parameters extraction method for PEMFC model is presented in table 6.6.

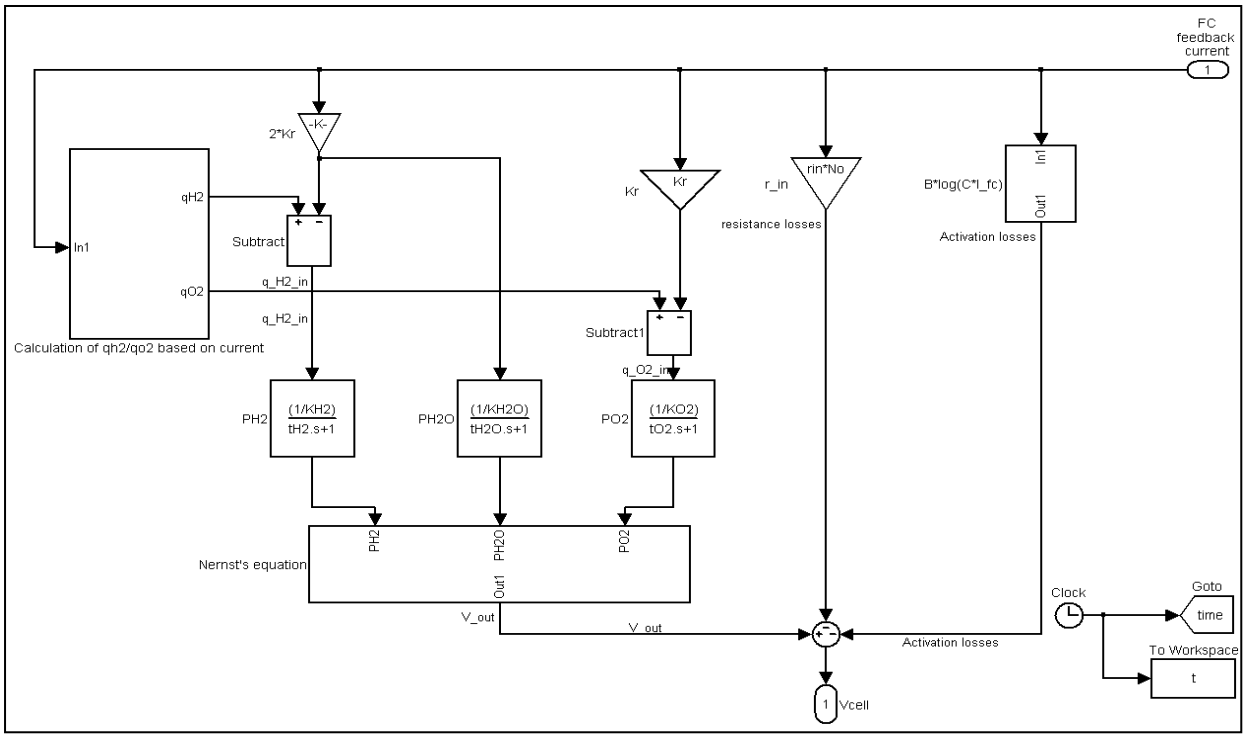

Figure 6.4 PEMFC stack model

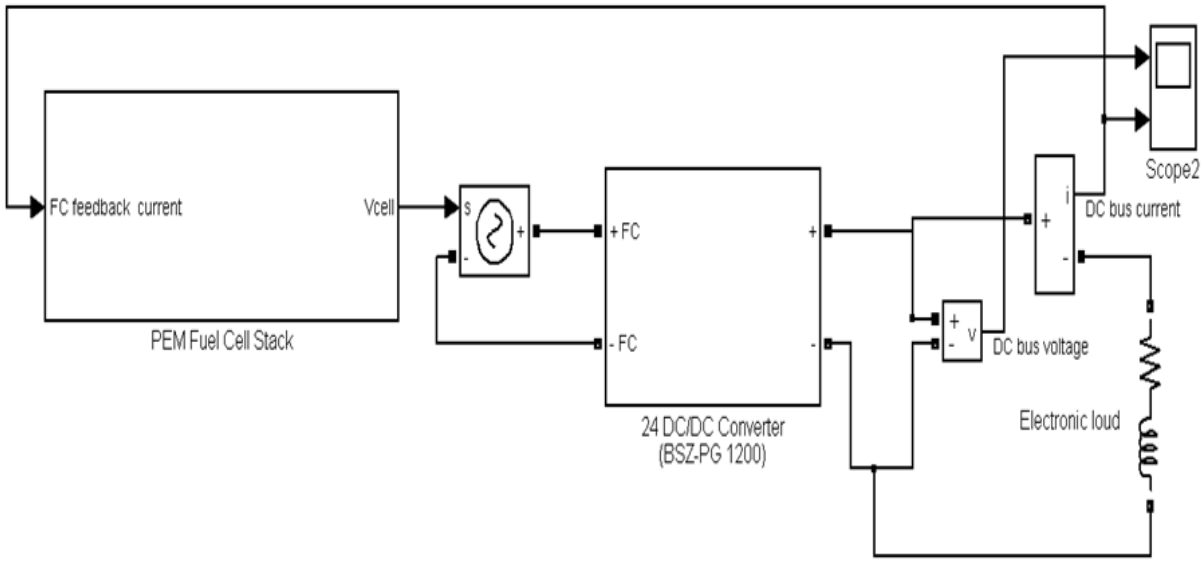

Figure 6.5 PEMFC stack connection to DC/DC converter then to the load

Table 6.1Model parameters

Symple	Description	Value
k_{H2}	Hydrogen valve molar constant	1.012370 kmol s−1 atm
k_{H2O}	Water valve molar constant	5.6640×10-4 kmol s−1 atm
k_{O2}	Oxygen valve molar constant	8.9294×10-5 kmol s−1 atm
k_{an}	Anode valve constant	kmol s−1 atm
q_{H2}	Molar flow of hydrogen	kmol s−1
q_{H2O}	Molar flow of water	kmol s−1
q_{O2}	Molar flow of oxygen	kmol s−1
q_{H2}^{in}	Hydrogen input flow	kmol s−1
q_{H2}^{out}	Hydrogen output flow	kmol s−1
q_{H2}^{r}	Hydrogen flow that reacts	kmol s−1
P_{H2}	Hydrogen partial pressure	atm
P_{H2O}	Water partial pressure	atm
P_{O2}	Oxygen partial pressure	atm
τ_{H2}	Hydrogen time constant	2.62889×10-9 s
τ_{H2O}	Water time constant	4.6988×10-7 s
τ_{O2}	Oxygen time constant	2.9875×10-6 s
M_{H2}	Molar mass of hydrogen	kg kmol s−1
M_{H2O}	Molar mass of water	kg kmol s−1
M_{O2}	Molar mass of oxygen	0.0319988 kg kmol s−1
V_{an}	Volume of the anode channel	7.59×10-4 m3
V_{ca}	Volume of the cathode channel	7.59×10-4 m3
R	Universal gas constant	8314.47 (J kmol−1 K)
r_{h-o}	Oxygen flow ratio	1.168
C_{O2}	Oxygen concentration	0.21%
T	Stack Temperature	343K
N_o	Number of FCs in the stack	46
I	Stack current	Amp
F	Faraday's constant	96484600 C kmol−1
k_r	Modelling constant = No/4F	1.1919001×10-7 kmol s−1A
V_{Cell}	DC output voltage of FC system	V
E	Nernst voltage	V
E_o	Open cell voltage	0.6V
ηohmic	Over voltage due to ohmic loss	
ηact	Activation over voltage	

B	Activation voltage constant	0.04777A−1
C	Activation voltage constant	0.0136V
$q_{methanol}$	Methanol flow rate	0.000015kmol s−1
CV	Conversion factor	2 kmol of HO2 kmol−1 of methanol
τ_1, τ_2	Time constants	
U	Utilization rate	
k3	PI gain	
τ_3	Time constant of the PI controller	
s	s domain	
R^{int}	Stack internal resistance	0.00303 Ω
X	Line reactance	0.05 Ω

6.4 Experimental Analyses

In order to gain a deeper understanding and learn more about the 1.2 Nexa fuel cell dynamic behaviours and to track changes in output parameters, the following four tests were performed as part of the initial experimental analyses:

- Start-up state
- shut-down state
- step-up load state
- Irregular load variation state

The test values are plotted as a function of time in order to make it easier to take notice of any trend changes of these parameters.

6.4.1 The Start-up Sequences Transient Response

The 1.2kW Nexa FC system is equipped with a fully automated control system. Thus, the 24V batteries must be connected to support start-up and shut down load, and the system must be provided with an adequate hydrogen fuel supply. The transient responses of transmitted status, current and voltage during the start-up states for 35 seconds are shown in Figures 6.9 and 26. Before applying the battery power, the FC system remains in the OFF state.

The starting-up process began by powering the FC control system with a 24 V from external batteries. The system requires 2 seconds from pressing the start button until

reaching the stand-by mode. At the stand-by mode FC control system has already energized all actuators and sensors, performed all safety checks and then begun to continuously collect and record system data and signals. By pressing the start button again, the system will be initiated by a 5 V start signal. The hydrogen valve will be opened to allow hydrogen to fill cells anode side. At the same time the air pump, purge valve and cooling fan will be turned on.

The cell voltages began to increase at 13 seconds and reached about 46V. At this state, the output current was zero. After 21 seconds, the current gradually increased to about 1.2A, and the voltage decreased to 42V, which presents starting-up operation in this time. At 28 seconds, when normal operation was reached, the Nexa FC system power supply was automatically transferred from external batteries to the FC internal generated power. At the same time a control signal was sent to connect the FC to the external load. As a result of this, the FC shocked up and its current increased with overshoot due to air pump fast response, and the voltage decreased with undershoot as shown in Figure 6.9.

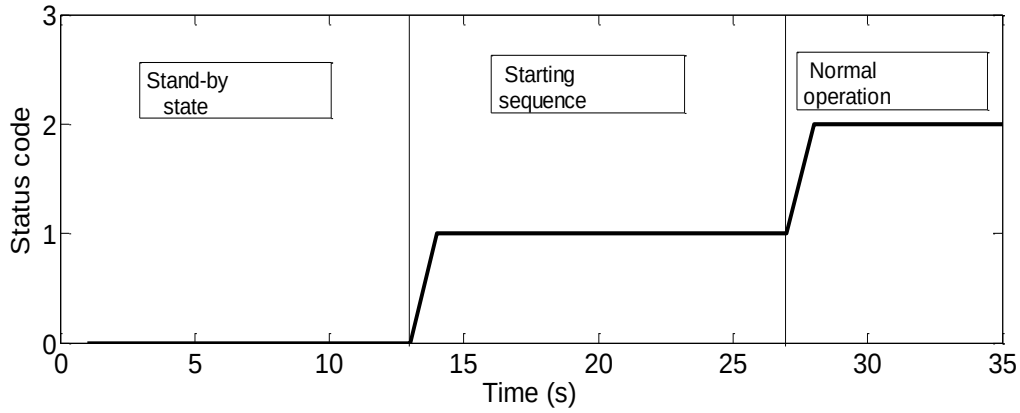

Figure 6.6 Nexa transmitted status in starting-up state

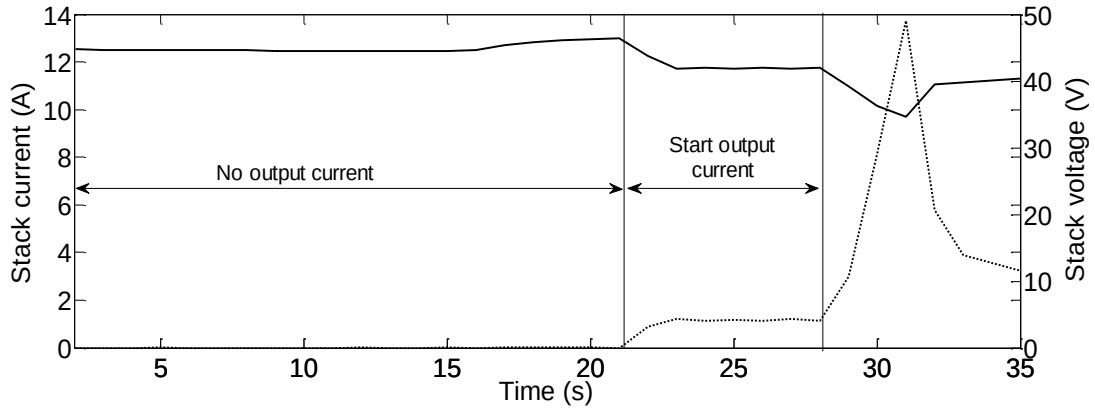

Figure 6.7 The stack output current (A) & voltage (V) transient responses in the start-up state

After the stand-by sequence, the air pump and cooling fan voltages jumped from 0 to 43% and 50%, respectively as shown in Figure 6.12. The air flow rate fluctuated from around 20 slpm, then overshot at the beginning of starting-up and then went back to about 20 slpm at normal operation states as illustrated in Figure 6.11. Just after connecting the external load to the FC at 28 seconds, the air pump voltage increased with overshoot. This reaction is to provide enough oxygen and to remove the residual water from the stack channels. It is important to notice that just after FC start up at low load, the membranes were still dry and there was not enough water. It is very important to keep minimum flow rate of water at the membranes to maintain the reaction at FC [36]. Contrarily, the cooling fan voltage dropped to about 35% so as to regulate the FC stack temperature. In reality, as shown in Figure 6.14, there is no sudden change to stack temperature but only gradual temperature decrease. The cooling fan was kept at about 35 %, even though FC stack current increased to its maximum level.

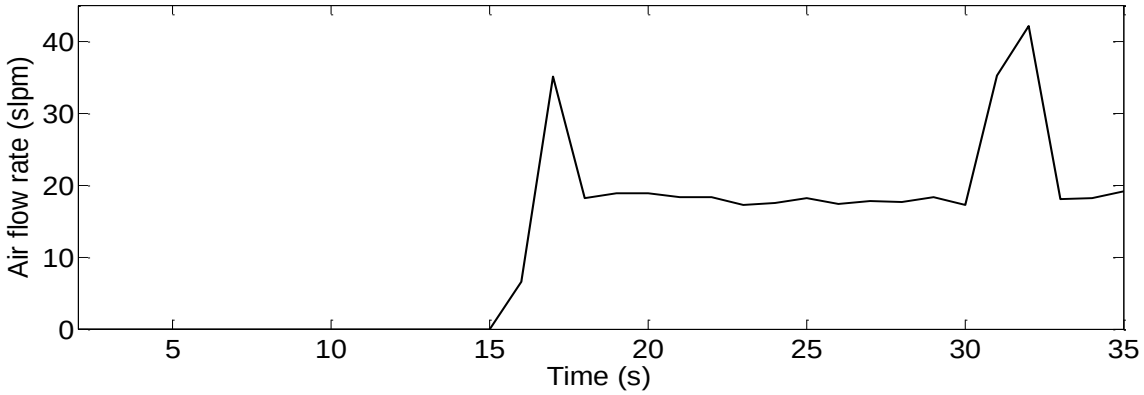

Figure 6.8 Air flow rate in starting-up state (slpm)

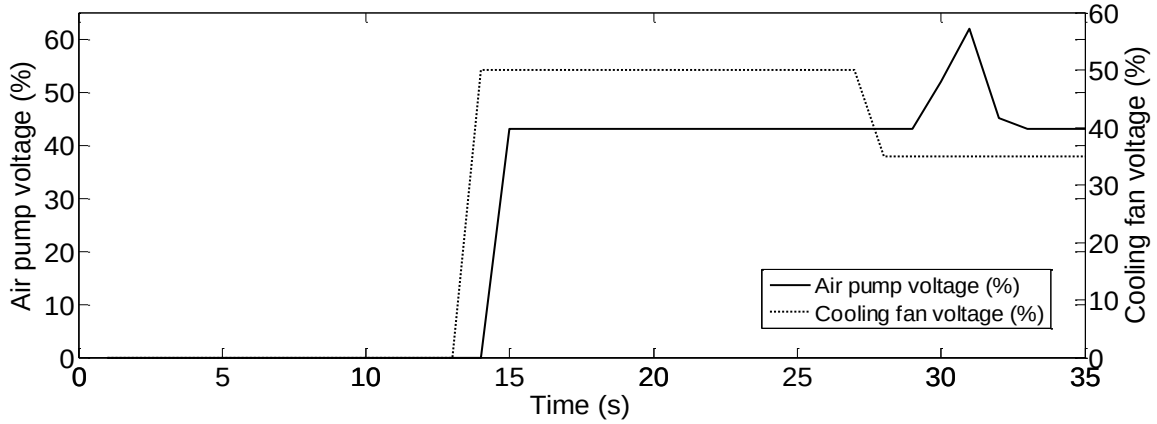

Figure 6.9 The air pump and cooling fan voltage in the start-up state

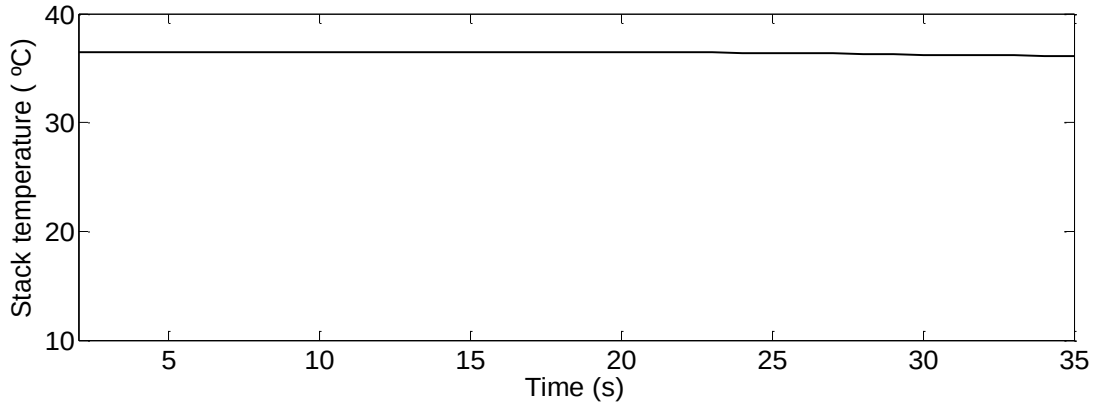

Figure 6.10 Stack temperature in the starting-up state

6.4.2 The shut-down Transient Response in Sequence

In the shut-down mode, the 5V start signal was removed from the FC stack and then FC stack was isolated from external load by switching the load relay to open position. Since the FC sufficiently operated for longer than 5 minutes, as part of the shutdown procedure, the air pump and water purge valve continued running to ensure that all water residual were removed.

System behaviour during the shut-down states is shown in Figures 6.13, 6.14, 6.15 and 6.16. The shut-down began from about 419 seconds, the current dropped to about 1.58A within 1 second, while the stack voltage increased to 42 V. In this period, at about 438 seconds, the control system internally transferred parasitic load from the FC stack internal power back to the external batteries, which caused current small undershoot and voltage small overshoot. From 447 seconds, the current dropped almost to zero while the voltage gradually increased until it reached the Open Circuit Voltage (OCV) of about 46 V, and the air pump continued running to ensure removing all residual water as shown in Figure 6.16. The air flow rate increased from 20 slpm to 59 slpm in the period from 438 to 482 second then dropped to zero as shown in Figure 5.15. At 452 seconds, the voltage of the cooling fan fell from 35 % to zero, later on at 482 seconds, the air pump dropped sharply to zero as shown in Figure 6.15. The stack temperature gradually decreased as the system shut down as shown in Figure 6.14.

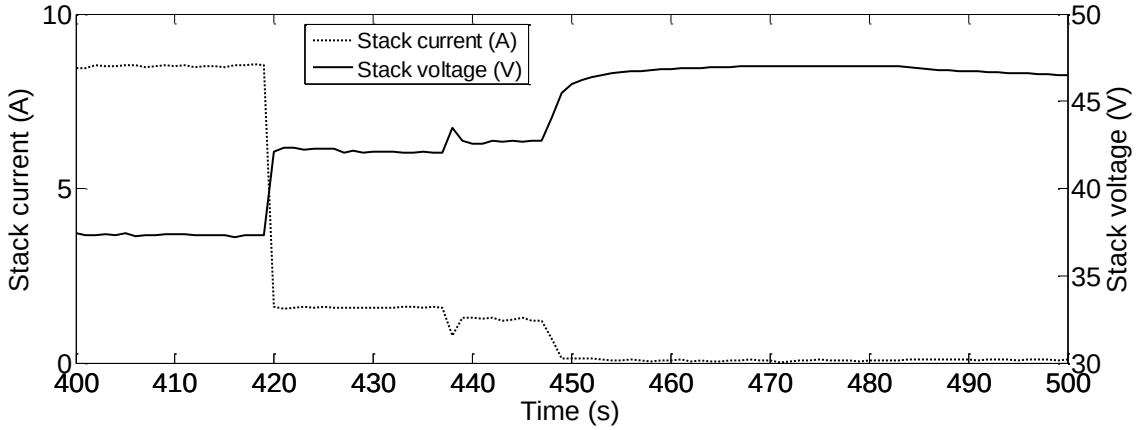

Figure 6.11 The stack output current (A) and voltage (V) Transient responses during shut-down state

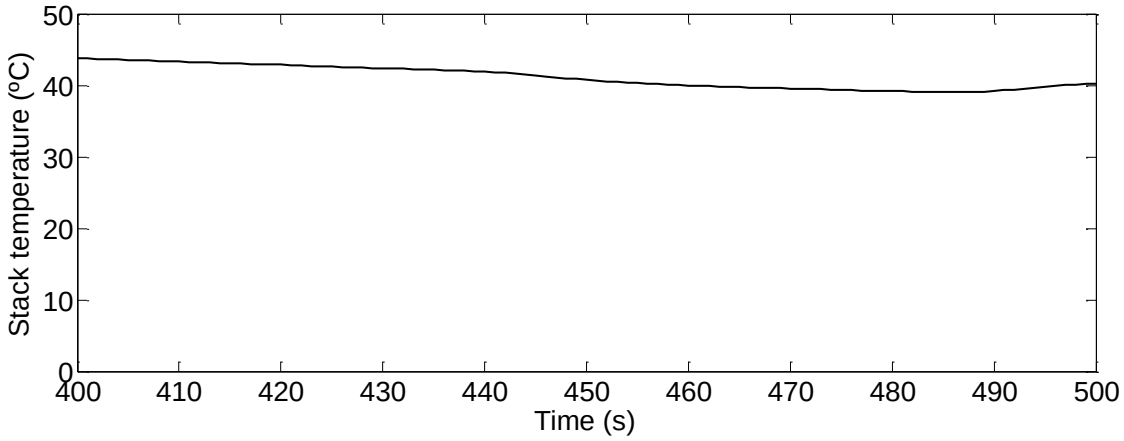

Figure 6.12 Stack temperature in the shut-down state

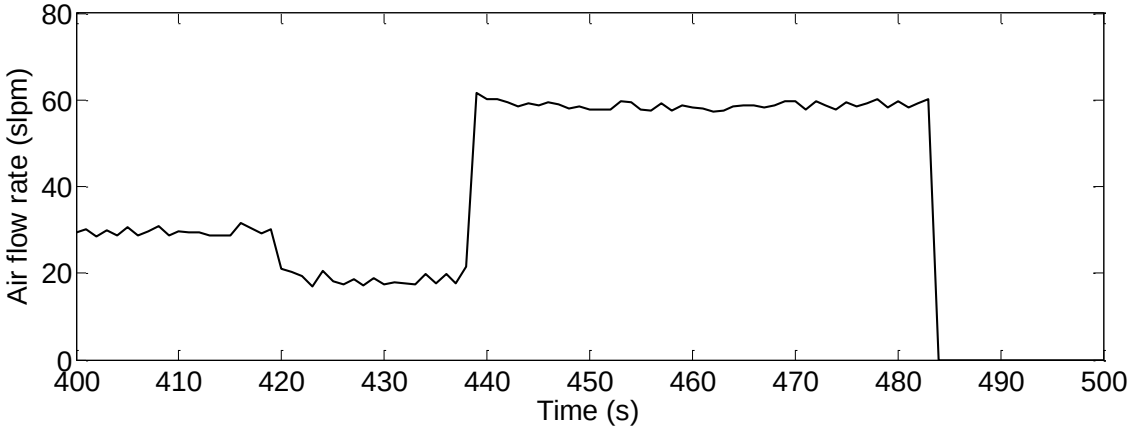

Figure 6.13 Air flow rate in shut-down state (slpm)

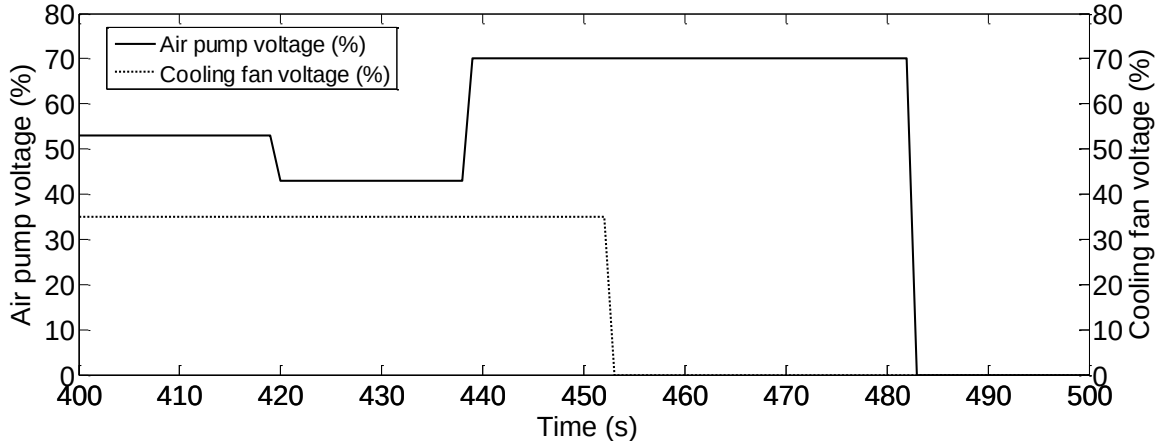

Figure 6.14 The air pump and cooling fan voltage in the shut-down state

6.4.3 The Step-Up Load States Transient Response

The results of this test describe the transient responses of FC parameters (stack current, stack voltage, air pump voltage ... etc.) during step-up load variation as shown in Figures 6.17, 6.18, 6.19, 6.20 and 6.21. The overall stack current increases from 10A to 40A, while the overall stack voltage declines from 35V to 30V. A 10A interval value was used to increase the stack current from 10 A to 40A. The maximum power of 1.2 kW was reached at about 919 seconds at 30V stack voltage and current respectively. It is important to notice that the purge valve operating frequency increases as the current increases just to prevent water flooding in the anode channel and anode gas diffusion layer, the interval between purge valve open and closed is about 96 seconds in the low-current region of around 10A, and the interval increases to 30 seconds at stack current 40A, which is the logical response to remove the increased water production as shown in Figures 6.20 and 6.21.

The ‘red’ circle in Figure 6.17 is focusing on stack voltage undershoot and current overshoot phenomena that occurs as the current suddenly increases from 20A to 30A. The current overshoot possibility is elevated for two reasons. The first is the rapid current change after a relatively long steady operation, which disturbed water saturation level at membrane. The second reason is that the membrane wettability is affected by both the produced and humidified water. Therefore, the sudden load change leading to voltage undershoot is due to electro-osmotic drag and air overflow on the anode side and on the cathode side respectively, which leads to a short term dehydration. As result of that membrane resistance increases which leads to cell voltage drop [51, 52].

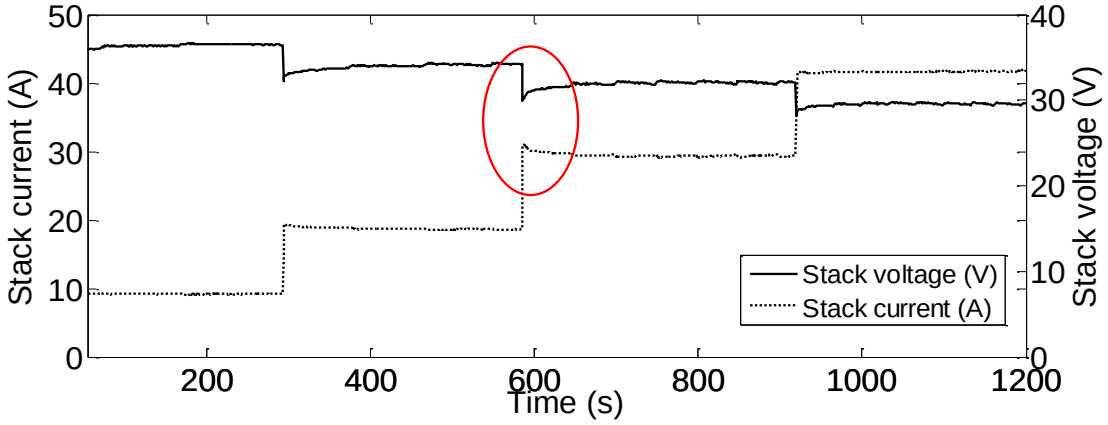

Figure 6.15 Transient responses of the stack output current (A) and voltage (V) during step-up load states

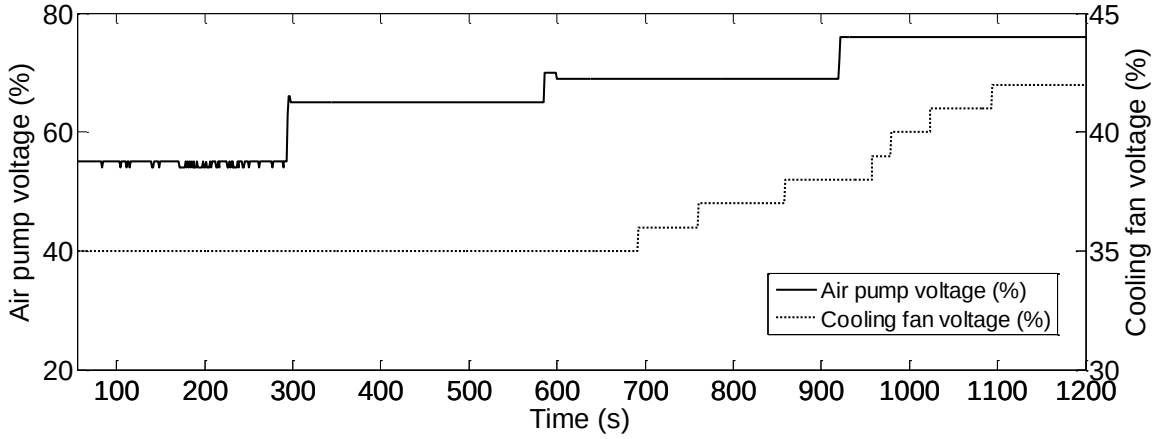

Figure 6.16 The air pump and cooling fan voltage during step-up states

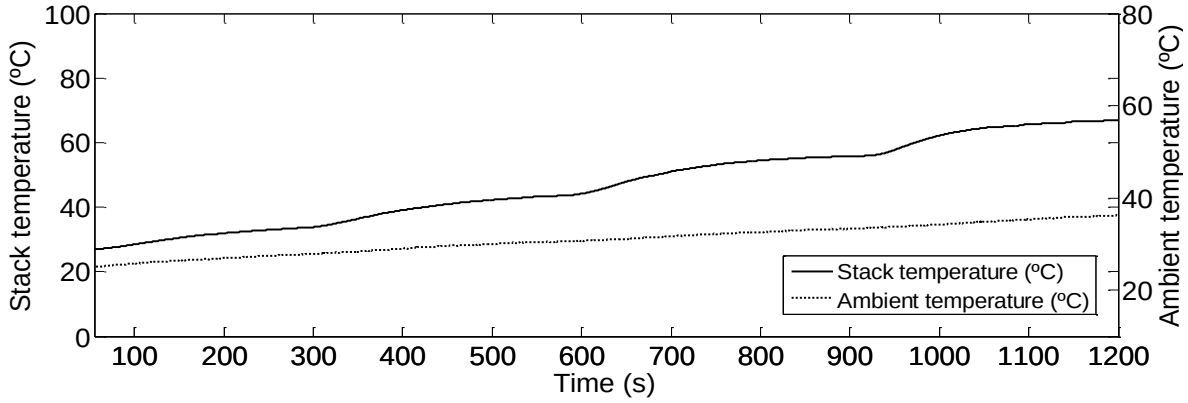

Figure 6.17 Stack and ambient temperatures during step-up states

Figure 5.19 shows a direct relation between the stack's temperature and current. The stack temperature directly increases as the stack current increases. Also the air pump voltage behaves in similar manner to stack current increases as shown in Figure 34. While the cooling fan voltage at the beginning remains constant at 35 % until 700 seconds, after 700 seconds it starts to step up following the current

increases as shown in Figure 6.20. Figure 6.21 is showing the FC stack voltage behaviour under a constant current of about 30 A for the period from 650 to 900 seconds. It can be noticed that at purge valve operation, stack voltage experienced periodic fluctuations as marked by the red circle in Figure 6.20. At these points, voltage declines from 32.2 to about 31.7 V due to water flooding. Just after water purge valve opening, the performance improves which leads to sharp voltage increases. Figure 6.21shows purge valve opening status, at 1 the valve is fully open and at 0 the valve is fully closed.

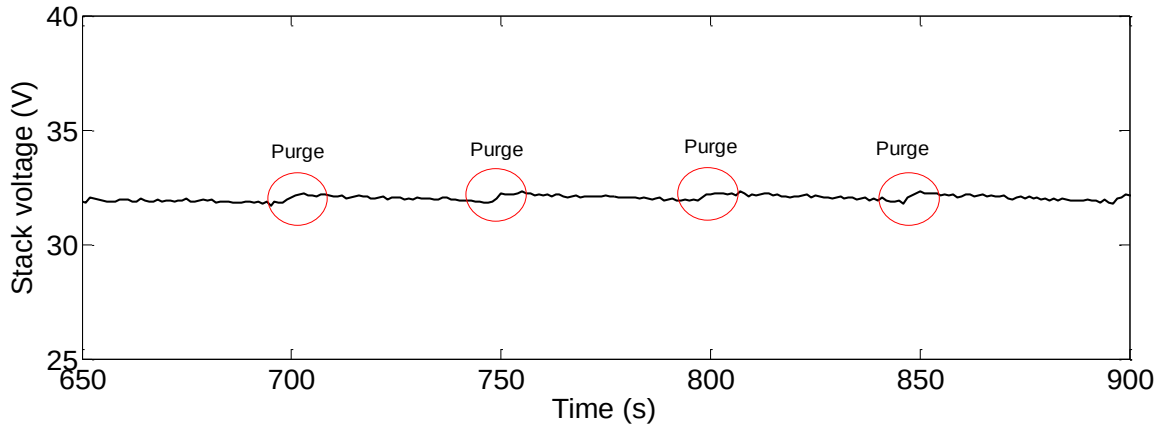

Figure 6.18 Effect of purge valve operation on PEMFC stack voltage during constant load

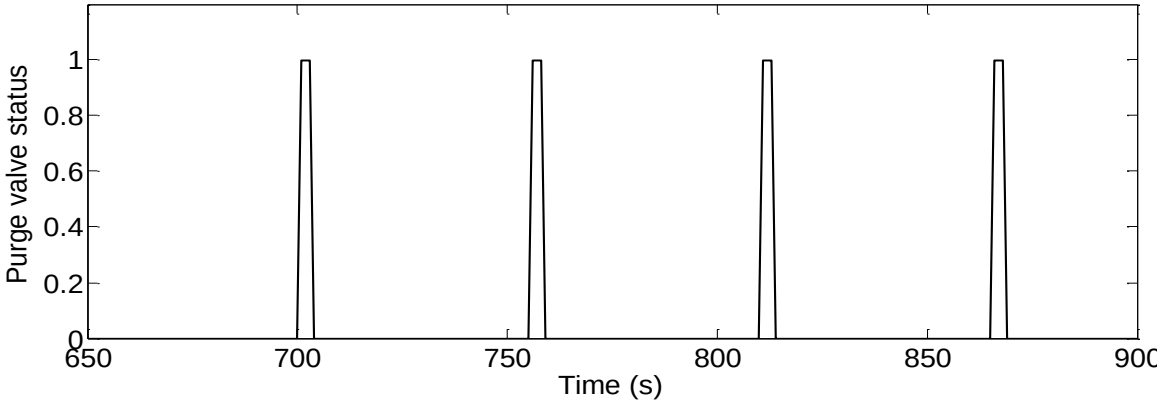

Figure 6.19 Purge valve status during constant load
(0 = valve closed, 1 = valve open)

6.4.4 Irregular Load Variation Transient Response

This test's main objective is to study the effects of air pump flow rate and stack temperature on the FC stack dynamic performance. In the test the FC supply power to variable load over about 1600 seconds; experimental results are illustrated in Figures 6.22, 6.23 and 6.24. The temperature commonly exists during the FC operation in the form of exothermic reaction heat transfer and internal heat dissipation. PEM FC stack temperature continuously changes with the load current. However, the temperature directly affects the rate of chemical reactions and the transport of water and reactants. Thus, operations under too-low or too-high temperatures in reality are normally not preferred except for in extreme circumstances such as sub-zero application [53], where this can be regulated by proper thermal control. The stack temperature and current are directly linked with FC stack load changes in a similar manner, so that they both increase and decrease as the load changes. However, temperature changes slowly without overshoot or undershoot as shown in Figure 6.22.

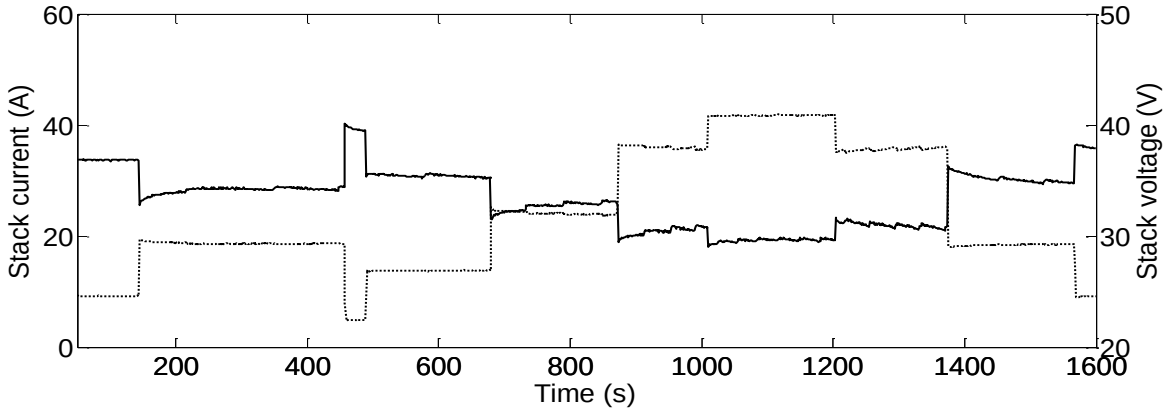

Figure 6.20 Transient responses of the stack output current (A) and voltage (V) asymmetrical load variation

Figure 6.24 presents the air pump and cooling fan voltages of the Nexa FC; it can be seen that the air pump flow rate changes in the same manner as the current responses with no delay. However, the decrease in the air flow rate results in oxygen depletion from the FC cathode channel during power generation. Furthermore, the Nexa FC operation shows that the air flow does not have a significant effect on the FC stack dynamic performance.

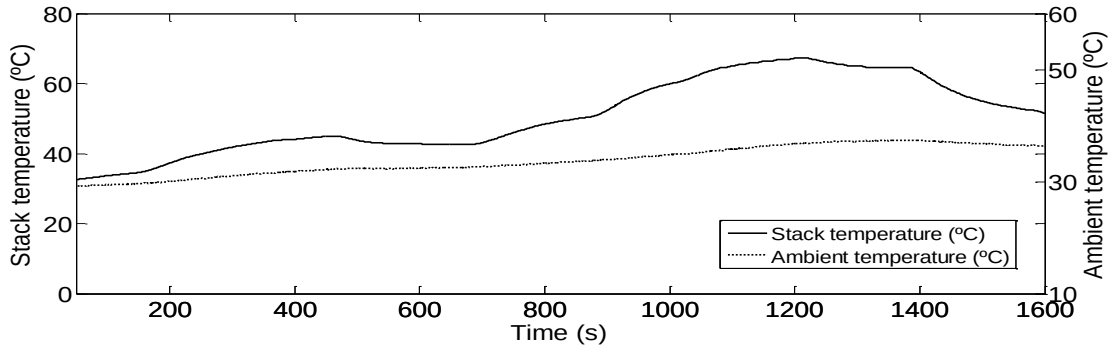

Figure 6.21 Stack and ambient temperatures during asymmetrical load variation

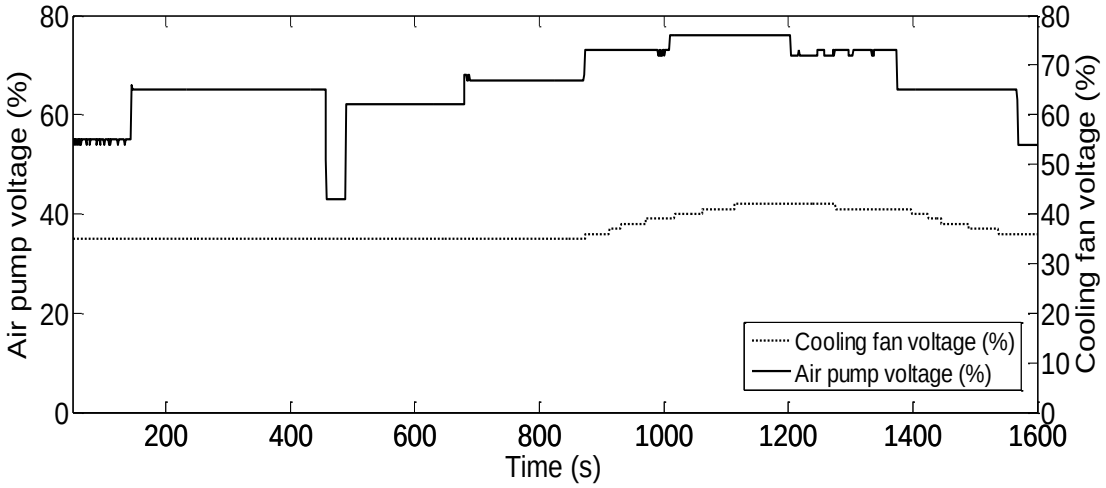

Figure 6.22 The air pump and cooling fan voltage during asymmetrical load variation

6.4.5 Photovoltaic Panel Simulation Model

For many years, many different mathematical models have been developed to describe the PV cell I-V characteristic curve The one-diode, the two-diode, and the empirical model are the main three common models most commonly used by researchers to describe the behaviour of the equivalent electrical circuit of a PV cell [60, 61].

<u>One-diode model:</u>

The one-diode model is the most popular model; due to it is simplicity and reasonably good accuracy [1, 5, and 15]. This model is based on five unknown parameters I_L, I_d, n, Rsh and Rs which describe the electrical characteristic of the pn-junction [59]

<u>Two-diode model:</u>

This is a more complex model which is based on seven unknown parameters I_L, $I_{d1,}$ $I_{d2,}$ n1, n2 Rsh and Rs. The two-diode model allows for a more detailed description of the recombination process of charge carriers both on the surface and in the bulk material.

<u>Impirical model:</u>

The empirical model is defined based on the curve fitting method of the I-V curve. The number of parameter is less than the other models. The main parameters (Pmax, Isc, Voc, etc.) of this model can be found on the solar panel supplier data sheet.

Due to the simplicity and accuracy of the one-diode model, it has been selected for this study.

6.4.6 One-Diode Model

The One-Diode equivalent circuit is one of the most commonly used models to describe the PV cell behaviour as shown in figure 6.23 [57, 58 and 61]. This model is based on four variables, two input parameters and two output parameters.

The two input variables are affected by bother geographical location and time:

- Solar Radiation G (W/m^2)
- Ambient temperature Ta (°C)

On the other hand, the two output variables which are affected by physical material properties of cells are presented by the internal resistance:

- Cell current I (A)
- Cell voltage V (V)

A commonly used assumption for ideal cell serial resistance (Rs) and Shunt resistance (Rsh), Rs=Rsh=0 is true at the open circuit condition [58].

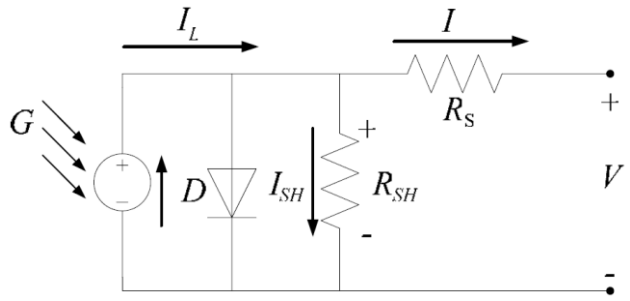

Figure 6.23 One- diode equivalent circuits [58].

By applying Kirchhoff's law to the equivalent circuit shown in figure 6.23 the circuit load current can be expressed as following:

$$I = I_L - I_d - I_{sh} \quad (6.12)$$

Where

$$I_d = I_0 . \left(e\left[\frac{q(V+IRs)}{nkT}\right] - 1\right) \quad (6.13)$$

Where

I	Load current [A]
I_L	Light current [A]
I_d	Diode current [A]
I_{sh}	Shunt current [A]
I_0	Saturation current [A]
V_c	Cell voltage [V]
q	Electron charge, 1.6×10^{-19} (C)
Rs	Series resistance [Ω]
n	Diode ideality factor
k	Boltzman's constant, 1.13×10^{-23} [j/k]
Tc	Absolute Temperature of the Cell, [K]

Because Shunt resistance is very high, the shunt current I_{sh} is assumed to be zero to simplify the model. Therefore equation 5.12 can be rewritten to [58].

$$I = IL - I_0 . \left(e\left[\frac{q(V+IRs)}{nkT}\right] - 1\right) \quad (6.14)$$

Where I_L is Light current, I_0 is Saturation current V and generated voltage are dependent on other factors like solar cell temperature as shown in the following equations.

$$I_{L=} I_L (T_1) + K_0 (T-T_1) \quad (6.15)$$

$$I_L (T_1) = I_{sc} (T_{1,\,nom}) \frac{G}{G(nom)} \quad (6.16)$$

$$K_0 = \frac{I_{sc}(T_2) - I_{sc}(T_1)}{(T_2 - T_1)} \quad (6.17)$$

$$I_{0=} I_0 (T_1)\, x\, (\frac{T}{T_1})^{\frac{3}{n}} e^{\frac{V_q(T_1)q}{nk\left(\frac{1}{T}-\frac{1}{T_1}\right)}} \quad (6.18)$$

$$I_0(T_1) = \frac{I_{sc}(T_1)}{\left(e^{\frac{q\,V_{OC}(T_1)}{nKT_1}-1}\right)} \quad (6.19$$

$$T_c = T_0 + T \quad (6.20)$$

Cell internal and connection cell resistance R_s are calculated as per the following equations [58].

$$R_{s=} - \frac{dV}{dI_{Voc}} - \frac{1}{X_V} \quad (6.21)$$

$$X_V = I_0(T_1) \frac{q}{nKT_1} e^{\frac{qV_{OC}(T_1)}{nKT_1}} - \frac{1}{X_V} \quad (6.22)$$

All parameter definitions are given below:

I_L	Light current (A)
I_s	Saturation current (A)
I_s	Diode current (A)I Load current (A)
I_{sc}	Short circuit current (I)
V	Output voltage (V)
V_{oc}	Open circuit voltage (V)
Rs	Series resistance (Ω)
Rsh	Shunt resistances (Ω)
n	Diode ideality factor
k	Boltzman's constant, 1.13 x 10^{-23} (j/k)
q	Electron charge, 1.6 x 10^{-19} (C)
G_0	reference solar radiation, 1000 [W/m²]
Ns	number of cells in series, 60/Panel
Eg	gap energy voltage, [eV]
T_0	reference junction temperature, [K]
T_1	Ambient temperature, [K]
T	Absolute Temperature of the Cell, [K]
NOCT	normal operating cell temperature ≈ 45-49 °C

Table 6.2 Main technical specification for the SCHOTT poly 230 panel

Parameter	Variable	Value
Nominal power (w)	P_{mpp}	230
Voltage at nominal Power (V)	V_{mpp}	30
Current at nominal power (A)	I_{mmp}	7.66
Open Circuit Voltage (V)	V_{oc}	36.9
Short-Circuit current (A)	I_{SC}	7.66
Module efficiency level (%)	μ	13.7
Normal Operating Cell Temperature (°C)	NOCT	≈ 45-49
Number of cells in series	Ns	60/Panel
Number of panels	-	2

6.4.7 Solar Panel Model Validation

Based on the mathematical model explained in section 6.8.1, a Matlab/Simulink model has been developed. The model result was compared with the experimental result as shown in figure 6.28.

The experimental result was obtained from Cranfield Laboratory by considering the manufacturer open circuit votage (Voc) and short circuit current (Isc), and by using variable load in very clear sky. The current was increased gradually by 0.1 A until it reached the open circtuit current.

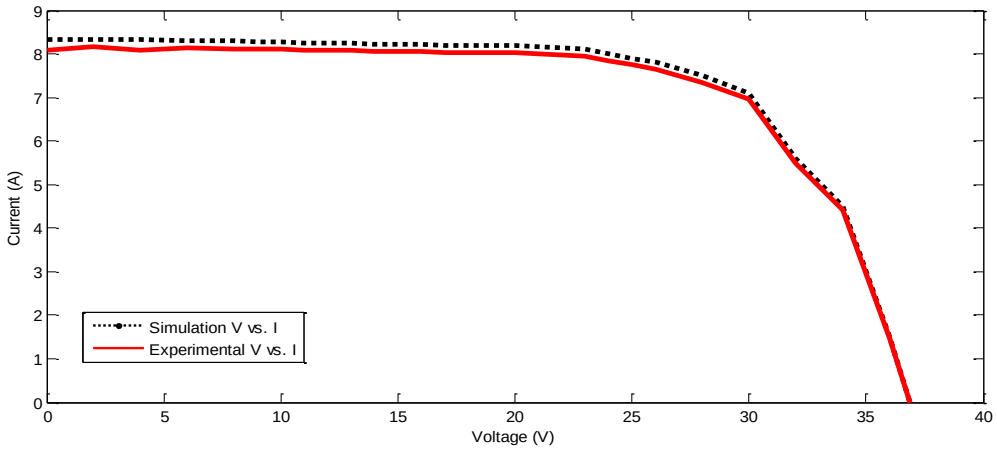

Figure 6.24 Experimental and simulation voltage vs. current comparison

6.5 Solar Panels Simulation results

This section will show different solar panel simulation results based on the developed Simulink model as shown in figure 6.27. The model will show solar panel output voltage, current and power for different environmental conditions and geographical locations.

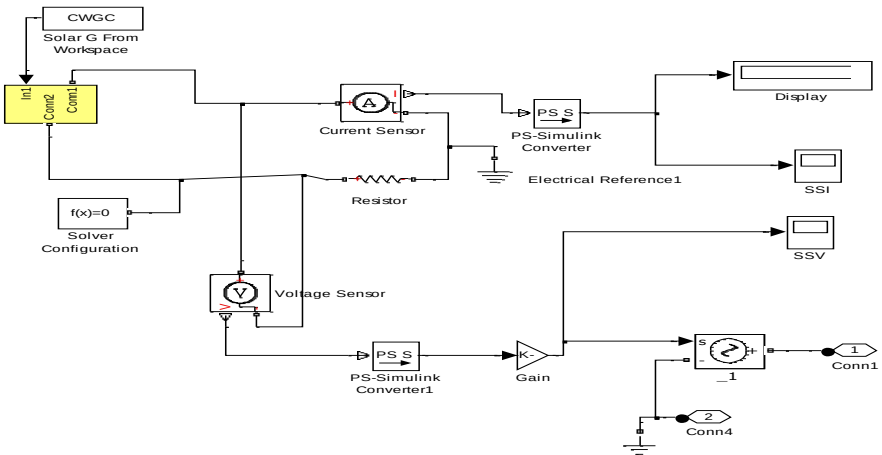

Figure 6.25 Solar panel model

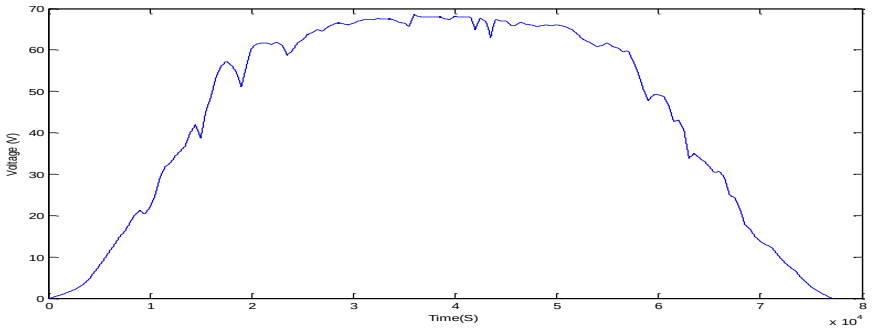

Figure 6.26 Solar panels before the converter voltage Abha- one day in August

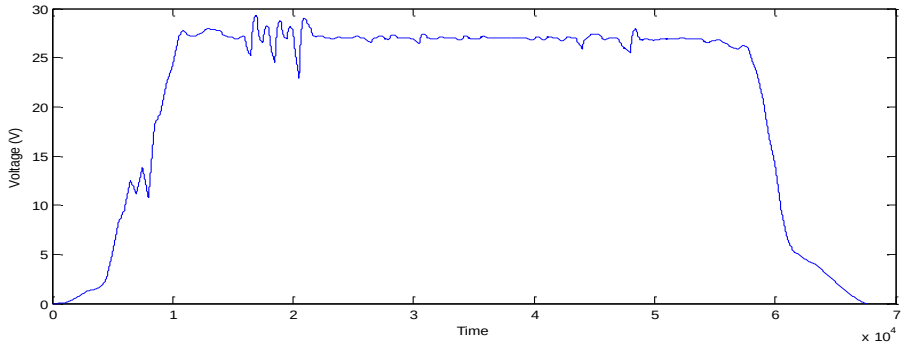

Figure 6.27 Solar panels after the converter voltage Abha- one day in August

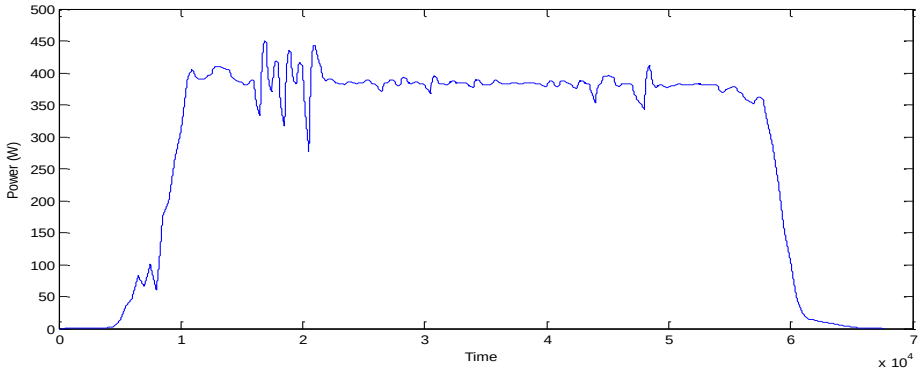

Figure 6.28 Solar panels power Abha- one day in August

6.6 Sealed Lead Acid 12V Battery Model Validation

The battery model used in this study is based on the battery block model obtained from Simulink SimPowerSystems® tool box, whose parameters can be modified to fit most popular rechargeable batteries. The model parameter was modified according to the sealed lead acid battery (WP18-12) data sheet used in the lab.

To verify the model a fully charged sealed lead acid battery (WP18-12), was connected to a constant 10A load. The battery voltage before connection to the load was 12.7 V. After connection, the voltage gradually started dropping; after 58 minutes the voltage dropped sharply and reached 9.9 V. Figure 6.31 shows a comparison of the experimental and simulation graphs of battery discharge voltage changes vs. time.

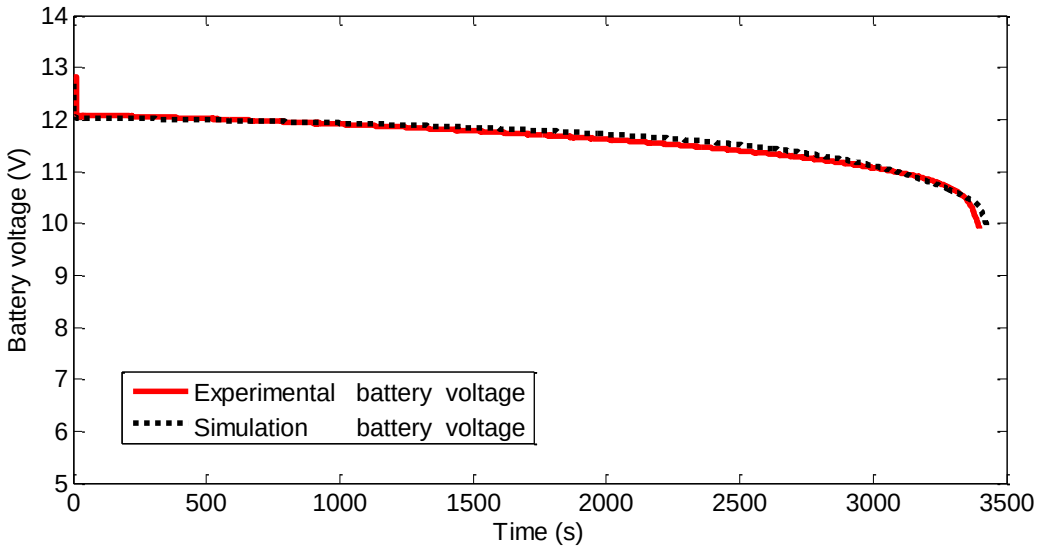

Figure 6.29 Experimental and simulation battery voltage comparison

6.7 HPS Overall Model

In the previous sections of this chapter HPS components model were developed and verified. In order to represent the overall HPS, individual models of fuel cell, solar panels, batteries and converters were integrated in Matlab Simulink and PI controller was implemented as shown in Figure 6.32.

6.7.1 Parameters of HPS Model Components

Each sub-model of the HPS requires a certain number of parameters which are essential to run the model. The corresponding parameters of the HPS sub-models are calculated and validated in previous sections.

6.7.2 HPS Model Input Data

This model is designed to perform long and short term studies and analysis of the HPS in different geographical areas, providing that following input data is available:

- Solar Radiation
- Ambient temperature
- Load profile (Water consumption and water tank level)
- H2 storage tank level

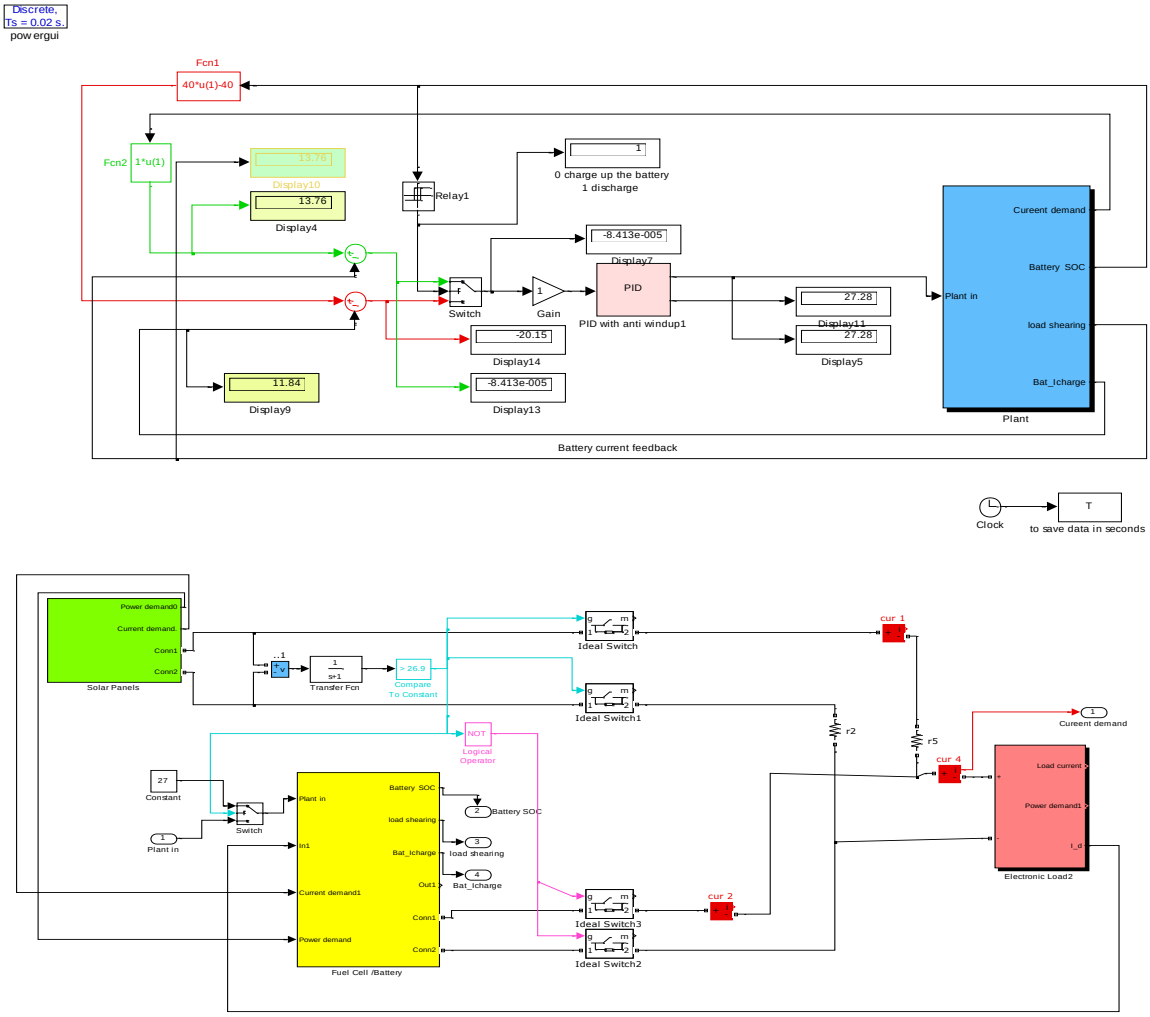

Figure 6.30 HPS Module Structure

6.7.3 HPS Modle Output Data

The developed simulation model provides sufficient information about the performance of each component and the system. During the program execution, all necessary system variables needed for a performance analysis are recorded in a simulation output file. For example, battery charge status generated current by solar panel, load current, the required current either by battery or fuel cell to compensate Solar deficiency to satisfy the load demand, water tank level etc. These output results can be analysed to cover all performance aspects of the overall system.

6.8 Chapter Summary

This chapter began by defining the simulation model and the importance of defining the model boundary, model input and output data.

The Fuel Cell model was then presented by highlighting model assumptions and showing mathematical model development details. After that, the model was validated by comparing experimental and simulation results which show good agreement. The Fuel Cell model was run for different operation conditions to study the Fuel Cell performance and behaviour. After different commonly used Photovoltaic models were discussed and why One-Diode model was used in the project, the PV model was validated by comparing experimental with simulation results, which also showed a good agreement. Finally the batteries model was explained and verified.

7 CASE STUDIES, RESULTS AND DISCUSSION

In this chapter, two main scenarios will be explored to validate the hybrid system performance in two different geographical and environmental conditions.

The first case is based on Saudi Arabian environmental conditions, where it is hot and sunny most of the year. This scenario allows more utilization of power generated from sunlight via PV cells and reduces the dependence on power produced by fuel cells.

In the second case, the hybrid system was examined in UK environmental conditions, where it is cold and cloudy most of the year. In this case sunlight is at a minimum leading to higher dependence on fuel cells.

7.1 Introduction and Background

Providing power for low power applications in remote areas is challenging. For such applications it is not feasible from a cost and environmental point of view to connect them to the main power grid. Therefore, local standalone HPS is an attractive option for such applications.

A case study based on the FC/PV system to provide power for a water pump and storage system for a small community (about 6,500 litres/day consumption) will be considered. The system will utilize photovoltaic (PV) as the primary power generator, PEMFC as the secondary back up power generator and a batteries bank as the power storage device (to store any excess power). The advantage of the proposed system is that, in addition to being environmentally friendly, it also has lower maintenance costs and noise footprint.

Work will be based on the FC/PV/batteries hybrid system to power a water pump, which will be used to fill an elevated water storage tank. This tank will be used to maintain a water supply to a small community of about 10 houses. A simple sketch of the proposed system is shown in Figure 7.1.

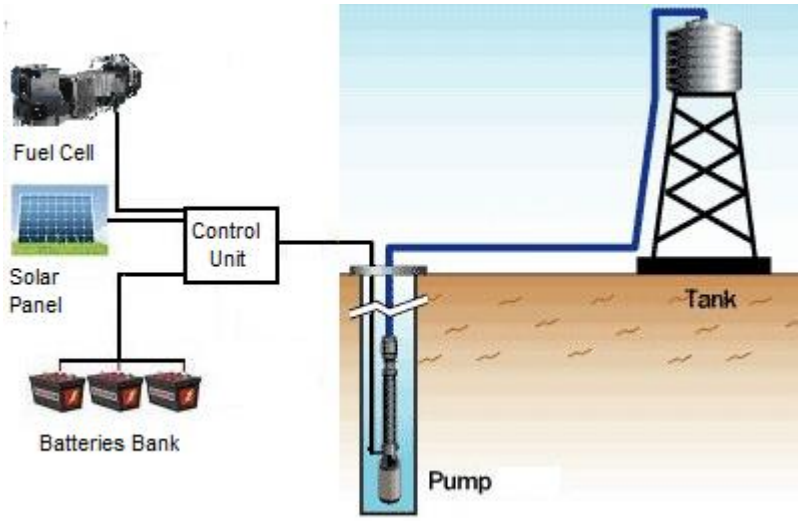

Figure 7.1 FC/PV/Battery hybrid water pumping & storage system

7.2 **HPS Simulation**

The FC/PV HPS individual components were modelled in detail in section 5 using Matlab Simulink. The system components have been grouped together to make the hybrid system as shown in figure 7.2.

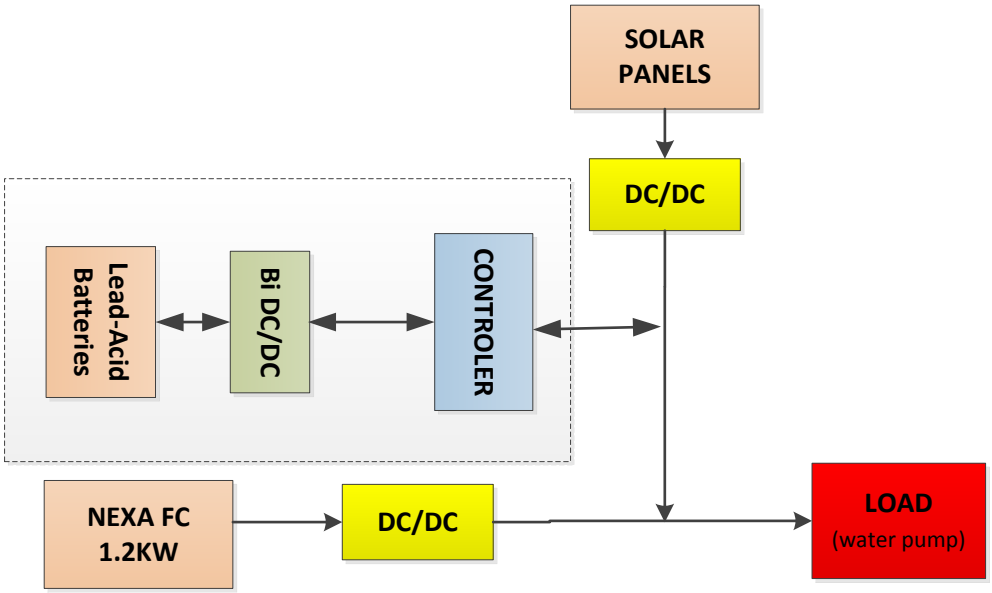

Figure 7.2 HPS set-up schematic diagram

This developed model allows us to perform long and short term studies and analysis of the HPS in different geographical areas, providing that weather data (including daily solar radiation and temperature) and load demand for each area are available.

7.3 **Simulation input and output data**

In order to perform the simulation, it is very important to gather enough data about the system. Some site data is not available so therefore assumptions need to be made. Power demand also needs to be established.

Two main categories of input data are required for this simulation. The first is based on component technical characteristics. This data is mainly related to the simulation which can be expressed mathematically as studied in detail in the earlier chapters. The second category of data is based on geographical and weather information and the load demand.

7.3.1 Load demand

An important point in designing the hybrid power system is to define the power demand and estimated consumption. It is important to consider both short and long term requirements.

The following sections show in detail the proposed system expected load demand.

7.3.1.1 Assumptions

In order to establish the bases of this project, a few assumptions have been made as follows:

- This system will be installed to supply water to houses in a remote community with no power supply from the national grid
- It is assumed that there are 10 houses and in each house there is an average of 4 people. This means there are 40 people living in the community. It is assumed that there are about 50 sheep
- It is assumed that each person will consume about 150 litres each day and each sheep will drink about 15 litres [34]. Therefore, the total expected daily water consumption is about 6,500 litres
- It is assumed that the underground water is about 3 to 6 metres deep
- The tank will be elevated above the ground for 6 metres, to create enough pressure to allow water distribution by gravity
- The Nexa system is fuelled by dry, high purity hydrogen.

7.3.1.2 System Design and Equipment Selection

The project's key objective is to achieve a practical, working system. Since the test will be connected in the laboratory, an electronic load will be used to map the pump load and power consumption.

The main systems components are listed below and more details are shown in Table 7.1:

- Based on the water need, a 10,000 litres elevated water tank has been selected
- 0.5 HP (373W) water pump
- 2 x SCHOT POLYTM 230 Photovoltaic (PV) Solar panel each Nominal power of 230
- BALLARD 1.2kW Nexa power module PEMFC
- DC/DC converters
- Power management system and control unit
- Power storage system batteries (12V, 18 Amp x 3).

7.3.2 Weather data

Since solar radiation (W/m²) and ambient temperature (°C) have a direct impact on Photovoltaic solar panel power generation, it is important to obtain this data on an hourly basis as a minimum. Weather information is for the two proposed locations, Abha - Saudi Arabia and Cranfield University –UK.

Figures 7.3 and 7.4 show the monthly average solar radiation and temperature in both Abha and Cranfield. The measured average global solar radiation over the Abha area is almost double the solar energy at Cranfield. This highlights the difficulty of generating electric from solar panels during winter months in the UK.

Table 7.1 Main systems components summary

Water Tank	Unit	Value
Water tank		
Quantity		1
Capacity	Litre (l)	10,000
Height	Meter (m)	6
Water pump		
Type		Shallow well jet Pump.
Quantity		1
Power Max.	Watt (W)	373
Flow rate Max.	litre/hour (l/hr)	2,274
Suction left Max	Meter (m)	7.6
Discharge pressure Max.	Psig	58
Suction pipe size	Inch	1
Discharge pipe size	Inch	1
Photovoltaic solar panel (PV)		
Model		SCHOTT POLY^{TM} 230
Quantity		2
Nominal power for each panel	Watt (W)	230
Voltage at nominal power	Voltage (V)	30
Current at nominal power	Current (A)	7.66
Open-circuit voltage	Voltage (V)	36.9
Short-circuit current	Current (A)	8.33
Module efficiency level	%	13.7
Fuel Cell		
Model		BALLARD 1.2kW Nexa power module PEMFC
Power		
Rated net power	Watt (W)	1200
DC voltage range	Volt (V)	22 - 50
Rated voltage	Volt (V)	26
Rated current	Ampere (A)	46
Fuel		
Purity	%	≥99.99 H2
Pressure	Psig	10-250
Consumption	SLPM	≤18.5
Emissions		
water	mL/hr	≤870
Noise	dBA @ 1 m	≤72

7.3.3 Weather data

Since solar radiation (W/m²) and ambient temperature (°C) have a direct impact on Photovoltaic solar panel power generation, it is important to obtain this data on an hourly basis as a minimum. Weather information is for the two proposed locations, Abha - Saudi Arabia and Cranfield University –UK.

Figures 7.3 and 7.4 show the monthly average solar radiation and temperature in both Abha and Cranfield. The measured average global solar radiation over Abha area is almost double the solar energy at Cranfield. This highlights the difficulty of generating electricity from solar panels during the winter months in the UK.

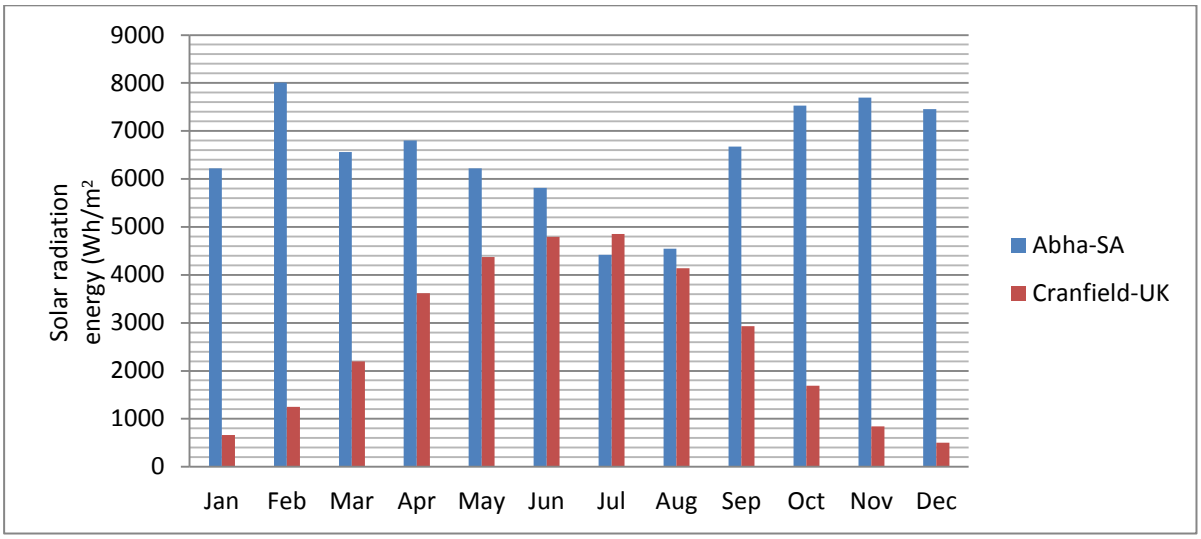

Figure 7.3 Monthly average solar radiation in Abha and Cranfield

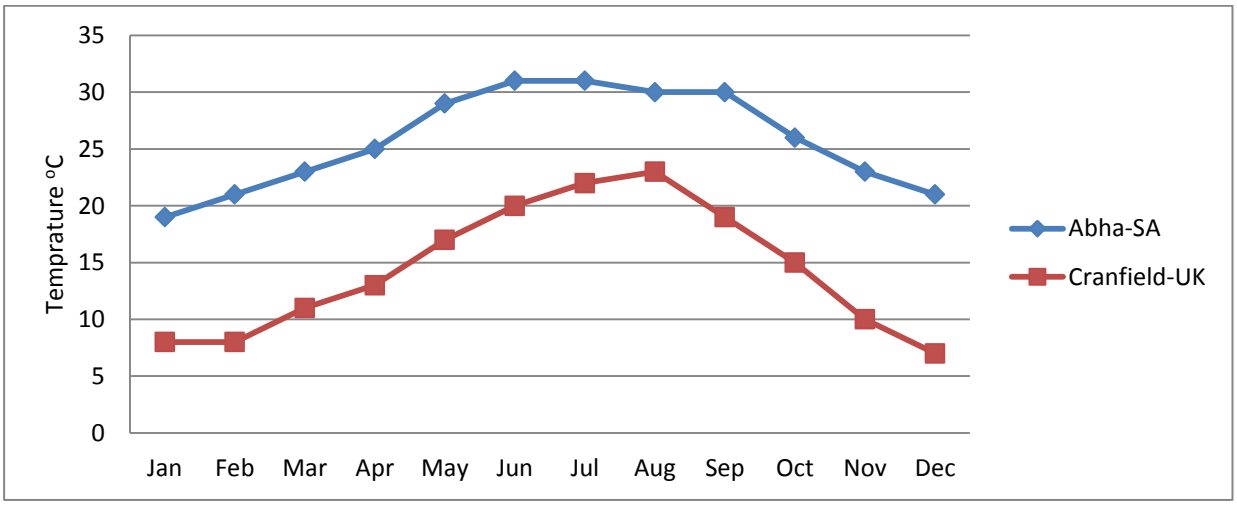

Figure 7.4 Monthly average ambient temperature in Abha and Cranfield

7.3.4 Study Scenarios

In this study, four study scenarios have been chosen to run the model in two different geographical locations. The first location is Abha in Saudi Arabia. In this location, two days have been selected: one in August and the second in January. The radiation and temperature for Abha were obtained from King Abdulaziz City for Science and Technology (KACST).

The second location is based at Cranfield University in the U.K. Two days have also been considered: again, one day in August and the second in January. The radiation and temperature data for Canfield were obtained from PVGIS © European Communities.

Water consumption was developed based on the earlier assumption made in section 7.3.1.

It was assumed that water consumption in summer is 10% higher than in winter months as shown in figures 7.5 and 7.4.

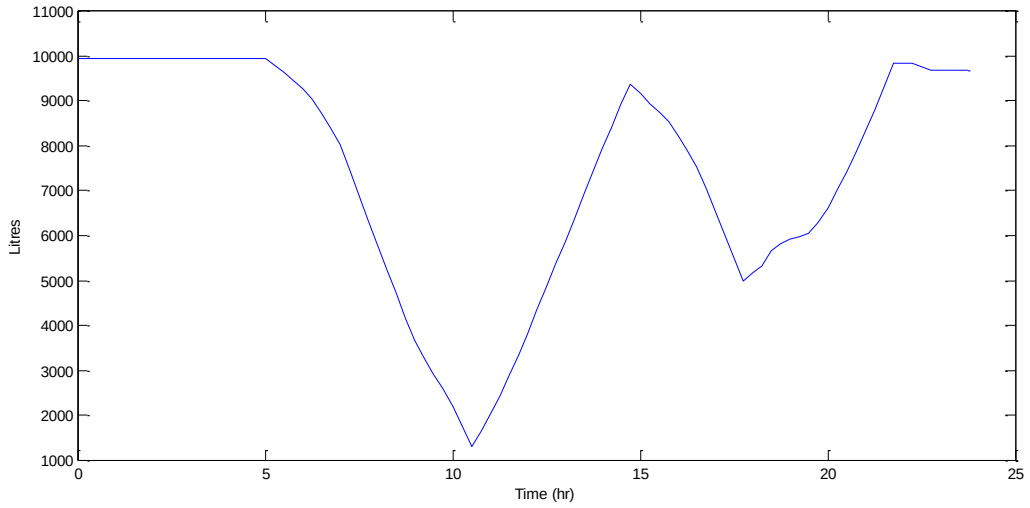

Figure 7.5 summer storage tank water capacity (Litres)

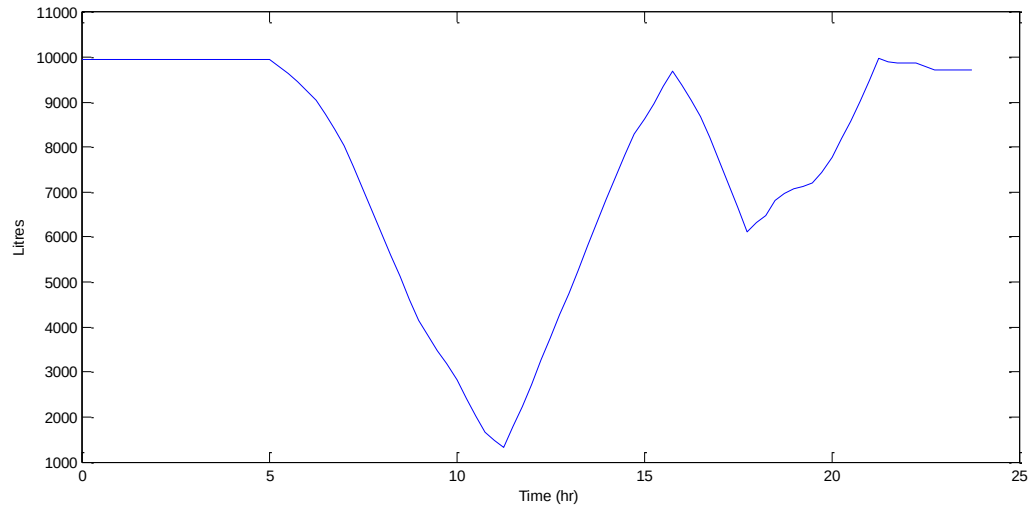

Figure 7.6 Winter storage tank water capacity (Litres)

It is important at the beginning of the study to highlight a few assumptions:

- Tank low level control is set at 10% of the tank capacity equivalent to 1000 litres
- The battery will stop giving power at 70% of its fully charged capacity.

- The battery maximum charging rate is 5.2 A based on 20% of the battery maximum power.

7.3.5 Abha Summer

The first two case study scenarios are to simulate the HPS behaviour in a remote area near Abha City**,** Saudi Arabia. Radiation and temperature were obtained from King Abdulaziz City for Science and Technology (KACST).

The load data has been set based on figure 7.5, a typical summer day based on radiation temperature data from 6th of August 2003.The model ran for 24 hours from 12:00 am to 11:45 pm.

As shown in figure 7.7, during early morning there was no water consumption. The water consumption started at about 5:00 am and reached its peak of 38 L/min at about 8:00 am, where most people are getting ready for work and watering the animals in the early morning. Water consumption then goes down during noon and starts to pick up again in the evening between 5:00 to 8:00 pm.

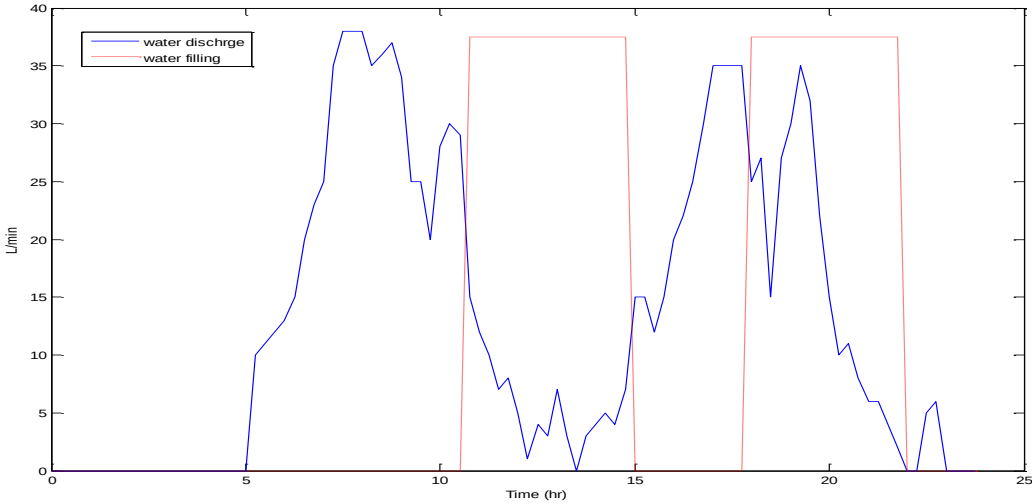

Figure 7.7 Abha summer water filling vs discharge flow rate (Litres/min)

At about 11 am the tank level reached the low level; at this point the water pump started and continued operating at constant flow for about 4 hours until the tank reached the maximum level. In the evening, the water pump began filling the tank again using batter power, even if the water level did not reach the low level, just to ensure there would be enough water during the night for any emergency need. Once the battery reached 70% of its power the fuel cell started to power the water pump and charge the battery. As shown in figure 7.8, for about 1 hour the fuel cell supplied

about 697 watts, then once the tank was full the fuel cell continued to charge the battery. Once the battery reached 90 % (fully charged) the fuel cell stopped.

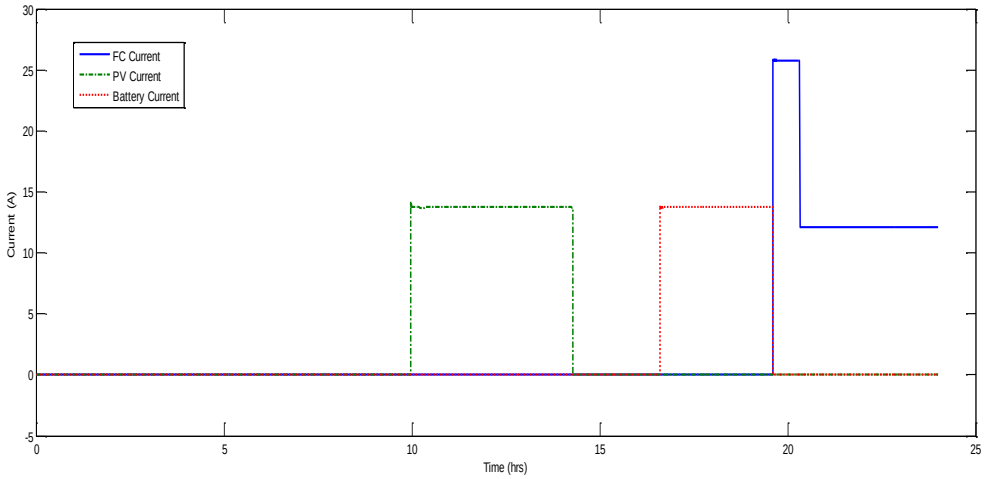

Figure 7.8 Abha summer power supply share

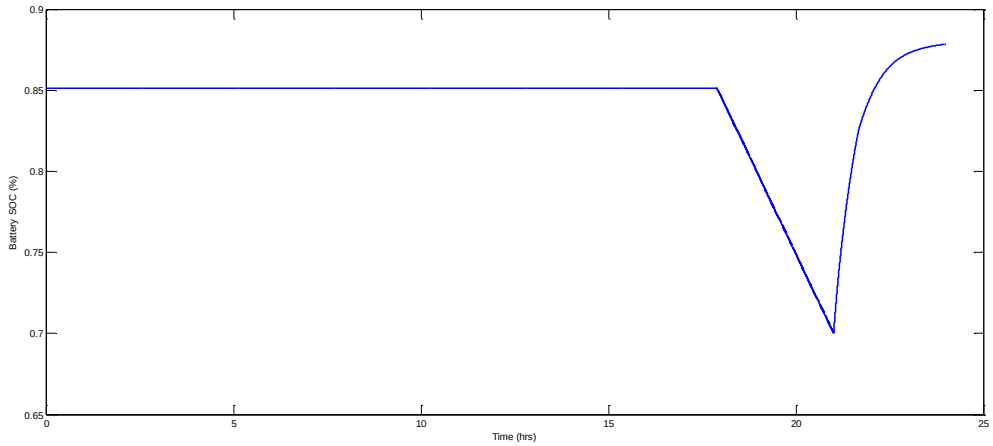

Figure 7.9 Abha summer battery charge status

7.3.6 Abha Winter (Cloudy Day)

This case is based on a cloudy day in January 2003.The effect of shade on the PV efficiency is very clear: by looking at figure 7.11, the power generated by the PV panels is unstable and fluctuating sharply. Connecting the battery in parallel with PV panels is essential in this case. The battery response to compensate the dramatic change in PV generated power is very good. The curve is showing over and undershoots which makes the operation unstable. A more advanced controller needs to be investigated in future work. Once solar power was lost the system stopped. Then after few hours the FC was started on a higher power rate to provide about 25 A to power the pump and charge the battery simultaneously. As the tank reached the

maximum level the FC cell current reduced to about 12 A to continue charging the battery.

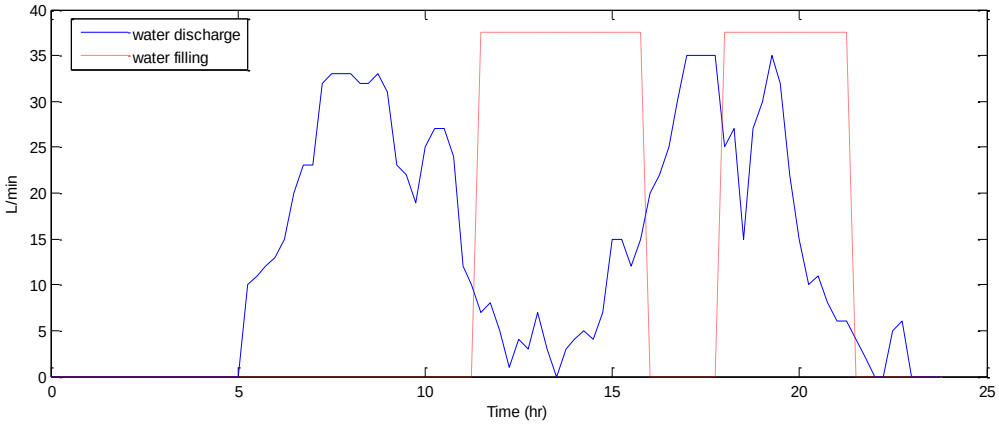

Figure 7.10 Abha winter water filling vs discharge flow rate (Litres/min)

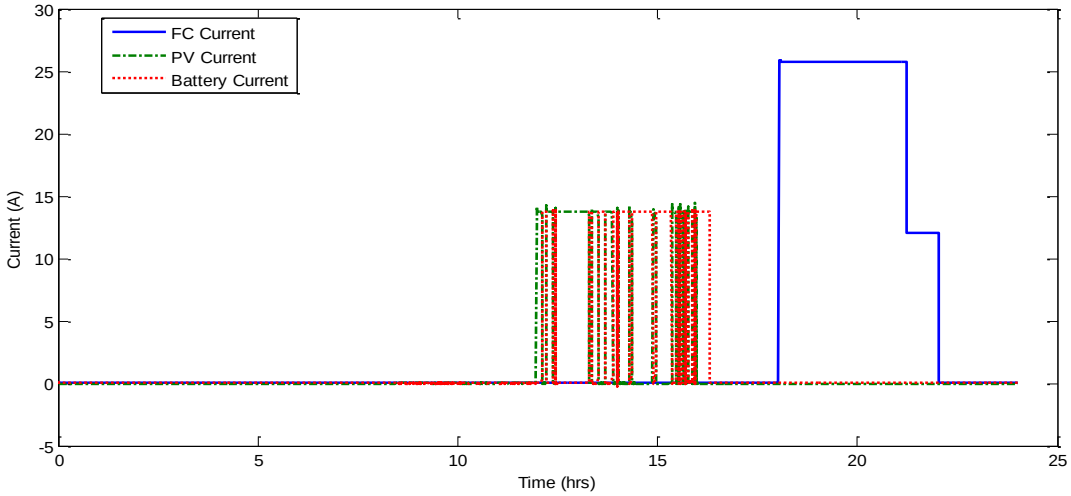

Figure 7.11 Abha winter power supply share

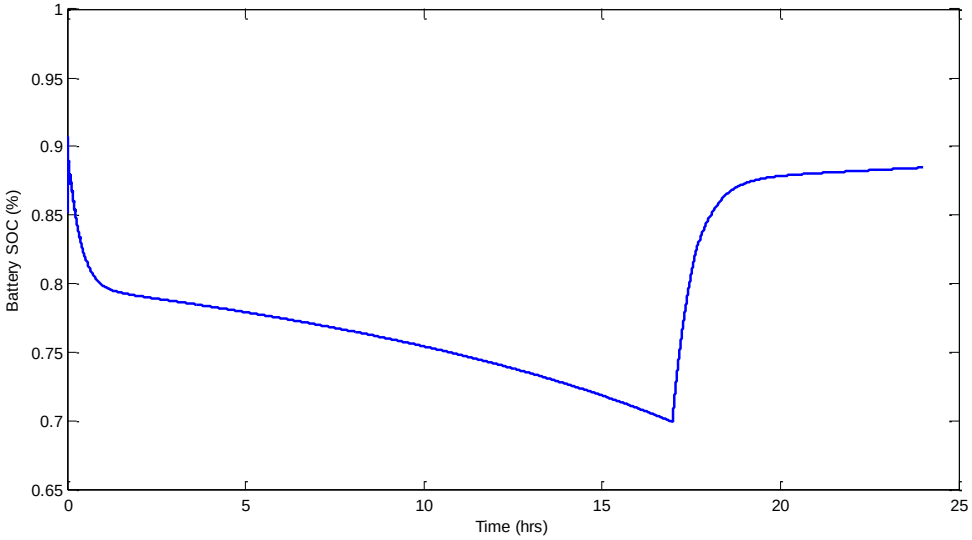

Figure 7.12 Abha winter battery charge status

7.3.7 Cranfield Summer

The second two case study scenarios are to simulate the HPS behaviour at Cranfield University - UK. The radiation and temperature were obtained from PVGIS © European Communities.

The load data has been set based on figure 7.5. A typical summer day was selected based on radiation temperature data of August average solar radiation. The model runs for 24 hours from 12:00 am until 11:45 pm.

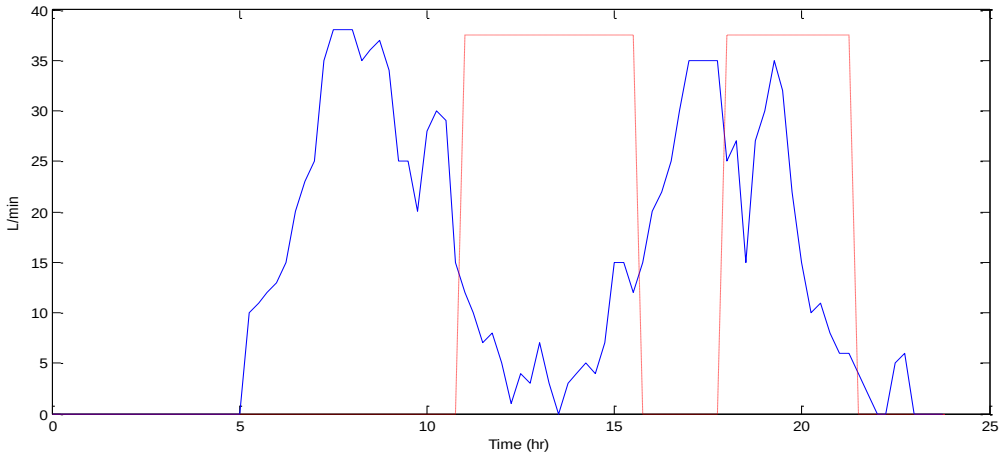

Figure 7.13 Cranfield summer water filling vs discharge flow rate (Litres/min)

As shown in figure 7.13 the water consumption starts declining early evening to zero consumption. From about 11:00 pm until 5:00 am during early morning there was no water consumption. Then as people woke up and started washing and showering, water consumption reached the maximum between 8:00 to 9:00 am. Water consumption then decreased around noon, picking up again in the evening between 3:00 and 8:00 pm.

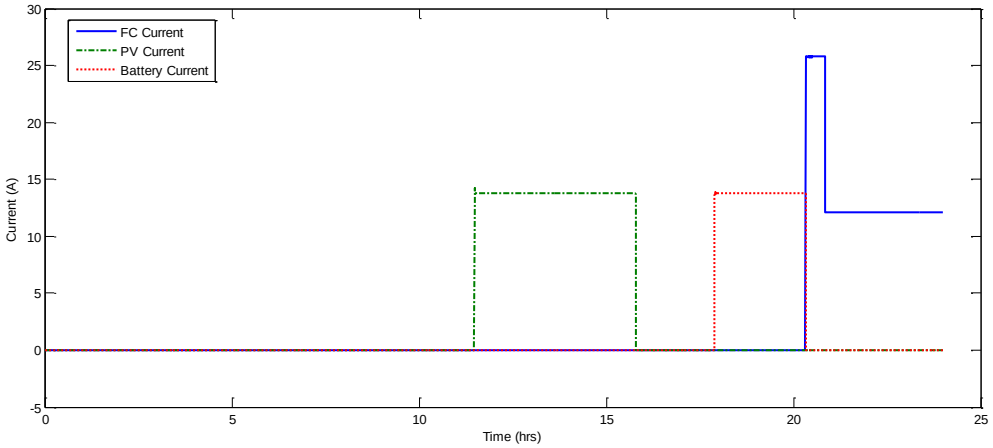

Figure 7.14 Cranfield summer power supply share

By looking at power supply share curves as shown in figure 7.14, the system in the morning shows the tank water level, battery charge level and the available power from the radiation. The battery charge in the morning was about 90%; therefore no charging process will take place.

Once the water tank water reaches low level, the solar power is used to pump the water as its primary source, backed up by the battery bank. It can be noticed that between 2:30 and 4:30 the solar could not meet the power demand, therefore the battery bank compensated for the shortage. Simultaneously, whenever there is access to solar power, the system utilizes this power to charge the battery optimize power use.

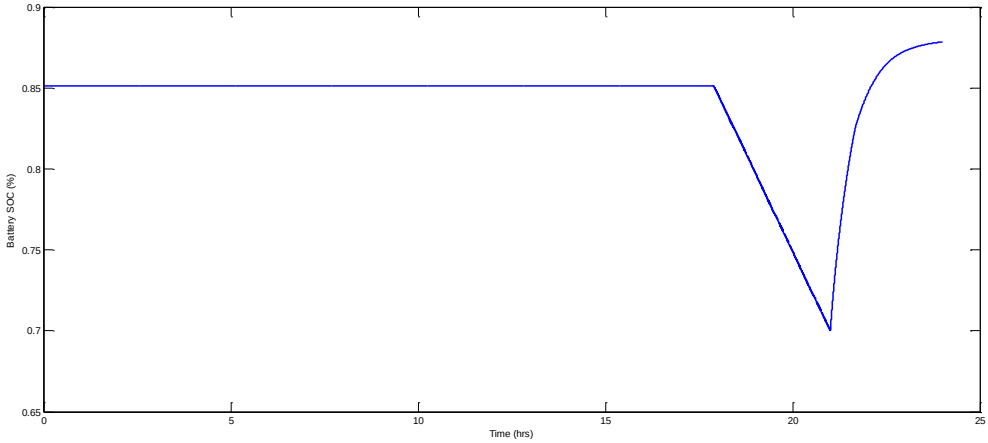

Figure 7.15 Cranfield summer battery charge status

7.3.8 Cranfield Winter

The solar radiation data obtained for this scenario is based on January average solar radiation in the Cranfield area. At an overall glance it is clear that the major effect of the geographical location and the time of the year on the system. (Figure 7.17) shows that no power has been generated from the solar panel, although the sun is shining. The solar radiation in winter in the earth's northern atmosphere reaches its minimum.

The voltage generated from the solar panel could not reach 27 V, the minimum input voltage the DC converter required to operate. Therefore, as the tank water reached low level, the system control checked the available power based on defined priority order. Because the system did not detect any power from the solar panel, the water pump load was obtained from the battery back-up.. The battery powered the pump

full load until battery reached 70% of its charge, and then the controller stopped the pump.

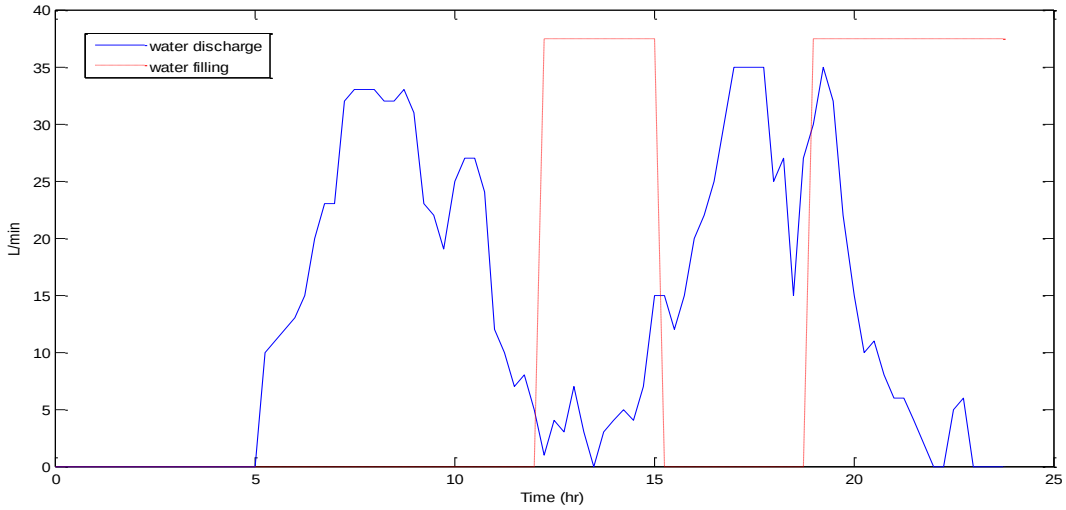

Figure 7.16 Cranfield winter water filling vs discharge flow rate (Litres/min)

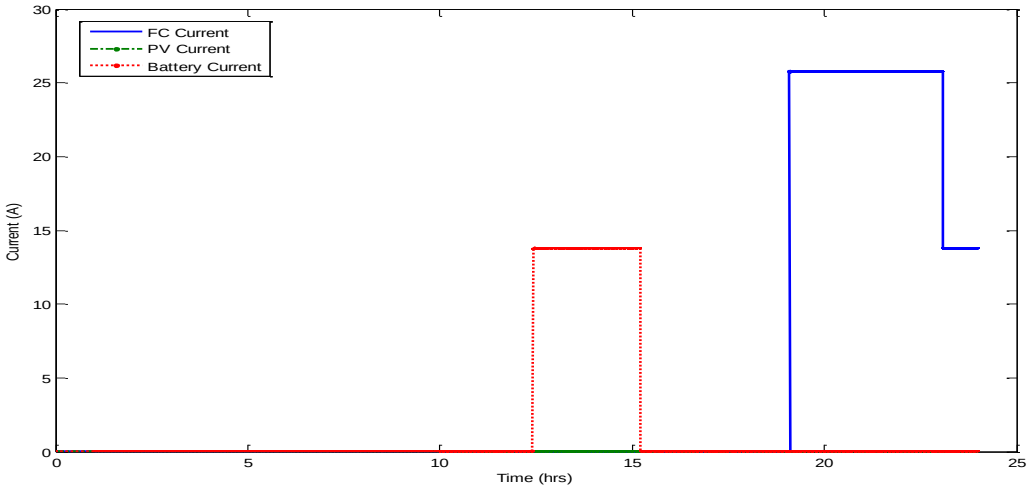

Figure 7.17 Cranfield winter power supply share

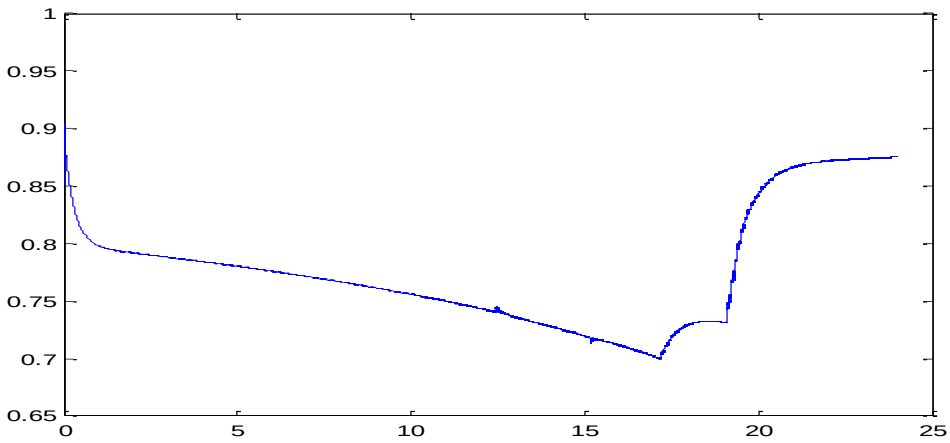

Figure 7.18 Cranfield winter battery charge status

By the time the battery bank reached 70% of its capacity, the water tank had only reached about 7000 litres. To minimize the use of FC, the controller did not start the FC cell to take over the battery supplying power to the pump. Alternatively, the HPS turned to stand by status until the water tank reached low level. The FC was then started to power the water pump and charge the battery at the same time.

The main advantage of this scenario is to minimize the start- stop of FC as much as possible and to ensure that the FC operates at a higher power rate to utilize FC cell best efficiency zone.

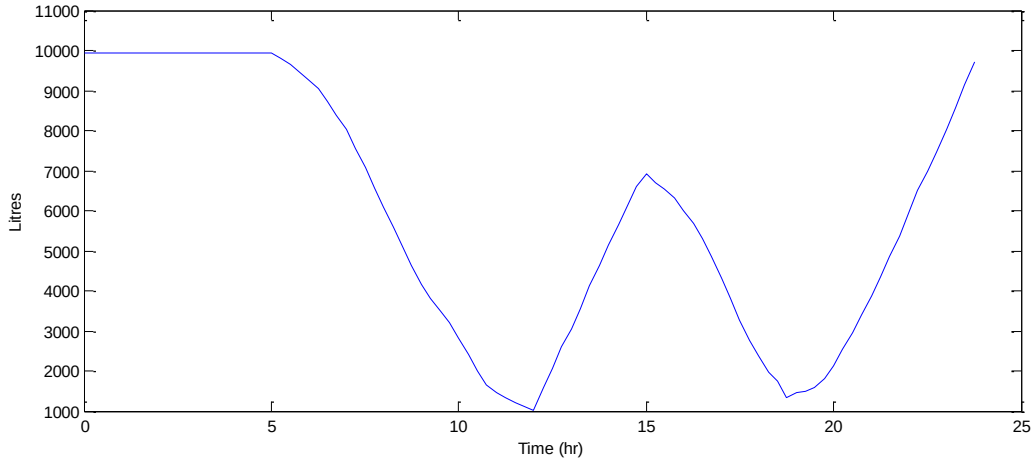

Figure 7.19 Storage tank water capacity (Litres)

Once the battery had charged to 100%, the fuel cell load reduced to 373 watts to meet the water pump load. Once the water tank reached high level, the fuel cell stopped and the HPS status changed to standby.

7.4 **Chapter summary**

In this chapter two main cases were explored to validate the hybrid system performance in two different geographical and environmental conditions. In each case two scenarios were studied: the first scenario was based on a simulation during 24hrs in the month of August, the second on a simulation of 24hrs in the month of January. In this chapter, the weather conditions of both locations were compared, and then study assumptions, input/output data and load demand were defined.

The first case was based on Saudi Arabian environmental conditions, where it is hot and sunny most of the year. This scenario allowed more utilization of power generated from sunlight via PV cells and reduced the dependence on power

produced by fuel cell. In Abha it was clear that in both scenarios (winter and summer), the solar radiation did not vary that much to affect operational stability.

In the second case, the hybrid system was examined in UK environmental conditions, where it is cold and cloudy most of the year. In this case was at minimum especially during winter, which leads to higher dependence on the fuel cells. It was clear from this scenario that there was not enough solar radiation in winter during the month of January, therefore the system was powered by Fuel Cell and batteries.

8 CONCLUSIONS AND RECOMMENDATIONS

This thesis presented an overview of the world's energy, the current high power consumption and expected future demand. Recent high power prices and rising public awareness are the main driving force behind the growing research interest in clean, renewable energy alternatives.

The main overall goal of this project was to investigate the operation and feasibility of a stand-alone FC/PV /Battery Hybrid Power System, which can be installed in a remote area to provide the power to pump water from a well to an elevated tank to supply water for a small community. The main conclusion and recommendations are summarized in the following sections.

8.1 **Hybrid Power System (HPS)**

Connecting remote areas such as islands or small communities in deserts to the grid can be very expensive and is not commercially viable. Therefore a standalone power system is the more viable choice. Due to the increased cost of fuel and the increased interest in finding cheaper and clean choices, HPS were introduced. These are either integrated with the conventional power generator (PV/ Diesel/ Battery HPS) or used as a combination of renewable HPS (PV/Wind turbine/FC HPS). Based on an actually implemented project, the PV/Diesel generator/Battery HPS installed in Tanzania 2006, the life cycle cost is cheaper than traditional Diesel generator as explained in section 3.4.3

8.2 **Simulation of FC/FV/Battery HPS**

In this research project, PV/FC/ Battery HPS has been developed using MATLAB/Simulink to predict system operation and performance in different environments and geographical conditions. To achieve that a model was developed for each of the system sub-components, including the 1.2 KW Nexa PEMFC, Photovoltaic solar panel, lead acid batteries, bi-directional DC/DC converters and the step down DC/DC converters. Experimental data was obtained to validate each part of the model. The result showed a good agreement between the experimental and model result as was shown in chapter 5.

8.2.1 PEMFC Model

The PEMFC model developed was based on an electrochemical modelling approach. A Mathematical model was first obtained and then implemented in Simulink. Following the model validation, the dynamic performance and transient responses were investigated under different loads. Different dynamic responses were performed for different cases: start-up, shut-down, irregular load variation. The main point to highlight regarding the PEMFC dynamic response is its limitation of response to sudden load change; for example an instant increase in the load from 5A to 35A caused the Nexa PEMFC to shut down. This is important in application where there is a recruitment of fast response to connect the Nexa system in a hybrid configuration, e.g. consisting of batteries or a super capacitor.

8.2.2 PV Solar Panel Model

Following on from the literature review, the one-diode model was used in this study due to its simplicity and reasonable accuracy. The model was validated by comparing experimental and simulation data which showed a good agreement.

8.3 Case studies

Two main scenarios were explored to validate and investigate the HPS performance in two different geographical and environmental conditions. In each location the model was run for 24 hours, once in summer and the other in winter.

8.3.1 Abha City Saudi Arabia

In this case, the hybrid system was examined in Abha city, which is located in the south of Saudi Arabia. This area is hot and sunny for most of the year. Two conditions were studied; one during summer and the second during winter.

In the summer, the power generated by solar panels was stable and enough to power the pump.

The winter case was based on a cloudy day when the power generated by the solar panels was unstable and fluctuating sharply. Connecting the battery in parallel with solar panels essential in this case, to ensure stable power supply to meet demand requirement. As a future work, an advance controller needs to be investigated to improve the load sharing.

8.3.2 Cranfield UK

In the test case at Cranfield, UK, the environmental conditions were mostly cold and cloudy for a large part of the year. Again two cases were studied one during the summer and one in winter. The summer scenario showed that the solar panel was providing enough power to operate the pump, apart from few hours in the afternoon when the battery was needed to share the load.

As for the winter case, solar radiation–was very low. The pump, therefore, was powered first by the battery and then, as battery level dropped to about 70%, the fuel cell started to supply power to the pump and to also charge the batteries. It is clear from this case that, during winter, the solar panel cannot provide sufficient power to operate the pump and charge the battery in climates similar to those of the UK.

8.4 Recommendations and Future Work

To improve the efficiency and performance of the HPS the following future work is recommended:

- During designing the HPS it is important to consider the geographical data to investigate the best combination of the HPS component which most fits the specific area/location. For example, by using wind turbine the system will reduce the dependence on fuel cells at night. Specifically in climates similar to the UK, this could also be used, during winter or cloudy days.
- Electrolyser can be added to the system. This will utilize the generated unused electricity and generate hydrogen which can be used and stored to fuel the fuel cell.
- Using pure Oxygen for the fuel cell instead of air can improve fuel cell efficiency which can be extracted from the electrolyser if included.
- Improving model accuracy with regard the effect of ambient temperature and wind speed and install temperature sensor and wind speed meter.

REFERENCES

[1] Sen, Z., (2008), "Solar Energy Fundamentals and Modeling Techniques Atmosphere, Environment, Climate Change and Renewable Energy", Springer-Verlag London Limited.

[2] SWMM5 - Stormwater Management Model [Online]. Available at: http://www.swmm2000.com/forum/topics/global-carbon-cycle [Accessed: 09 Feb., 2013].

[3] International Energy Outlook 2010 [Online]. Available at: http://www.eia.doe.gov/oiaf/ieo/world.html [Accessed: 09 Feb. 2013].

[4] Current World Oil Situation [Online]. Available at: http://planetforlife.com/oilcrisis/oilsituation.html [Accessed: Feb. 09, 2013].

[5] International Electric Energy Usage/Demand [Online]. Available at: http://www.geni.org/globalenergy/library/energytrends/currentusage/index.shtml [Accessed: 09 Feb. 2013].

[6] Edwards, P. P., Kuznetsov, V. L., David, W. I. F. and Brandon, N. P. (2008), "Hydrogen and fuel cells: Towards a sustainable energy future", Energy Policy, vol. 36, no. 12, pp. 4356-4362.

[7] European Photovoltaic Industry Association, Photovoltaic energy, electricity from the sun Available at: http://www.epia.org/publications/epia-publications.htm [Accessed: 09 Feb. 2013].

[8] Alliance for Rural Electrification [Online]. Available at: http://www.ruralelec.org [Accessed: 03 Feb. 2013].

[9] Wireless Network of Small-scale Hybrid solar generators integrated with Fuel-cell: a step towards the Solar-Hydrogen Economy [Online]. Available at: http://www.elettronicasanterno.it/system/Ffiles/documents/materiale/EuroSun_Wireless.ppt [Accessed: 09 Feb. 2013].

[10] Stand Alone Power System Coupling a PV Field and a Fuel Cell: Experimental Results of the FC System [Online]. Available at: http://www.pvfcsys.cma.fr/publications/articleFrDeFconf.pdf [Accessed: 03 Mar. 2013].

[11] Zhenchao, X., Chaejoo, M., Younghak, C., Jungmin, L.and Taegon, K. (2008), "Remote Monitoring of Wind-Photovoltaic Hybrid Generation System Using Mobile Phone and Internet"[Online]. Available at: http://www.energy.wesrch.com/paper_details/pdftext/TR16RRXEWDCTX/remote-

monitoring-of-wind-photovoltaic-hybrid-generation-system-using-mobile-phone-and-internet [Accessed: 05 Feb. 2013].

[12] Isolated Hybrid installation demonstration to cover single family house electrical consumptions with Hydrogen storage (IHAVU Project), IEA Hydrogen Implementing Agreement Task 18 Case Study Subtask C [Online]. Available at: http://www.ieahia.org/pdfs/Task18_IHAVU_CaseStudy(Spain).pdf [Accessed: 05 Feb. 2013].

[13] Dehghan, S., Kiani, B., Kazemi, A. and Parizad, A. (2009), "Optimal sizing of a hybrid wind/PV plant considering reliability indices", Proceedings of World Academy of Science, Engineering and Technology, vol. 56, pp. 527-535.

[14] El-Shatter, T. F., Eskander, M. N. and El-Hagry, M. T. (2006), "Energy flow and management of a hybrid wind/PV/fuel cell generation system", Energy Conversion and Management, vol. 47, no. 9-10, pp. 1264-1280.

[15] Rajashekara, K. (2005), "Hybrid fuel-cell strategies for clean power generation", IEEE Transactions on Industry Applications, vol. 41, no. 3, pp. 682-689.

[16] San Martín, J. I., Zamora, I., San Martín, J. J., Aperribay, V. and Eguia, P. (2010), "Hybrid fuel cells technologies for electrical microgrids", Electric Power Systems Research, Vol. 80, no. 9, pp. 993-1005.

[17] Dihrab, S. S. and Sopian, K. (2010), "Electricity generation of hybrid PV/wind systems in Iraq", Renewable Energy, vol. 35, no. 6, pp. 1303-1307.

[18] Pecen, R. and Stigliani, W. (2005), "Design and Implementation of 5 kW Hydrogen Fuel-Cell Station using Wind Solar, and Hydro resources at Hickory Hills Park in Iowa, USA", Proceedings International Hydrogen Energy Congress and Exhibition IHEC

[19] Somasak, T., Boonbumrung, U., Tanchareon, S., Jeenkaokam, N. and Jovacate, C. (2004), "PV- diesel Stand Alone Hybrid System at a Royal Project Research Station: Observations on Power Quality", Technical Digest of the International PVSEC-14, Thailand, 2004.

[20] Uchida, H., Haraki, T., Oishi, K. and Miyamoto, Y. (2005) "A wind & Solar Hybrid Energy storage system using Nano-structured Hydrogen storage alloy", Proceddins international Hydrogen Energy Congress and Exhibition IHEC 2005.

[21] Larminie, J. and Dicks, A. (2003), "Fuel Cell System Explained Second Edition", John Wiley & Sons Ltd.

[22] Spiegel, C. (2008), "Fuel Cell Modeling and Simulation Using MATLAB", Elsevier Inc.

[23] Mattos, L.V. and Noronha, F.B. (2005) "Hydrogen production for fuel cell applications by ethanol partial oxidation on Pt/CeO2 catalysts: the effect of the reaction conditions and reaction mechanism", Journal of Catalysis, vol. 233, pp. 453-463.

[24] U.S. department of energy, Hydrogen Production [Online]. Available at: http://www.hydrogen.energy.gov/production.htm [Accessed: 03 Feb. 13].

[25]Hydrogen and fuel cell Review of national R&D Programs (2002), International Energy Agency [Online]. Available at: http://www.iea.org/books [Accessed: 03 Feb. 2013].

[26]Hydrogen energy and fuel cells – a vision of our future, European Commission, Directorate-General for Research [Online]. Available at:, <http://europa.eu.int/comm/research/rtdinfo_en.html> [Accessed: 03 Feb. 03, 2013].

[27] Krichen, L. (2007), "Modeling and Control of a Hybrid Renewable Energy Production Unit", ICGST-ACSE Journal, Volume 7, Issue 1, May 2007.

[28] Fadali, H.. (2008), "Fuel Cell Distributed Generation: Power Conditioning, Control and Energy Management (unpublished Master thesis)", University of Waterloo, Canada.

[29] Lehman, P., Chamberlin, C., Zoellick,C., Engel, R. and Rommel, D. (2002) "Fuel Cell/Photovoltaic Integrated Power System For a Remote Telecommunications Repeater", Manuscript for 14th World Hydrogen Energy Conference, June 2002

[30] Hybrid power systems based on renewable energies: a suitable and cost-competitive solution for rural electrification [Online]. Available at: http://www.ruralelec.org/fileadmin/DATA/Documents/06_Publications/Position_papers/ARE-WG_Technological_Solutions_-_Brochure_Hybrid_Systems.pdf [Accessed: 05 Feb. 2013].

[31] Ben Slama, S., Ben Chaabène, A. and Chérif, A (2012) "Efficient Design of a Hybrid (PV-FC) Water Pumping System with Separate MPPT Control Algorithm", IJCSNS International Journal of Computer Science and Network Security, VOL.12 No.1, January 2012

[32] EG & G Services (2000), "Fuel Cell Handbook" (Fifth Edition) Parson, Inc., West Virginia, USA.

[33] Ballard (2003), "Nexa™ Power Module User's Manual", MAN5100078, Ballard Power Systems Inc, Canada.

[34] Average water used per person per day[Online]. Available at: http://www.data360.org/dsg.aspx?Data_Set_Group_Id=757 [Accessed: 03 Feb. , 2013].

[35] El-Sharkh, M. Y., Rahman, A., Alam, M. S., Byrne, P. C., Sakla, A. A. and Thomas, T. (2004), "A dynamic model for a stand-alone PEM fuel cell power plant for residential applications", Journal of Power Sources, vol. 138, no. 1-2, pp. 199-204.

[36] The online Fuel Cell information resources, (2000) [Online]. Available at: www.fuelcells.org/basics/apps.html [Accessed: 03 Feb. 2013].

[37] Amphlett, J. C., Baumert, R. M., Mann, R. F., Peppley, B. A., Roberge, P. R. and Rodrigues, A. (1994), "Parametric modelling of the performance of a 5-kW proton-exchange membrane fuel cell stack", Journal of Power Sources, vol. 49, no. 1-3, pp. 349-356.

[38] Padullés, J., Ault, G. W. and McDonald, J. R. (2000), "An integrated SOFC plant dynamic model for power systems simulation", Journal of Power Sources, vol. 86, no. 1-2, pp. 495-500.

[39] History: Photovoltaics Timeline 1960 to present [Online]. Available at: http://inventors.about.com/od/timelines/a/Photovoltaics_2.htm [Accessed: 03 Feb. 2013].

[40] A walk through time [Online]. Available at: http://www.pvresources.com/en/history.php [Accessed: Mar. 05, 2013].

[41] Photovoltaic History[Online]. Available at: http://www.sunlightelectric.com/pvhistory.php [Accessed: 03 Feb. 2013].

[42] Global market outlook for photovoltaics until 2014, May 2010 update, European Photovoltaic Industry Association [Online]. Available at: <www.epia.org> [Accessed: 03 Feb. 2013].

[43] Handbook for Solar Photovoltaic (PV) Systems[Online]. Available at: http://www.ema.gov.sg/images/files/handbook_for_solar_pv_systems.pdf [Accessed: 03 Feb. 2013].

[45] Malaysie Building Integrated Photovoltaic- Project (MBIPV) (2009), PV Industry Handbook, Malaysian Industrial Development Authority.

[46] Honda Soltec to Release New Enhanced Thin-film Solar Cell in 2011 [Online]. Available at:

http://world.honda.com/news/2011/c110126Solar-Cell/index.html?r=r [Accessed: 03 Feb. 2013].

[47] Solar photovoltaic system[Online]. Available at: http://www.greenenergygreenhome.com/solar-photovoltaic-system[Accessed: 05 Feb. 2013].

[48] How do Photovoltaics Work? [Online]. Available at: http://science.nasa.gov/science-news/science-at-nasa/2002/solarcells/ [Accessed: 03 Feb. 2013].

[49] Kleinkauf, W., Ibrahim, M., Haas, O. and Gruß, B. (2003), "Basics of Hybrid Technology for Grid Compatible Stand-Alone Plants", 2nd European PV-Hybrid and Mini-Grid Conference, Kassel, Germany, 2003, pp. 61-67.

[50] Caselitz, P., Lehmkuhl, D. and Panahandeh, B. (2003) "ISET Alternative Power Library- Universal Model Library for Simulation of Decentralised Power Supply Systems", 2nd European PV-Hybrid and Mini-Grid Conference, Kassel University, Germany, 2003, pp. 456-461.

[51] Li, X., Qu, S., Yu, H., Hou, M., Shao, Z. and Yi, B. (2009), "Membrane Water-Flow Rate in Electrolyzer Cells with a Solid Polymer Electrolyte (SPE)", Journal of Power Sources, vol. 190, no. 2, pp. 534-537.

[52] Nam, J. H. and Kaviany, M. (2003), "Effective Diffusivity and Water-Saturation Distribution in Single- and Two-Layer PEMFC Diffusion Medium", International Journal of Heat and Mass Transfer, vol. 46, no. 24, pp. 4595-4611.

[53] Tang, Y., Yuan, W., Pan, M., Li, Z., Chen, G. and Li, Y. (2010), "Experimental Investigation of Dynamic Performance and Transient Responses of a kW-Class PEM Fuel Cell Stack under Various Load Changes", Applied Energy, vol. 87, no. 4, pp. 1410-1417.

[54] Hydrogen Gas Safety Self-Study [Online]. Available at: http://www.usmra.com/repository/category/mine_gases/hydrogengassafety.pdf [Accessed: 03 Feb. 2013].

[55] Im218. Step Down DC/DC Converter. Zahn Electronics , Inc, Franksville, WI, (2001) [Online]. Available at: http://www.zahninc.com/httpzahninc.comssloose.html [Accessed: 03 Feb. 02, 2013].

[56] Ramsden, E., (2006), "Hall-Effect Sensors - Theory and Application", 2nd Edition, Elsevier.

[57] Tsai,H., Tu, C. and Su, Y. Member, IAENG(2008) "Development of Generalized Photovoltaic Model Using MATLAB/SIMULINK", Proceedings of the World Congress on Engineering and Computer Science 2008.

[58] Francisco M. González-Longatt, (2005), “Model of Photovoltaic Module in Matlab™”, 2DO CONGRESO IBEROAMERICANO DE ESTUDIANTES DE INGENIERÍA ELÉCTRICA, ELECTRÓNICA Y COMPUTACIÓN (II CIBELEC 2005).

[59] Mohsen Taherbaneh, Gholamreza Farahani and Karim Rahmani, (2011), “Evaluation the Accuracy of One-Diode and Two-Diode Models for a Solar Panel Based Open-Air Climate Measurements”, Solar Cells – Silicon Wafer-Based Technologies, Prof. Leonid A. Kosyachenko (Ed.), ISBN: 978-953-307-747-5, InTech [Online]. Available at: http://www.intechopen.com/books/solar-cells-silicon-wafer-based-technologies/evaluation-the-accuracyof-one-diode-and-two-diode-models-for-a-solar-panel-based-open-air-climate-m [Accessed: 03 Feb. 2013].

[60] Huan-Liang Tsai, (2010), “Insolation oriented model of photovoltaic module using Matlab/Simulink”, Solar Energy Vol. 84, (2010) 1318-1326.

[61] F. Adamo, F. Attivissimo, A. Di Nisio, A. M. L. Lanzolla, M. Spadavecchia, (2009), “Parameters Estimation for a Model of Photovoltaic Panels”, XIX IMEKO World Congress, Fundamental and Applied Metrology, September 6-11, 2009, Lisbon, Portugal

Appendix A
Nexa Power Module Product Specification Definitions

Beginning of Life (BOL)	Within the first 40 hours of module operation, within 90 days of receipt from Ballard.
End of Life (EOL)	Characterised by performance below 22V or a non-repairable fuel cell stack failure.
Cold Start	The temperature of the entire Nexa TM power module is at equilibrium with the ambient air temperature.
Indoors or Outdoors	Any location where the Nexa TM power module is protected by the end product outer enclosure against wet, marine, freezing or other inclement conditions and against sand, dust or other particulates.
Uninstalled	Not installed into an enclosure nor integrated with an external thermal management system, fuel supply system or power conditioning system.
Standard Conditions	Evaluated at sea level at an ambient (cooling air and oxidant air) temperature of 30°C.
Voltage at Rated Power	Measured as the minimum 60 second running average within the first 30 minutes of continuous use. At time of module shipment, Rated Power and Voltage will be within +/- 5% of listed specifications.

OUTPUTS	Requirement	Definition	Quantity
Power[1]	Rated Power	Capacity at Standard Conditions, BOL	1200 W
	Voltage	Operating voltage range	22 V to 50 V
		Voltage at Rated Power	26 V
	Start-up Time	Minimum time to achieve Rated Power from a Cold Start condition	2 minutes
Emissions	Noise	Maximum noise emission at 1m	72 dBA
	Water	Maximum quantity of liquid water produced at Rated Power	870 mL/hr
Physical	Dimensions	L x W x H	56 x 25 x 33cm
	Mass	Total system mass	13 kg
Lifetime	Operating Life	Minimum number of operating hours before EOL	1500 hours
	Cyclic Life	Minimum number of start-up & shut-down cycles before EOL	500
	Shelf Life	Minimum storage (non-operation) before EOL	2 years
INPUTS	Requirement	Definition	Quantity
Fuel	Purity	Lowest acceptable concentration of hydrogen	99.99% H_2 (vol)
	Pressure	Allowable range of inlet supply pressure[2]	70 – 1720 kPa(g)
	Acceptable Impurities	Maximum total inert fluids (including helium, argon, nitrogen and water vapour)	0.01% (vol)
		Maximum CO and CO_2 combined	2 ppm (vol)
		Maximum total hydrocarbon	1 ppm (vol)
		Maximum oxygen	500 ppm (vol)
	Consumption	Maximum fuel consumption at Rated Power	<18.5 SLPM
Power Conditioning	Current Ripple	Maximum acceptable current ripple at 120 Hz, with respect to average DC net output current	24.7% RMS 35% peak-peak
DC Power Supply	Voltage	Allowable range of input voltage	18 V to 30 V
	Power	Maximum power draw during start-up	60 W
Operating Environment	Location	Acceptable locations for use	Indoors & Outdoors
	Temperature Range	Range of acceptable ambient, cooling air and oxidant air temperatures	3°C - 40°C
	Relative Humidity	Range of acceptable ambient relative humidity	0% - 95% (non-condensing)
	EMI Tolerance	Tolerant to and operates safely in the EMI environment specified by	UL 991

Appendix B
Nexa Power Module User's Manual

enter a Non-Restartable mode for safety reasons. In these cases, the system must be reset by a BALLARD Field Service or Customer Support representative.

7.3 Communications

A serial port is used to communicate information about fuel cell operation to the OEM and to communicate diagnostic and instructional information from the OEM to the Nexa™ system. The serial port interface uses full duplex communication, a pair of wires for transmission, and a pair of wires for reception. The full duplex communication allows asynchronous data transmission without needing to handle bus contention. The differential voltage levels used by the serial port are defined by the RS-485 standard. The following items outline the features of the serial port communications:

1. Communication is asynchronous at 9600 baud, with the Nexa™ system sending a data stream to the OEM approximately once every 200 ms.
2. SLIP (Serial Line Internet Protocol, Internet RFC 1055) is used to encode and decode the messages sent between devices. The SLIP code uses a one-byte tag (0xC0) at the beginning and at the end of each message. Three other special characters called "escape characters," 0xDB, 0xDC, and 0xDD are required to handle cases where 0xC0 must occur in the middle of the message.
3. The message from the Nexa™ power module to the OEM will always include a 40 bytes segment at the beginning of the message that includes all relevant operating data for the OEM. Up to an additional 100 bytes may be added for diagnostic and fault code retrieval purposes to the end of the message. These bytes should be considered unused bytes by the OEM except for the purposes of computing the checksum at the end of the message.
4. In addition to the varying length of the message that accounts for the diagnostic transmission, additional bytes are required to handle the transmission of the "escape characters".
5. A check sum is computed over the entire message and displayed as the last byte at the end of the message. The check sum is computed as a simple summation of the message bytes. Overflow bits are discarded. The Check Sum does not include the Tags or any "escape characters."
6. Each character is sent containing 1 start bit, 8 data bits, no parity bit, and 1 stop bit.
7. The format for the message from the Nexa™ system to the OEM is given below:

Tag	Status	Fail Code	Warning Bitmap	Last Command Acknowledge	Stack Temperature	Stack Voltage	Stack Current	Hydrogen Pressure

Hydrogen Concentration	Cumulative Hydrogen Consumption	Oxygen Concentration	Ambient Temperature	Purge Cell Voltage

Additional diagnostic and fault code bytes (0 to 100 extra bytes)	Check Sum	Tag

8. Information in the message header and footer (the 2 Tags, the Status, the Fail Code, the Warning Bitmap, the Last Command Acknowledge, and the Check Sum) are sent as single bytes.

9. The Nexa™ system has the following Status Codes:

   0x00 = Standby
   0x01 = Start up
   0x02 = Normal Operation
   0x03 = Warning
   0x04 = Normal Shut Down
   0x05 = Failure Shut Down
   0x06 = Non Restartable

10. The Nexa™ system has the following Fail Codes:

    0x00 = Normal Operation
    0x01 = High Fuel Cell Stack Temperature
    0x02 = Low Fuel Cell Stack Voltage
    0x03 = High Fuel Cell Stack Current
    0x04 = Low Cell Voltage
    0x05 = Low Fuel Pressure
    0x06 = Fuel Leak Detected
    0x07 = Low Oxygen Concentration
    0x08 = Low Ambient Temperature
    0x09 = Low Purge Cell Voltage
    0x0A = Low Battery Voltage
    0x0B = Startup Time Expired
    0x0C = Self Test Fault
    0x0D = General Software Fault
    0x0E = Spurious Interrupt Fault

11. The Nexa™ system has the following Warning Bitmap Codes:

    0x00 = No Warnings
    0x01 = High Fuel Cell Stack Temperature Warning
    0x02 = Low Fuel Cell Stack Voltage Warning
    0x04 = High Fuel Cell Stack Current Warning
    0x08 = Low Fuel Pressure Warning
    0x10 = Fuel Leak Warning
    0x20 = Low Oxygen Concentration Warning
    0x40 = Low Purge Cell Voltage Warning

    These warning codes are designed so that more than one warning can be issued at one time. The bitmap is a combination of the warnings present. The warning codes are combined with "OR" logic to form a single byte. For example, to send Low Fuel Cell Stack Voltage and Low Fuel Pressure Warnings simultaneously, the code 0x0A would be sent.

12. The Last Command Acknowledge is a repetition of the last command received from the OEM. See below for the structure of commands sent to the Nexa™ system.

13. The data (Fuel Cell Stack Temperature, Voltage, Current, Hydrogen Pressure, Hydrogen Concentration, and Cumulative Hydrogen Consumption, Oxygen Concentration) are sent as floating point numbers using the following 4 byte format as follows:

Sign (1 bit)	Exponent (8 bits)	Mantissa (23 bits)

The 4 bytes are arranged in the following fashion:

Sign (1 bit) + Exponent (7 MSB's)	Exponent (LSB) + Mantissa (7 MSB's)	Mantissa (8 bits)	Mantissa (8 LSB's)
Fourth Byte Sent	Third Byte	Second Byte	First Byte

The mantissa and the exponent are arranged so that the Most Significant Bit (MSB) is on the left and the Least Significant Bit (LSB) is on the right. To convert this format into a decimal number, the following formula is used:

$$X = (-1)^{\text{Sign}} \cdot (2^{(\text{Exponent}-127)}) \cdot (1.\text{Mantissa})$$

Where: Sign is either 1 or 0
Exponent is 8 bits (0 to 255)
Mantissa is 23 bits

Example: The number +46.28 would be sent as 0xB8, 0x1E, 0x39, 0x42, in that order.

14. The engineering units for the data are as follows:

Data Name	**Engineering Unit**
Fuel Cell Stack Temperature	° C
Fuel Cell Stack Voltage	volts
Fuel Cell Stack Current	amps
Hydrogen Pressure	bar (gauge)
Hydrogen Concentration	ppm
Cumulative Hydrogen Consumption	standard litres
Oxygen Concentration	percent (%)
Ambient Temperature	° C
Purge Cell Voltage	volts

15. Messages from the OEM to the Nexa™ control board are always 5 bytes long. The format for the message is given below:

Tag	Command	Failure Acknowledge	Check Sum	Tag

16. All of the information in the OEM command will be single bytes with the check sum computed in the same fashion as above.

17. The commands needed by the Nexa™ system are developed for customer-specific diagnostic and field service functions.
18. The Failure Acknowledge will be a repetition of the last Fail Code received from the control board.

Appendix C
ICMET Conference paper

Experimental Analysis of the Dynamic Performance of PEM Fuel Cell under Various Load Changes

A. Oheda, B. Omar, S. C. Chai, A. Aseeri and A. Savvaris

Dynamics, Simulation and Control Group, Department of Aerospace Sciences, School of Engineering

June 2010

Abstract

The dynamic performance is one of the most important specifications for Fuel Cell system (FCs). In this paper, practical experimental investigation of dynamic performance and transient responses of Proton Exchange Membrane (PEM) FC under various load conditions are presented using Ballard Nexa (1.2kW) PEMFC system. In order to test different characteristics of FCs, the practical tests have been separated into four different categories: instance start-up, shut-down, step-up load, and irregular load variation. It is observed that the external load changes the current output proportionally and reverses stack voltage consequently. The purge operation benefits performance recovery and improvement during a constant load and its time constant completely depends on the current working point. Overshoot and undershoot behaviours were observed throughout start up and transience. Magnitudes of overshoot/undershoot voltage show a discrepancy under different current intensities conditions.

The operating temperature of the system reacted quickly to current load without observation of overshoot or undershoot event. At the same time the air flow rate is directly affected by the dynamics load demand. Whereas, the increased amount of air flow rate during different step-changes is not identical, but depends on the requirement of internal reaction and flooding intensity. The results presented in this paper can be extended for validation of dynamic behaviour for different FC models.

1. Introduction

FC play a very importance roles in the new power generation filed due to its inherit virtue such as inherently clean, efficient and reliable service. Comparing with the traditional fossil-fuels technologies, FC system has strong robustness over whole load range in the case of little variation. Due to high module structure, FC system can be scaled to variety size to improve the performance and efficiency. However, for further practical deployment, FCs are expected to become more competitive in terms of cost, performance and reliability.

Among the various types of FCs, the Proton Exchange Membrane (PEM) FC has been drawing more attention due to its low operating temperature, ease of start-up and shut-down and compactness [1]. However, it is not able to respond promptly to a load step change due to the delay time for the fuel flow rate to adjust [2].

The majority of recent research focused on steady-state performance of PEM FC by presenting the polarization curves. Since experimental limitations and practical design problems, most of research works are carried out through modelling approaches [3]. However, the dynamic behaviour plays a very important role in evaluation of the whole system performance and obtains stable performance under various operating conditions. Generally, the dynamic performance of PEM FCs is affected by water, heat and gas management. In order to test the several technical problems related with the FC dynamic performance, the practical experiments have been carried out under strong conditions. This review divided into three parts as follows:

i- Temperature operation and gas management

Jong-Woo and Song-Yul [4] proposed a new temperature control strategy based on a thermal circuit. The thermal circuit consists of a bypass valve, a radiator with a fan, a reservoir and a coolant pump. Classic PI controllers and a state feedback control were used for the thermal circuit. In addition, the heat source term, which is dependent upon the load current, was feed-forwarded to the closed loop. The results show that the temperature rise in the catalyst can be kept within an allowable value and duration. The oxygen excess ratio can be maintained at an optimal value by minimizing the influence of temperature variations in the gas flow channel, and the power consumption of the blower reduced by more than 15% by compensation, and 5% by the controlling bypass valve at a multi-step load profile.

Three dimensional simulation of transient response of PEM FCs with consideration of heat balance was carried out by Shimpalee, S., [5] The results showed that the current overshoots the final state value during a change in the electrical load with fixed flow rates of hydrogen and air. Shimpalee, S. et al. [6] they carried out the effects of different operating parameters on the performance of PEM FC by using pure hydrogen on the anode channel and air on the cathode channel. They presented experiments with different FC operating temperatures, different cathode and anode humidification temperatures. Their experimental results are showed the effects of the various operating parameters on the performance of the PEM FC. Ferng, Y. M et. al. [7] they presented a study of the single cell performance covering the effects of operating temperature and pressure on performance and the flow characteristics within the cell. Their work confirms that the temperature and pressure have effect on the performance of a single PEM FC.

ii- Water management:

Yan, W., [8] presented a totally developed 3D model to calculate the steady state and transient phenomena of PEM FCs. They found that the vapour condensation

dynamics prolonged the cell response time particularly when compared to a liquid production model. Also [9-11] achieved a lot of work with the transient phenomena of gas and water transport. They found the dynamic response time was around 10s due to the mass transport interval. However, the system only required 0.4s to reach the 90% response. Also, they recognized the time for reaching the steady-state to the water content in the membrane particularly during the start-up procedure.

iii- Overshoot and undershoot behaviours:

Peng et al. [12] investigated the transient response of high temperature PEM FC They showed the relationship between overshoot and undershoot actions and the air mass flow rate. Tang, Y. et al. [3] Investigate the dynamic performance and transient responses of PEM FC under various load changes, their study showed the Overshoot and undershoot behaviours during transience.

Overall, the dynamic performance of PEM FC is extremely affected by operating conditions for instance temperature, gas flow rate, pressure and load changes. The current research [14-16] working on experimentally investigation of the dynamic characteristics and transient responses of PEM FCs undergoing load changes, and found out the relationship of the dynamic behaviour by employing a commercial PEM FC stack of Ballard Nexa power module.

2- Dynamic tests are carried out

2.1. Start-up state

Before starting up; the FC system was in OFF state. As an energy storage system 24 V battery power was applied to the control board, the system transited to STANDBY state. In this state, sensors and actuators were energized and the onboard microprocessor began to continually deliver system data and status signals.

After, a 5 V start signal to the Nexa system control board will begin the STARTING sequence. The hydrogen solenoid valve opens and the purge valve periodically cycled to fill the FC stack with hydrogen and the air pump turned on to provide air to the FCs.

After all, the cooling fan ran for thermal regulation as well as dilution of purged hydrogen. Once the external load increased from zero to the first step value, the current would accordingly begin to rise until the system reached a normal operating state.

2.2. Shut-down state

Once the 5V start signal is removed from the FC system, it transitions to the normal shut down state, and the external load relay was initiated to isolate the FC stack from the load. Then a shut-down sequence continued to remove residual product water from the anode and cathode flow channels using the air pump and hydrogen purge valve. After the start line was totally turned off and the battery power was disconnected, the system returned to OFF-state.

2.3. Step-up load state

In this state, four load steps were taken for step-up load investigation. The current increased from 0 to 40 Amp with break value 10 Amp. As the external load changed, the stack voltage and current responded dynamically to new operating conditions until reaching next steady state. In the meantime, other operating parameters changed as a result during each step state, and then adapted themselves to the new state. Among the whole process, the dynamic cell performance under constant load at 20 Amp was particularly discovered for investigation of purge effects.

2.4. Irregular load variation state

In this state, The FC system had to go through rough load changing since the external load did not follow step-by-step regulations. In order to get deeper insight of effects of air flow rate and operating temperature on the FCs dynamic performance, a longer test was carried out for dynamic evaluation.

3. Test apparatus

In this paper, the experimental data was obtained from Ballard Nexa (1.2kW) PEM FC system, the module consists of a Ballard stack with 47 cells set in series and other auxiliary subsystems including hydrogen system, oxidant air system, cooling system, electronic control system and safety system with sensors and microprocessors integrated on board. The dry hydrogen (>99.99%) is supplied by prepared high-pressurized hydrogen cylinder, while the oxidant air is supplied by air pump and humidified in a humidity exchanger before entering the FC stack in order to maintain water saturation of the membrane.

A cooling fan at the base of the unit is utilized to blow air through vertical cooling channels, Figure 1 shows the whole FC system schematically. A multi-functional data acquisition (DAQ) unit is supplied facilitating status monitoring and data record. Feedback signals as well as operating parameters (e.g. temperature, pressure, flow rate, gas concentration, current, voltage and so forth) can be captured through serial port communication. For real-time control and experimental observation Lab-View based software program is used.

4. Experimental set up

The experimental was based on a 1.2 kW PEM FC, a battery (2-batteries connected together, providing 12V each) as energy storage system or backup are connected to DC/DC converter then to electric load as shown in Figure 2. A series of dynamic experiments were performed under different operating conditions.
The whole process included four experimental states: start-up, shut-down, step-up load, and irregular load variation. The most important task of this paper was to identify the dynamic performance of each state and characterize relevant transient response to variable load.

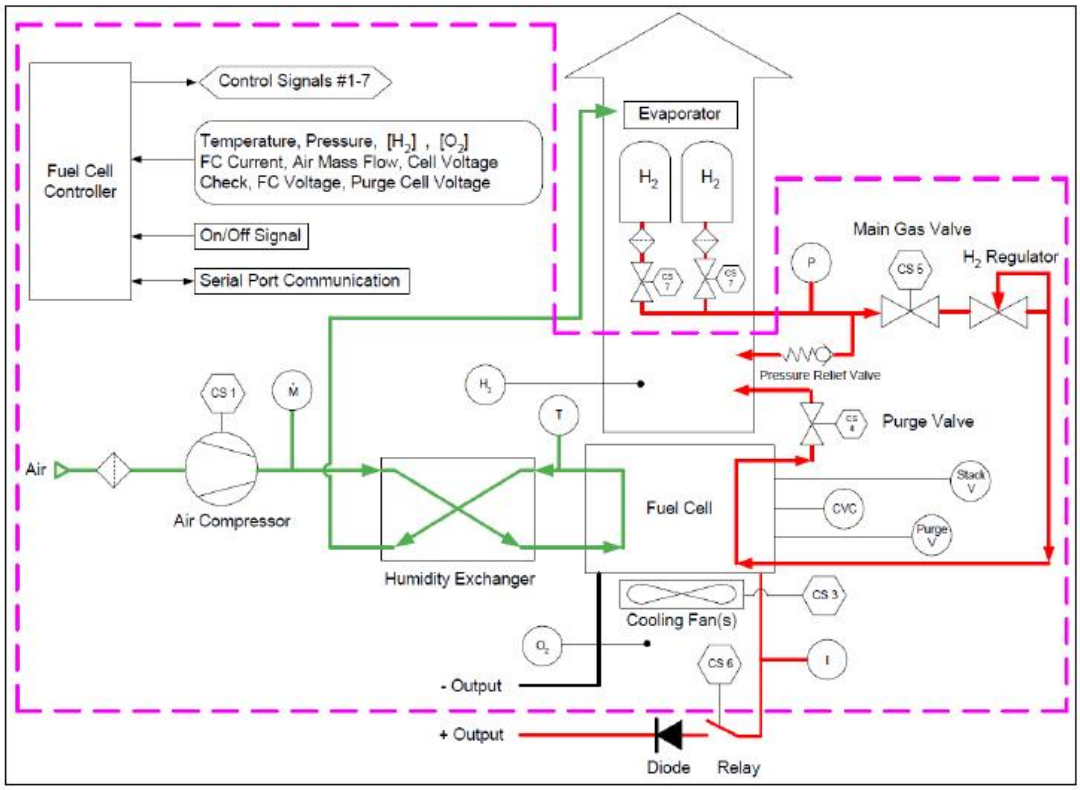

Figure: (1) Nexa™ System Schematic

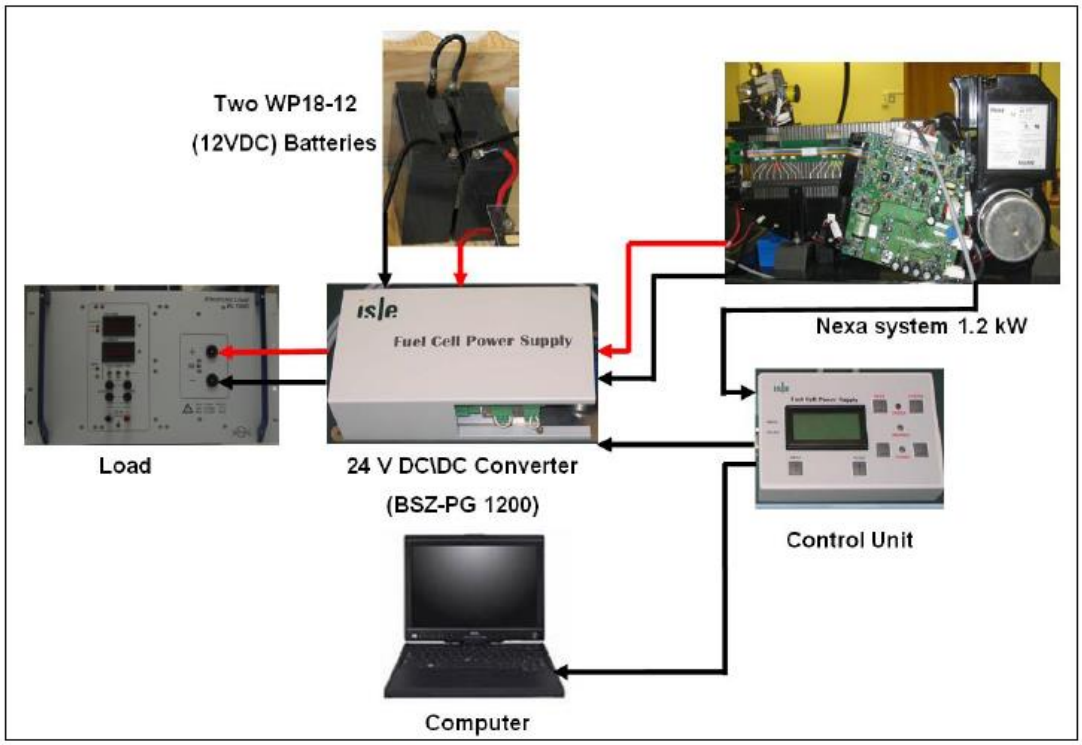

Figure: (2) Experiment set up

3

5. Results and Discussion

To track changes in output parameters and other factors these values are treated as a function of time and then plotted. This makes it a lot easier to take notice of any trend changes of these parameters.

5.1. Transient response in the start-up sequences

The 1.2kW Nexa power module FC provides fully automated operation and load response. Thus 24V batteries must be connected to support start-up and shutdown load; and the system must be provided with an adequate hydrogen fuel supply. The transient responses of transmitted status, current and voltage during the start-up states for 35 second are shown in Figures 3 and 4. Before applying the battery power, the FC system remains in the OFF state. The starting-up process began by applying 24V battery power to the control board, the system transited to stand-by state in 2 seconds. In this state, sensors and actuators were energized and the onboard microprocessor began to continually deliver system data and status signals. Subsequently a 5V start signal initiates the starting sequence. The hydrogen solenoid valve opened and the purge valve periodically cycled to fill the FC stack with hydrogen. And the air pump turned on to provide air to the FC. Finally, the cooling fan turned on for temperature regulation as well as dilution of purged hydrogen.

The cell voltages began to increase at 13 seconds and reached about 46V. During this state, no current output delivers to external load. After 21 seconds, the current gradually increased to 1.2 A and voltage decreased to 42V, which presents starting-up operation in this time. At 28 second, when normal operation was achieved, the Nexa module control board internally transferred parasitic load from the external battery to the FC stack. As well an external load relay control signal was sent to connect the FC to the external load. Due to this transmission the FC shocked up, it's the current increase with overshoot due to air pump fast demand, and the voltage decrease with undershoot as shown in Figure 4.

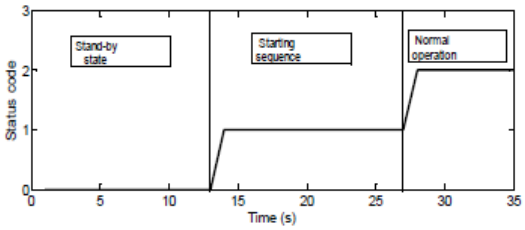

Figure: (3) Nexa transmitted status in starting-up state

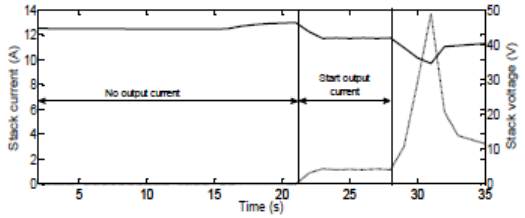

Figure: (4) Transient responses of the stack output current (A) & voltage (V) in start-up state

After the STAND-BY sequence, the air pump and cooling fan voltages jump from 0 to 43% and 50%, respectively as shown in Figure 6. The air flow rate is fluctuated around 20 slpm, its response has overshoot at the beginning of starting-up and normal operation states as illustrated Figure 5. When the external load was connected to the FC at 28 second, the voltage of the air pump increased with overshoot in order to supply enough oxidant air and flush the stack of residual water. The air flow rate goes up proportionally to satisfy the FC consumption. On the other hand, the membranes are still dry without enough water content at the beginning of a low load operation. An appropriate flow rate benefits water uptake and transport in the membrane FCs [36]. Contrarily, the cooling fan voltage drops to 35% so as to regulate the FC stack temperature. In reality, as shown in Figure 7 that the stack temperature does not change immediately. Therefore, even for a higher current level in the following running of the system, the cooling fan voltage is still kept constantly at 35%.

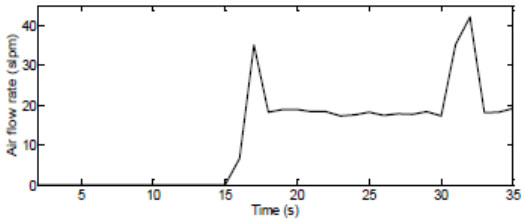

Figure: (5) Air flow rate in starting-up state (slpm)

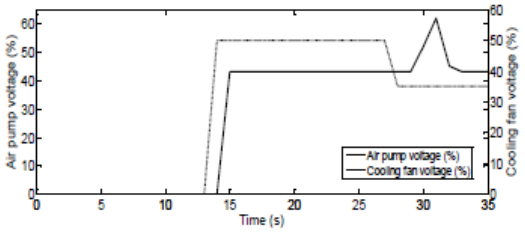

Figure: (6) The air pump and cooling fan voltage in the Start-up state

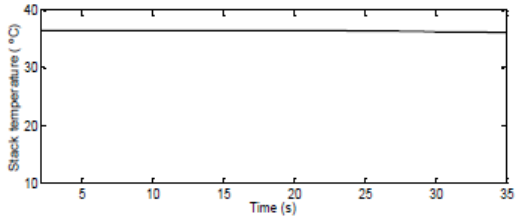

Figure: (7) Stack temperature in the starting-up state

5.2. Transient response in the shut-down sequence

In shut-down mode, the 5V start signal removed from the FC stack and the external load relay was open to isolate the FC stack from the load. Since the FC sufficiently operated longer than 5 -minute, then the shut-down sequence continued to remove residual product water from the anode and cathode channels using the air pump and hydrogen purge valve.

The transient responses during the shut-down states are illustrated in Figures 8, 9, 10 and 11. The shut-down begin from 419 second, the current drops to 1.58A within 1 second, while the stack voltage increases to 42 V. In this period at 438 seconds, the control board internally transferred parasitic load from the FC stack back the external battery, which cause current small undershoot and voltage small overshoot. From 447 seconds, the current drops almost to zero while the stack voltage increase gradually until reaches the OCV value of 46 V in idle state, and continually remove residual product water from the anode and cathode flow channels using the air pump and hydrogen purge valve as shown in Figure 8. The air flow rate increase from 20 slpm to 59 slpm in the period from 438 to 482 second than drops to zero as shown in Figure 10. At 452 second, the voltage of the cooling fan falls from 35 % to zero, later on at 482 seconds, the air pump drops sharply to zero as shown in Figure 11. Upon shut-down sequence, the stack temperature enters a decline phase but drops quite gently as illustrates in Figure 9.

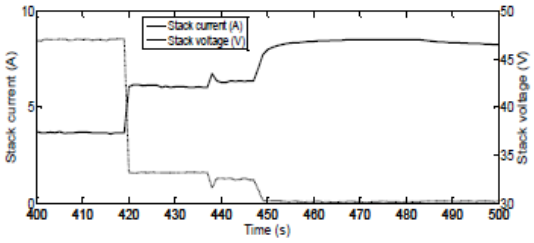

Figure: (8) Transient responses of the stack output current (A) and voltage (V) during shut-down state

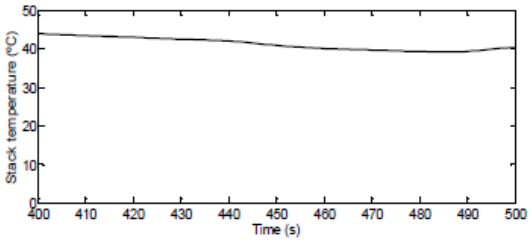

Figure: (9) Stack temperature in the shut-down state

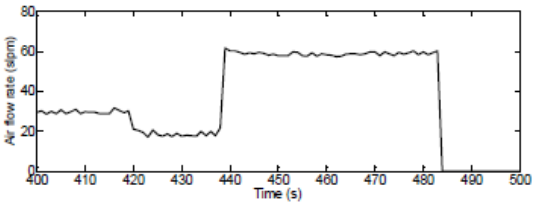

Figure: (10) Air flow rate in shut-down state (slpm)

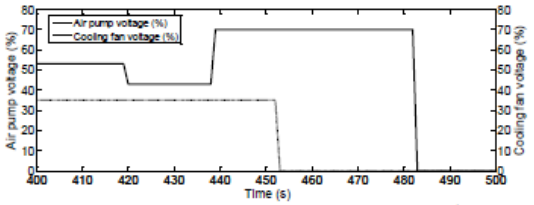

Figure: (11) The air pump and cooling fan voltage in the shut-down state

5.3. Transient response in the step-up load states

The results of this test describe the transient responses of FC parameters (stack current, stack voltage, air pump voltage ... etc) during step-up load variation as shown in Figures 12, 13, 14, 15 and 16. The current increases from 10 to 40 A, the stack voltage decline from 35 to 30V and the interval value was 10A. The maximum power of 1.2 kW occurs after 919 seconds as the current keeps stable at 40A. When the current increase, the frequency of purge valve operation also increases in order to prevent water flooding in the anode channel and anode gas diffusion layer, the interval between purge valve open and closed is about 96 seconds in the low-current region of around 10A, and become 30 seconds in the high-current region at 40A, which demonstrate the purging mechanism depend on the feedback of the FC dynamic behaviour as shown in Figures 15 and 16.

The 'red' circle in Figure 12 is focusing on stack voltage undershoot and current overshoot phenomena that occurs when the current transiently increases from 20A to 30A. The current overshoot possibility is elevated for two reasons: First, is that different operating condition leads to disparate water saturation level particularly after a long course of running. The second, is both the humidified water and product water alter the membrane wettability. The voltage undershoot because of an unexpected load action causes temporary dehydration due to electro-osmotic drag on the anode side, and air feeding starvation on the cathode side. The membrane resistance jumps and inevitably leads to a sharp drop of cell voltage [3].

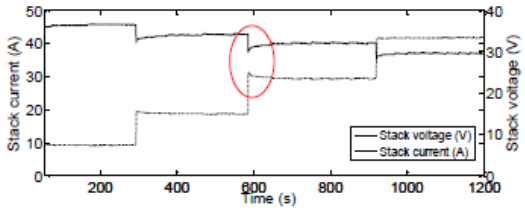

Figure: (12) Transient responses of the stack output current (A) and voltage (V) during step-up load states

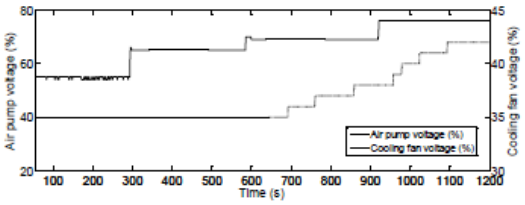

Figure: (13) The air pump and cooling fan voltage during step-up states

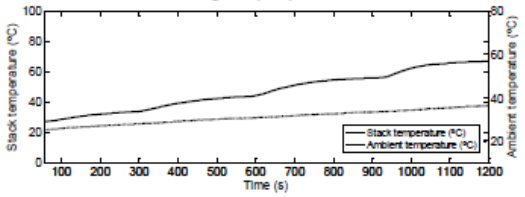

Figure: (14) stack and ambient temperatures during step-up states

The stack temperature changes proportionally with the current almost without any delay as illustrated in Figure 14. The air pump voltage also following the same step-up rhythm to the current increasing trend. The cooling fan voltage at the beginning is constant at 35%, after 700 seconds, it started to step up following the current increase as shown in Figure 13. Figure 15 is a detailed schematic plot of the FC stack voltage between 650 and 900 seconds under constant load. The current is around 30A during this period, while the FC stack runs without any load variation, the stack voltage actually experiences periodic degradation with purge valve operation that helps to remove water from the anode channel. During normal FC operation, liquid water condenses and accumulates because of dead-end configuration of the FC anode side. Before the purge valve opens, the stack voltage experiences a slight decline process from 32.2 to approximately 31.76V due to water flooding. An immediate performance enhancement after the purge valve open can be seen at the sharp voltage increase. The purge valve status values are '1' when the valve is open and '0' when the valve is closed as shown in Figure16.

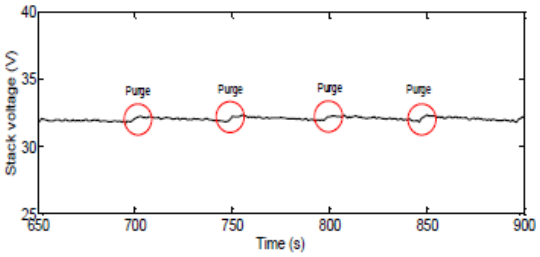

Figure: (15) Effect of purge valve operation on PEMFC stack voltage during constant load

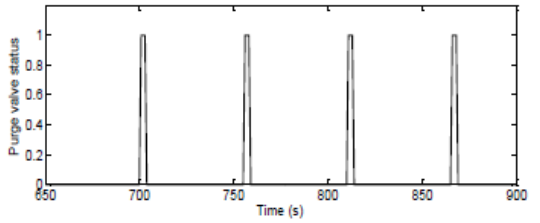

Figure: (16) Purge valve status during constant load (0 = valve closed, 1 = valve open)

5.4. Transient response under irregular load variation

The main objective of this test is to study the effects of temperature and air flow rate supplied by the air pump on the FC stack dynamic performance. In the test the FC supply power to irregular load variation over a longer course; experimental results are presented in Figures 17, 18 and 19. The temperature commonly exists during the FC operation in the forms of exothermic reaction heat transfer and internal heat dissipation. PEM FC stack temperature continuously changes with the load current. However, the temperature directly affects the rate of chemical reactions and the transport of water and reactants. Thus, operations under too-low or too-high temperatures in reality is always not recommended except for extreme circumstance such as sub-zero application [36], where it can be regulated by proper thermal control. The stack temperature response is following the load changes in a similar way to that of the current increase or decrease. However, changing slowly without overshoot or undershoot as illustrated in Figure 18.

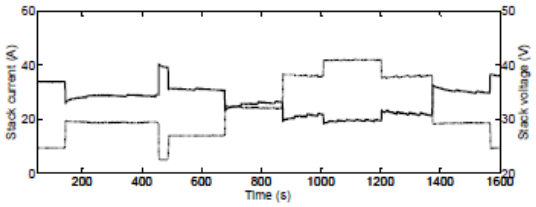

Figure: (17) Transient responses of the stack output current (A) and voltage (V) asymmetrical load variation

Figure 19 presents the air pump and cooling fan voltages of the Nexa FC, it can be seen that the air pump flow rate changes directly tracking the dynamic trend of current fluctuation without any delay. However, the decrease in the amount of air flow rate results in oxygen depletion from the FC cathode channel during power generation. Furthermore, the Nexa FC operation shows that the air flow does not significantly affect the FC stack dynamic performance.

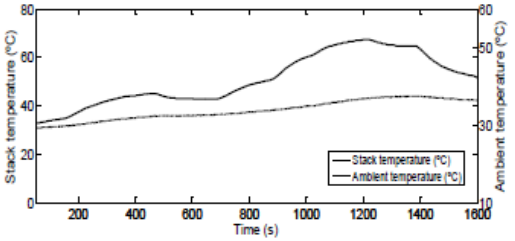

Figure: (18) Stack and ambient temperatures during asymmetrical load variation

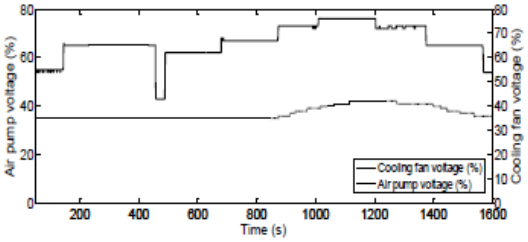

Figure: (19) The air pump and cooling fan voltage during asymmetrical load variation

6. Conclusions

The aim of this study was to investigate the dynamic performance of a PEM FC stack. To reach this goal, a set of experimental tests on Ballard Nexa power module were presented. The dynamic behaviours were checked during different operations conditions such as start-up, shut-down, and step-up and irregular load variation.

The control board internally transferred parasitic load from the external battery to the FC stack at start-up. Due to this transmission the FC shocked up, it's the current increase with overshoot due to air pump fast demand, and the voltage decrease with undershoot. In shut-down sequences control board internally transferred parasitic load from the FC stack back the external battery, which cause current small undershoot and voltage small overshoot.

When the current transiently increases from 20A to 30A, a current overshoot can be observed in the system responses due to two factors. The first factor is that different operating condition results in disparate water saturation level particularly after a long course of running. The second factor is that both the humidified water and product water alter the membrane wettability. Since temporary dehydration due to electro-osmotic drag on the anode side and air feeding starvation on the cathode side, a voltage undershoot was observed at the same time.

With the current increasing, the frequency of purge valve operation also increases in order to prevent water flooding in the anode channel and anode gas diffusion layer. The time interval between purge valve open and closed is about 96 and 30 seconds in the case of the low-current region of around 10A and 40A, respectively.

The stack temperature quickly responses to the load current without observation of overshoot/undershoot. The air flow also follows the same step-up rhythm to the current increasing trend. The cooling fan is constant at 35% at the beginning and steps up when the load current and stack temperature increase.

References

[1] Choi, W., Howze, J. W. and Enjeti, P. (2006), "Development of an equivalent circuit model of a fuel cell to evaluate the effects of inverter ripple current", Journal of Power Sources, vol. 158, no. 2, pp. 1324-1332.

[2] Uzunoglu M, Alam MS. Dynamic modeling, design and simulation of a PEM fuel cell/ultra-capacitor hybrid system for vehicular applications. Energy Convers Manage 2007;48(10):1544–53.

[3] Tang, Y., Yuan, W., Pan, M., Li, Z., Chen, G. and Li, Y. (2010), "Experimental investigation of dynamic performance and transient responses of a kW-class PEM fuel cell stack under various load changes", Applied Energy, vol. 87, no. 4, pp. 1410-1417.

[4] Ahn, J. and Choe, S. (2008), "Coolant controls of a PEM fuel cell system", Journal of Power Sources, vol. 179, no. 1, pp. 252-264.

[5] Shimpalee, S., Spuckler, D. and Van Zee, J. W. (2007), "Prediction of transient response for a 25-cm2 PEM fuel cell", Journal of Power Sources, vol. 167, no. 1, pp. 130-138.

[6] Wang, L., Husar, A., Zhou, T. and Liu, H. (2003), "A parametric study of PEM fuel cell performances", International Journal of Hydrogen Energy, vol. 28, no. 11, pp. 1263-1272.

[7] Ferng, Y. M., Tzang, Y. C., Pei, B. S., Sun, C. C. and Su, A. (2004), "Analytical and experimental investigations of a proton exchange membrane fuel cell", International Journal of Hydrogen Energy, vol. 29, no. 4, pp. 381-391.

[8] Wu, H., Berg, P. and Li, X. (2009), "Steady and unsteady 3D non-isothermal modeling of PEM fuel cells with the effect of non-equilibrium phase transfer", Applied Energy.

[9] Yan, W., Chu, H., Chen, J., Soong, C. and Chen, F. (2006), "Transient analysis of water transport in PEM fuel cells", Journal of Power Sources, vol. 162, no. 2 SPEC. ISS., pp. 1147-1156.

[10] Yan, W., Soong, C., Chen, F. and Chu, H. (2005), "Transient analysis of reactant gas transport and performance of PEM fuel cells", Journal of Power Sources, vol. 143, no. 1-2, pp. 48-56.

[11] Shimpalee, S., Lee, W., Van Zee, J. W. and Naseri-Neshat, H. (2006), "Predicting the transient response of a serpentine flow-field PEMFC: II: Normal to minimal fuel and AIR", Journal of Power Sources, vol. 156, no. 2, pp. 369-374.

[12] Zou, J., Peng, X., and Yan, W., (2006), "Dynamic analysis of gas transport in cathode side of PEM fuel cell with interdigitated flow field", Journal of Power Sources, vol. 159, no. 1 SPEC. ISS., pp. 514-523.

[13] Zhu, W. H., Payne, R. U., Cahela, D. R. and Tatarchuk, B. J. (2004), "Uniformity analysis at MEA and stack Levels for a Nexa PEM fuel cell system", Journal of Power Sources, vol. 128, no. 2, pp. 231-238.

[14] Del Real, A. J., Arce, A. and Bordons, C. (2007), "Development and experimental validation of a PEM fuel cell dynamic model", Journal of Power Sources, vol. 173, no. 1, pp. 310-324.

[15] Adzakpa, K. P., Ramousse, J., Dubé, Y., Akremi, H., Agbossou, K., Dostie, M., Poulin, A. and Fournier, M. (2008), "Transient air cooling thermal modeling of a PEM fuel cell", Journal of Power Sources, vol. 179, no. 1, pp. 164-176.

Appendix D
SCHOTT Solar polycrystalline Data Sheet

SCHOTT Solar polycrystalline solar modules

SCHOTT POLY™ 217/220/225/230

The long-established German company SCHOTT Solar is a world leader in the photovoltaic industry and has more than 50 years of experience in the development and production of components for solar applications.
SCHOTT Solar polycrystalline modules are specifically designed for both roof- and ground-mounted applications. Due to strict internal quality standards, all modules benefit from exceptionally long durability, which results in maximised profitability. The polycrystalline cells within each module are sorted to particularly narrow performance tolerances, thereby allowing series interconnections with minimal mismatch losses.

Double of the required standard: SCHOTT Solar tests its modules for twice as long as is required by the IEC.

High resistance to mechanical loads: The solid anodised aluminium frame ensures superior torsional resistance. SCHOTT Solar polycrystalline modules are also tested to an extreme loading pressure of 5,400 Pa – which equates to 550 kg per square metre and a reassuring level of security for your investment.

High performance output: All SCHOTT Solar polycrystalline modules hold a positive tolerance of their nominal power rating. This ensures a stable high-energy output and a quick return on investment.

Long-term reliability: SCHOTT Solar offers a power output guarantee of 25 years and a product warranty of five years.

Increased resistance to reverse current: SCHOTT Solar polycrystalline modules have a high resistance to reverse current, minimising the wiring costs.

- Double of the required standard
- High resistance to mechanical loads
- High performance output
- Long-term reliability
- Increased resistance to reverse current

SCHOTT POLY™ 217/220/225/230

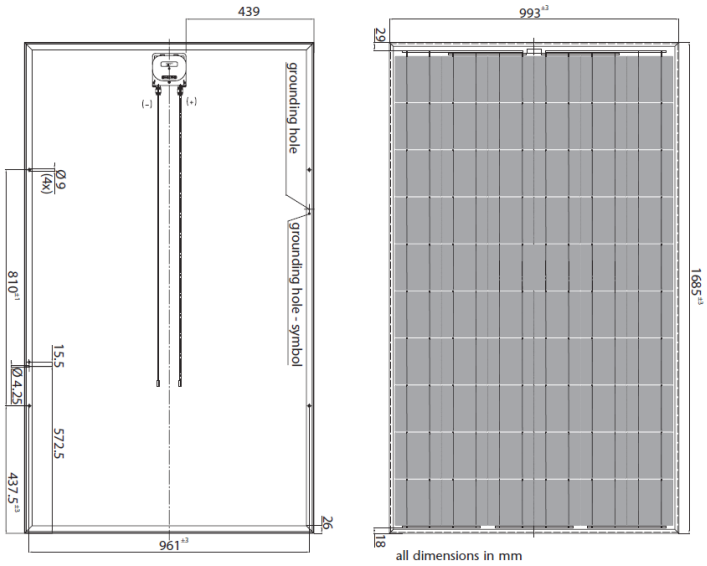

all dimensions in mm

Technical Data

Electrical data

Electrical data refer to Standard Test Conditions (STC):
Irradiance 1000 W/m², spectrum Air Mass 1.5 and cell temperature 25°C

Module type		SCHOTT POLY™ 217	SCHOTT POLY™ 220	SCHOTT POLY™ 225	SCHOTT POLY™ 230
Nominal power [Wp]	P_{mpp}	≥ 217	≥ 220	≥ 225	≥ 230
Sorting tolerance		-0 %	-0 %	-0 %	-0 %
Voltage at nominal power [V]	U_{mpp}	29.6	29.7	29.8	30.0
Current at nominal power [A]	I_{mpp}	7.33	7.41	7.55	7.66
Open-circuit voltage [V]	U_{oc}	36.4	36.5	36.7	36.9
Short-circuit current [A]	I_{sc}	8.10	8.15	8.24	8.33
Module efficiency level (%)	η	13.0	13.1	13.4	13.7

Sorting of module performance by flash data report (-0 %, positive tolerance only)
Rating tolerance for power output is ± 4 % and rating tolerance for all other parameters is ± 10 %.

Data at normal operating cell temperature (NOCT)

Irradiance 800 W/m², spectrum Air Mass 1.5, windspeed 1 m/s and ambient temperature 20°C

Nominal power [Wp]	P_{mpp}	156	158	161	165
Voltage at nominal power [V]	U_{mpp}	26.7	26.7	26.9	27.1
Open-circuit voltage [V]	U_{oc}	33.2	33.3	33.5	33.7
Short-circuit current [A]	I_{sc}	6.49	6.53	6.60	6.67
Temperature [°C]	T_{NOCT}	47.2	47.2	47.2	47.2

Rating tolerance for power output is ± 4 % and rating tolerance for all other parameters is ± 10 %.

Temperature coefficients

Power [%/K]	T_K (P_n)	-0.47	-0.47	-0.47	-0.47
Open-circuit voltage [mV/K]	T_K (U)	-122	-122	-123	-123
Short-circuit current [mA/K]	T_K (I)	2.43	2.45	2.47	2.50

Characteristic data

Solar cells per module	60
Cell type	MAIN-Iso (polycrystalline silicon, 156 x 156 mm², full-square)
Connection	Junction Box IP65 with 3 bypass diodes, solar cable (length: 1.1 m, diameter: 4 mm²) with Tyco Solarlok Interconnection
Dimensions junction box [mm]	110 x 115 x 25
Front panel	low iron solar glass 4.0 mm
Frame material	anodised aluminium

Dimensions and weight

Dimensions [mm]	1,685 x 993 (tolerance ± 3 mm)
Thickness [mm]	50 (tolerance ± 1 mm)
Weight [kg]	approx. 23

Limits

System voltage [V_{DC}]	1000
Maximum reverse current I_R [A]*	20
Operating module temperature [°C]	-40… +85
Maximum load (to IEC 61215 ed. 2)	Pressure: 5,400 N/m² or 550 kg/m²
Application classification (to IEC 61730)	A
Fire classification (to IEC 61730)	C

** No external voltage in excess of U_{oc} shall be applied to the module.*

Permission and certificates

The modules are certified to IEC 61215 ed. 2 and IEC 61730, Electrical Protection Class II and the CE-guidelines.

The **installation manual** contains additional information on installation and operation.

All information complies with the requirements of the standard EN 50380.

MANAGEMENTSYSTEM
Certified by DQS according to
DIN EN ISO 9001:2000 · Reg.-No. 2184
DIN EN ISO 14001:2005 · Reg.-No. 2184

SCHOTT Solar AG
Carl-Zeiss-Strasse 4
63755 Alzenau
Germany

Phone: +49 (0) 60 23 / 91 - 1712
Fax: +49 (0) 60 23 / 91 - 17 00
solar.sales@schottsolar.com
www.schottsolar.com

SCHOTT solar